On Using A Viscoelastic Material Model for Saline Ice

Lien Tran

School of Engineering

Thesis submitted for examination for the degree of Master of Science in Technology.

Espoo July 26, 2019

Supervisor

Prof. Arttu Polojärvi

Aalto University
School of Engineering

Aalto University
School of Engineering

Aalto University, P.O. BOX 11000, 00076 AALTO
www.aalto.fi
Abstract of the master's thesis

Author Lien Tran

Title On Using A Viscoelastic Material Model for Saline Ice

Degree programme Mechanical Engineering

Major Solid Mechanics **Code of major** 007

Supervisor and advisor Prof. Arttu Polojärvi

Date July 26, 2019 **Number of pages** 64+20 **Language** English

Abstract

In the current thesis, we attempt to understand the linear viscoelastic behaviour of S2 sea ice by studying its compliance function. Descriptions of the Power Law and the Generalised Kelvin models are provided. Starting with these analytic models, the compliance function was approximated with certain numerical techniques; truncated singular value decomposition (SVD), Tikhonov regularisation, and nonnegative least squares method were examined amongst all in this work. The approximate forms of the compliance function contain parameters that were determined by investigating strain response of ice to some given loading cases. Once the parameters were established, the numerical techniques that produced them were evaluated based on how well a resulting compliance function predicts experimental strain response. It was found that the truncated SVD gives the most reliable results. The test data for this project was extracted from creep tests and loading/unloading creep cycles at various stress rates and frequencies. Generally, the numerical methods were shown to determine the parameters of the approximate forms of compliance function rather well.

Keywords Linear viscoelasticity, S2 sea ice, saline ice, creep compliance, Power Law , Genralised Kelvin.

Preface

This thesis has been carried out during the years 2018-2019 in ice mechanics research group at Aalto University School of Engineering.

I wish to express my deepest gratitude to my supervisor Assistant Professor Arttu Polojärvi for providing me a chance to work in this project in his Ice Mechanics group. Without his guidance support and contribution, I would not have been possible.

From my deepest heart, I would like to show my greatest appreciation to Kari Santaoja for his teaching, support, and his warm heart as well as his precious advice during my years studying at Aalto. Special thanks also to Mingdong Wei for his generous support in performing experiments and treating data.

And without support and encouragement from my family and all of my friends, Bogdan M., Osama A., Mateo R., Anton V., Javier V., Espezanza L.,Anrea C., and Calos C., I could not have got this far. I am blessed to have you all as friends and I apologise for being aloof most of the time. Thank you for your questions, answers, and specially your belief in me.

Otaniemi, July 26, 2019

Lien Tran

Contents

Symbols and abbreviations

Symbols

B	body at the time of reference
B'	body at the current time
$\boldsymbol{B}$	left Cauchy-Green tensor
$\boldsymbol{C}$	right Cauchy-Green tensor
$\mathbb{E}$	Euclidean space
$\boldsymbol{F}$	deformation gradient tensor
$\boldsymbol{I}$	identity tensor
J	retardation/creep compliance function
$\boldsymbol{J}$	retardation/creep compliance tensor
G	moduli/relaxation function
$\boldsymbol{G}$	moduli/relaxation tensor
$\mathbb{N}$	set of natural numbers
$\mathbb{R}$	set of real numbers
t	time
$\boldsymbol{u}$	displacement vector
$\boldsymbol{U}$	right stretch tensor
$\boldsymbol{V}$	left stretch tensor
$\boldsymbol{X}$	spacial point in B
$\boldsymbol{x}$	spacial point in B'
ϵ	strain function
$\boldsymbol{\epsilon}$	strain tensor
$\boldsymbol{\varphi}$	deformation map
σ	stress function
$\boldsymbol{\sigma}$	stress tensor

Operators

det	determinant
$\frac{\mathrm{d}}{\mathrm{d}t}$	derivative with respect to variable t
$\frac{\partial}{\partial t}$	partial derivative with respect to variable t
$\sum_i$	sum over index i
$\mathbf{a} \cdot \mathbf{b}$	dot product of vectors $\mathbf{a}$ and $\mathbf{b}$

Abbreviations

SVD	singular value decomposition
NLS	nonnegative least squares
ppt	parts per thousands

1 Introduction

1.1 Motivations

In terms of geography, sea ice covers most of the primary cryospheric surface that takes about $5\% - 10\%$ of Earth's surface and it is still a vital topic in research and operational disciplines including physics, climatology, meteorology, oceanography, navigation, marine biology, and marine and offshore structural engineering. For instance, in the field of engineering, the influence of sea ice becomes one of the most significant factors to be considered by cold-climate ship and structure designers. In the severe Arctic climate conditions, offshore structures and ships can be critically damaged during the ice-structure interactions (see Fig.1.1). The sea ice failure process is driven by different parameters including the contact area between ice and structures, the local stresses, ice feature properties, geometry of the structures, and the mode of ice failure against the structures. Typical failure mechanisms in sea ice include creep, radial cracking, buckling, circumferential cracking, spalling, and crushing. The last mechanism has been observed to be the most critical failure mode for vertical structures due to the fact that it may cause the highest ice action and violent structural vibrations. This motivates the need to deeply understand sea ice and its properties and behaviour in order to protect the structures from encroachments of ice. The knowledge is essential for the economic and safe design of ships and marine structures. (Shokr & Sinha, 2015)

Conventionally, sea ice is defined as a conglomerate of fresh water crystals interlaced with or without the inclusion of brine that has formed between the crystals and crystal plates. In nature, sea ice exists as a composite material comprising of three phases of matter: solid, liquid and gas. During all stages of its development, influenced by a number of complex processes such as the constantly turbulent fluctuations of wind, wave, temperature, ocean water movement, fluxes of heat, and circulation between atmosphere and ocean, sea ice exhibits rather complicated characteristics. Due to its complex structure, sea ice is often regarded as a heterogeneous and anisotropic material. The term 'sea ice', by convention, covers all types of ice including saline ice formed from direct freezing of seawater. The classification of sea ice has been broadly defined on the basis of thickness and quality of consolidation and age with little concern for microstructural details. However, microstructural details of ice are of direct relevance to most ice-induced engineering problems as they determine the physical and mechanical properties of sea ice. (Shokr & Sinha, 2015)

Due to its inherently complex microstructure and the high homologous temperature condition in nature, sea ice tends to display rather complicated mechanical properties which make ice modelling more challenging. The major class of sea ice encountered in nature are columnar-grained ice or S2 ice which exhibits a regular and ordered crystalline structure. This particular type ice behaves like a brittle material when loaded for very brief periods but, under sustained loading conditions, it behaves like a ductile material. Ice properties and behaviour can be characterised in a form of a constitutive equation. Such an equation describes the behaviour of ice in a manner

Figure 1.1: A ship stuck in compressive ice and the damages that resulted from the ice load. (Riska, 2011)

which is independent of the geometry of the body but depends only on the material intrinsic nature. A constitutive equation is formulated through concepts of stress, strain, and rate of strain. In this thesis work, a viscoelastic constitutive relation of polycrystalline S2 sea ice is investigated in the framework of a linear theory.

In principle, the concept of stress is defined as force per unit area at the macroscopic level but it breaks down at the molecular level. The concept of strain enables us to capture the material deformation in terms of functions of space and time. Schematically, a typical strain history in polycrystalline ice during its sustained loading can be divided into two main stages: undamaged and damaged stage (see Fig. 1.2). At low-stress levels or in the undamaged stage, ice behaves elastically when deforms. Depending on the rate of deformation and the deformation history it displays a characteristic of a creeping, ductile material which is known as linear viscoelastic and non-linear viscoelastic behaviours. At this stage, the ice properties stay constant at any specific strain level in spite of the increase of stress. In other words, the deformation of sea ice is completely removed as the applied stress is removed. Opposite to that, in the damaged stage, ice deformation cannot be recovered after

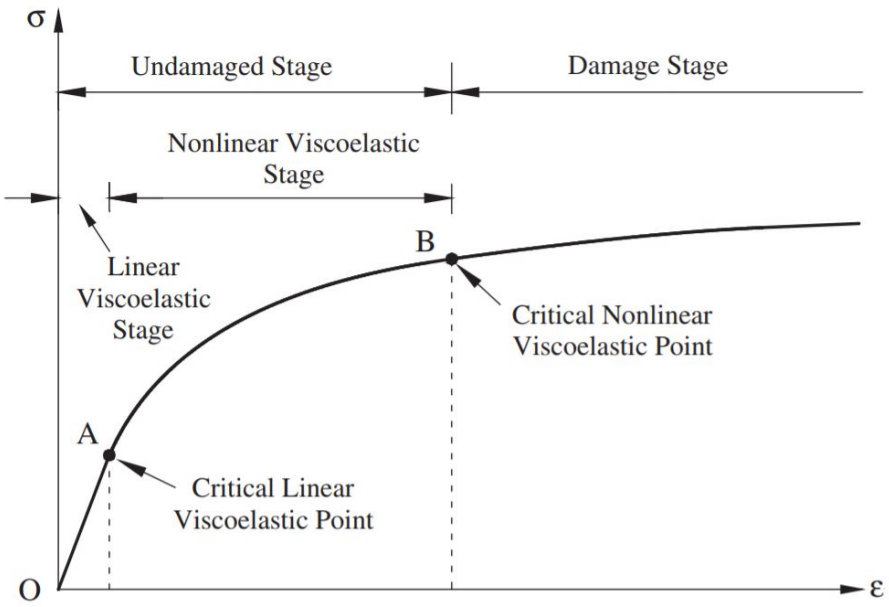

Figure 1.2: Typical stress-strain curve. In the direction of increase strain, sea ice may experience multiple stages including undamaged stage, consisting of the linear elastic stage, linear viscoelastic stage, and the nonlinear viscoelastic stage; and damage stage. (Luo et al., 2016).

unloading along with the fact that their properties keep varying as the strain level varies. (Luo et al., 2016) Subjected to relatively high-stress levels, ice behaves as an extremely brittle material which may fail by brittle fracture as a consequence of the formation and propagation of cracks. The transition between ductile to brittle phase in ice plays a central role in ice mechanics as it indicates the point where the stresses in ice attain their maximum magnitudes. In particular, it allows the critical forces exerted by sea ice on the man-made structure to be determined. Thus this transition stage is of special interest to Engineering.

1.2 Objectives and Scope

The principal aim of the thesis is to provide better insights into the linear viscoelastic property of sea ice subjected to various stress states. In particular, the present work develops a description of polycrystalline ice structure from the point of view of Continuum Mechanics and establishes the needed theoretical interrelations. Specifically, the formulations of isothermal linear viscoelastic stress-strain constitutive relations of sea ice are to be discussed. We examine different representations of the constitutive relations. Obviously, in order to understand these relations, certain material functions that link stresses and strains must be studied. It will be shown that one of such functions is the so-called creep compliance function. There exist several analytic representations that model compliance; they are to be discussed later.

The main contribution of this thesis is to develop numerical methods to approximate analytic forms of the sea ice creep compliance function. Depending on the analytical form of the compliance function, different numerical schemes are applied and evaluated. The schemes under examination include truncated singular value decomposition (truncated SVD), Tikhonov regularisation, and nonlinear least squares (NLS) optimisation. These numerical techniques are to be formulated and adapted for estimating the creep compliance function; then they are to be tested with numerically simulated loading and strain response that corresponds to it. Furthermore, these numerical methods are tested with stress and strain response data obtained from an experiment. The constitutive relations are then used to predict the strain response of sea ice under two loading scenarios; semi-static and cyclic. The predicted response is to be compared with measured values. Last but not least, we discuss the harmonic or complex compliance, which is a function of frequency, and which is obtained as a Laplace transform of the analytical form of the real-valued compliance.

1.3 Thesis Structure

This thesis is organised into five sections. The crystalline structure of sea ice and its kinematics, as well as its linear viscoelastic behaviour are covered in the Sec. 2. Different analytical models of material functions are investigated in the same section. Sec. 3 presents numerical methods to approximate the creep compliance function. In Sec. 4, the simulation results and comparison of the three models are provided. Sec. 5 gives a brief summary of the results and concludes the thesis.

2 Background

Theoretical background necessary to develop the viscoelastic models for S2 ice subjected to various loading scenarios is covered in the present section. Sec. 2.1 introduces general definitions, classifications, and characteristics of sea ice. Sec. 2.2 provides the theory of kinematics which is the foundation of linear elastic and linear viscoelastic theories. In the last subsection, Sec. 2.3, linear viscoelastic theory is studied in detail. Several representations of the theory are presented.

2.1 Polycrystaline Sea Ice

2.1.1 General Classification

Based on the scale of observation, ice in nature can be classified into two major groups: micro- to macroscale and mesoscale. The former one provides an important ice classification based on the grain structure and texture of ice. This ice classification plays a vital role in fields of ice engineering that are related to near-shore and offshore structures, as well as to ship designing. The latter group is based on age, history, size, and thickness of the ice cover, which is more useful for navigation and safety of structures, icebreakers, and ice-strengthened ships designing. (Shokr & Sinha, 2015)

The micro- to macroscale categorisation of ice can be sub-classified into five other subgroups: primary, secondary, superimposed (tertiary), random ice and glacier ice. According to the ice classification, the class that interests us the most is the secondary ice due to its commonality in nature. This class can be divided into five basic types by crystallography: S1, S2, S3, S4, and S5. Columnar-grained ice or S1, with c-axis (or optical axis which is discussed in the next section) in the vertical plane, has never been reported for sea ice. Type S1 ice usually forms under the calm conditions without any disturbance of snow deposition during the initial age of freezing. On the other hand, the S2 type can form in an area of rip water current and is defined as the transversally isotropic columnar-grained ice with the c-axis of the grains randomly oriented in the horizontal plane or normal to the growth direction. Ice of the type S3 has a similar structure to that of S2 but the c-axis of the grain tends to be oriented in a particularly preferred direction which is parallel to the current of the water under the ice sheet during the growing period. (Sinha, 1977; W. F. Weeks & Gow, 1978) Type S4 is prevalent which refers to the ice mixed with unfrozen dense slush. The last type of ice, S5, refers to the structure of oriented frazil ice whose crystals are usually needle-like or crushed needles. (Shokr & Sinha, 2015)

2.1.2 Pollycrystalline Sea Ice Structure

In the domain of crystalline structures, natural polycrystalline sea ice inherits an intrinsic characteristic of long range atomic or molecular order which consists of many crystals of varying shape, size, and orientation. The categorisation of polycrystalline ice is based on the basis of geometrical characteristics of its constituent

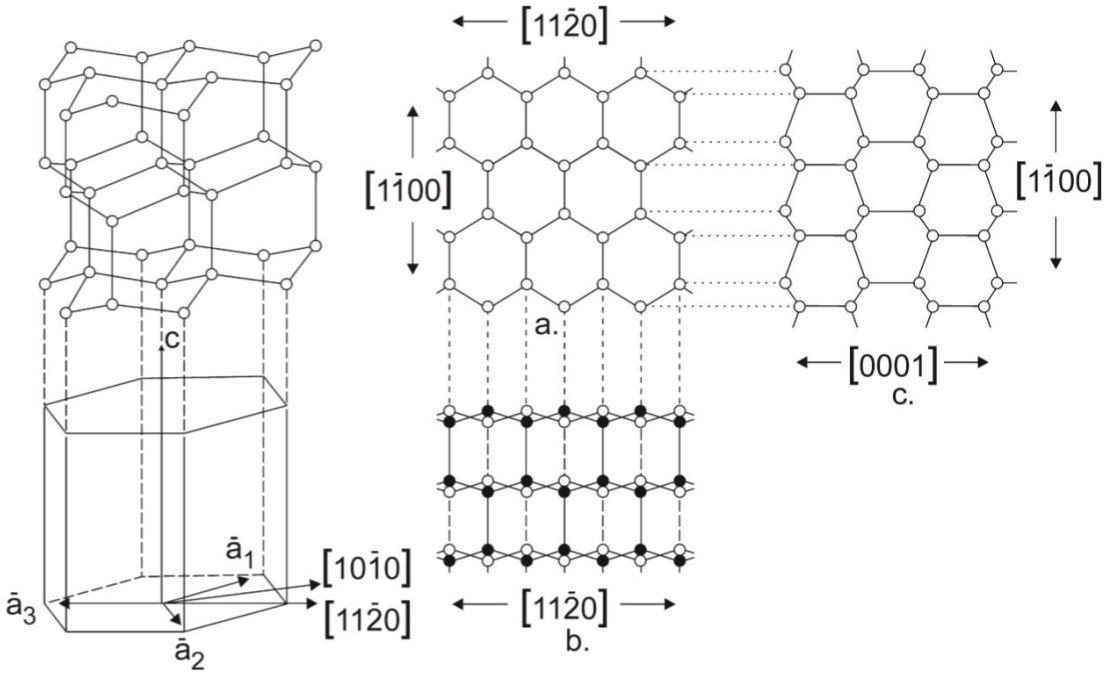

Figure 2.1: (a) Crystal structure of ice Ih, (b) top and (c) bottom (normal to the c-axis) views (W. Weeks et al., 1998).

crystals.(Shokr & Sinha, 2015) In general, the freezing of water on the Earth's surface under equilibrium condition leads to formation of the modification of ice Ih, where "h" indicates crystal symmetry in the hexagonal system. During the solidification process, water molecules (H_2O) arrange tetrahedrally around each other, with a sixfold rotational symmetry apparent in the so-called basal plane or basal face. This plane parallels to the crystal hexagonal bases while the lateral sides of the crystal are called prismatic planes. The principal crystallographic axis or c-axis is defined as a unit vector [0001] normal to the basal plane which corresponds to the axis of maximum rotational symmetry (see Fig. 2.1). The basal plane is defined by the crystal a-axes and is smooth at the molecular level, while, the crystal faces perpendicular to this plane are rough at the molecular level. (Thomas, 2017)

The main factor determining the microstructure and properties of sea ice is the amount of sea salt ion retained in liquid inclusions in the solid ice matrix. The percentages of dissolved salts and gases are directly related to the sea ice formation, composition, and growth. Water salinity is regularly measured as the ratio of the weight of salts in grams dissolved in one 1000g of seawater or parts per thousands (ppt or ‰). On average, seawater salinity is observed to be 35‰ in most marine area. The salts dissolved in seawater compose of sodium chloride (NaCl) primarily and other salts such as sodium sulfate, magnesium sulfate, and magnesium chloride in minor amounts.

During the of solidification, due to its tenacious resistance to incorporate salt ions in seawater, ice has a lower material density than its liquid state. The majority

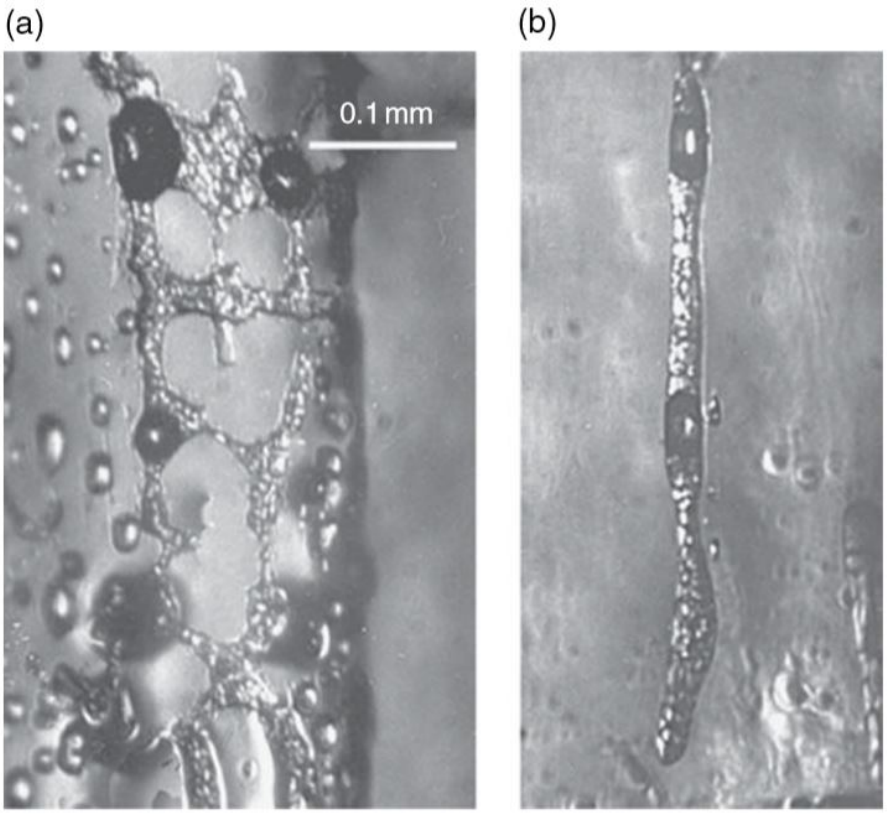

Figure 2.2: Photomicrographs of (a) irregular and (b) cylindrical brine pockets at -30^0C exhibiting precipitated salt crystals and air bubbles. (Shokr & Sinha, 2015)

of ions present in seawater are rejected by the advancing ice–water interface during crystal growth. In the ice crystal lattice, accommodation of sea salt ions is highly restricted except for very few species of ions and molecules. Among them are fluorine and ammonium ions, and some gases, which are allowed to incorporate in ice lattice in appreciable quantities based on constraints, size, and electric charge. The migration of salt ions and gas to ice lattice results in brine pockets (see Fig. 2.2) which

Table 1: Major salts in sea ice and their precipitation temperatures. (Shokr & Sinha, 2015)

Salt Name	Composition	Precipitating Temp. (^{0}C)
Calcium carbonate	$CaCO_3 \cdot 6H_2O$	-2.20
Sodium Sulfate	$Na_2SO_4 \cdot 10H_2O$	-8.20
Magnesium chloride	$MgCl_2 \cdot 8H_2O$	-18.00
Sodium chloride	$NaCl{\cdot}2H_2O$	-22.90
Magnesium chloride	$MgCl_2 \cdot 12H_2O$	-36.80
Calcium chloride	$CaCl2 \cdot 6H_2O$	-55.00

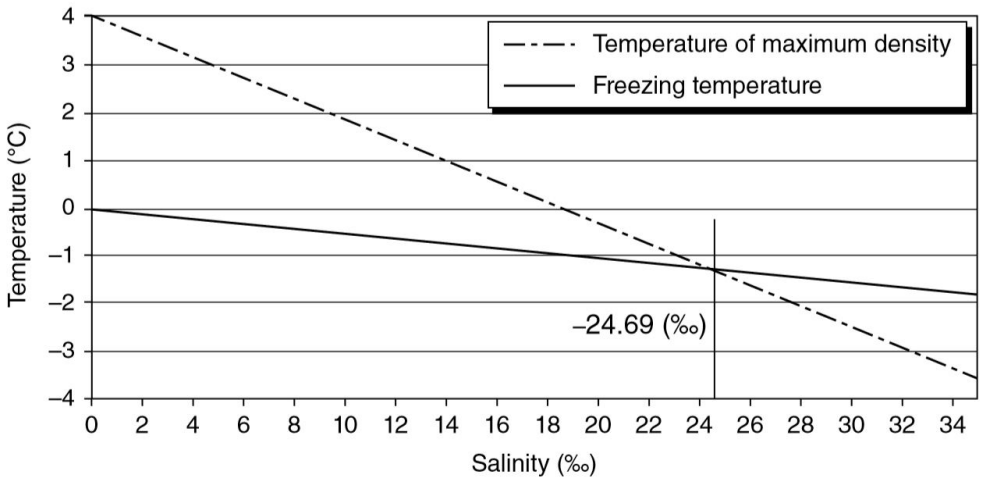

Figure 2.3: Dependence of the temperature of maximum density and the freezing point on water salinity; the two curves intersect at the salinity of 24.69 ‰. (Shokr & Sinha, 2015)

are located along boundaries and subboundaries of ice crystals. Depending on the temperature of the ice, the salinity of the liquid in the brine pockets is determined. As can be seen in table 1, different solutes in the brine start to precipitate at different temperatures. On the other hand, the large fraction of rejected ions stays in the underlying water column. As ice grows, the desalination of ice lattice causes the salt to build up ahead of the advancing interface and dissolve into the lower saline ocean water.

Sea ice density, as aforementioned, is lower than that of its liquid state. Depending on the salinity of the water, the density of seawater at the surface of the ocean varies between 1020 and 1029 kg/m^3. In its solid state, newly formed sea ice has a density marginally less than 1000 kg/m^{-3} and the particular hexagonal polycrystalline ice has a density of 916.7 kg m^{-3} at 0^{o}C. The temperature of maximum density and the solidification point of sea ice decrease almost linearly as the water salinity increases as demonstrated in Fig. 2.3. The sea ice critical saline point of 24.69 ‰ is achieved at a temperature of -1.32^oC which is also the temperature of maximum density. When the salinity exceeds the critical value, the freezing temperature is also higher than the temperature of maximum density. (Shokr & Sinha, 2015)

2.1.3 Properties and Mechanical Behaviour of Polycrystalline Ice

Early studies of sea ice have revealed that the mechanical properties of sea ice are commonly controlled by the sea ice substructure. In particular, the fracture surface subjected to tension tends to run parallel to the [0001] planes of the ice crystals (Anderson & Weeks, 1958). In these planes, the brine pockets and air bubbles are concentrated. In fact, the gas and brine inclusions reduce the percentage of the failure plane allowing failure to occur at lower bulk stress levels. Therefore, pure sea ice has strengths similar to that of freshwater ice. Whereas, very low strengths are

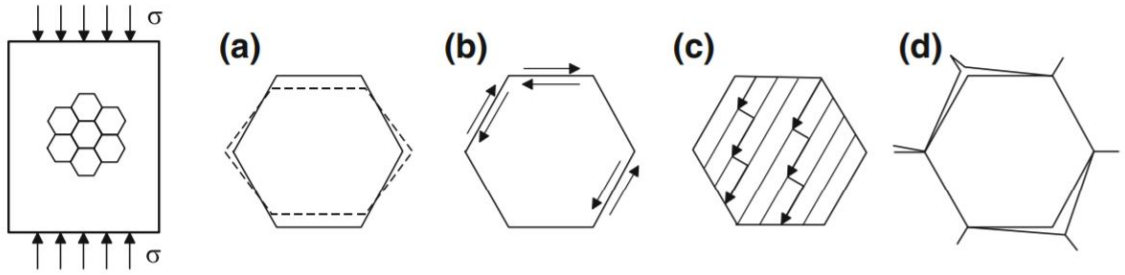

Figure 2.4: Schematic illustration of processes occurring at the grain level during loading of an ice sample: (a) purely elastic deformation; (b) delayed elastic deformation; (c) viscous deformation; (d) brittle deformation due to crack formation and propagation. (Staroszczyk, 2018)

found in sea ice with higher porosities. (W. F. Weeks & Ackley, 1986)

In nature, ice crystallites are usually found to be clustered into larger grains of random shapes and approximately of similar sizes. A grain may consist of one or several crystallites. The collection of grains of various shape, size, and orientation into larger structures, therefore, is called polycrystals. Despite the fact that a single ice crystal is hexagonally symmetric, its mechanical properties are similar to those of transversely isotropic medium. The explanation could be that the crystal c-axis is the axis of material symmetry and the crystal basal plane is the plane of isotropy. (Staroszczyk, 2018)

When polycrystalline ice is subjected to stress, individual ice grains in a polycrystal are stressed and then they deform themselves and interact with each other. The deformation mechanism depends considerably on the fashion in which the crystal basal planes are oriented to the applied stress field. Simultaneously, the crystal c-axes gradually rotate giving rise to the evolution of the preferred orientations of c-axes. Such a process is called induced anisotropy, and it is an evolution of the macroscopic properties of polycrystalline ice. (Staroszczyk, 2018)

In the next level or the grain level, grains deform in a purely elastic and reversible manner. This deformation gives rise to the bulk instantaneous elastic strain. Synchronously, an induced sliding takes place on the grain boundaries due to the shear stresses generated between grains. Since all the atomic rearrangement processes take place only at the boundaries, there is no permanent deformation inside the grains. The explanation for this mechanism is that there is some delay in the material response to changing stresses. Some elastic energy is assumed to be stored in the crystal during its deformation and is recovered when the applied compressive stress is relaxed. This process earns the grain boundaries time to slide in reverse directions. The reversible macroscopic deformation associated with this micro-mechanism is known as the delayed elastic strain. The irreversible macroscopic deformations, however, are likely to happen; they result in permanent changes in the grains. This deformation mechanism is usually referred to as creep. (Staroszczyk, 2018)

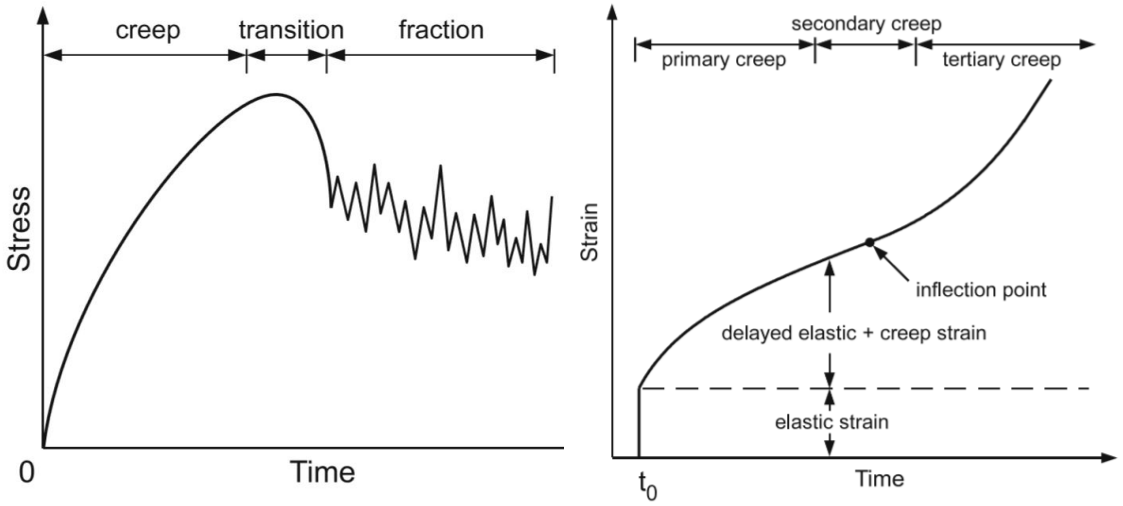

(a) (b)

Figure 2.5: (a) A typical history of stress in polycrystalline ice under sustained loading. At low stress levels, ice responds in an instantaneous elastic manner and is defined a creeping, ductile material. At high stresses and strain-rates, in turn, ice behaves as an extremely brittle material. At this level, ice may fail by brittle fracture as a result of the formation and propagation of cracks; (b) History of strain in polycrystalline ice under constant stress suddenly applied at time t_0. (Staroszczyk, 2018)

A typical deformation history during a constant-stress test on polycrystalline ice has the following scheme: elasticity, primary (or delayed elastic) creep, secondary (or viscous) creep, and tertiary creep (see Fig. 2.5b). As subjected to sudden stress, sea ice undergoes an instantaneous elastic strain which is fully recoverable. This strain is increasing approximately linearly with stress and typically of a magnitude 10^{-4} at a stress of 1 MPa. As stress keeps constant, a transient-time delayed elastic strain starts to develop, which is also recoverable upon the stress removal. In case of high stress applied, irreversible creep deformations develop and result in a permanent deformation in the material. This thesis, however, focuses only on reversible deformations including linear on polycrystalline ice. (Staroszczyk, 2018)

2.2 Kinematics

At the elementary level, strain is thought of as infinitesimal or relative deformation. However, in order to study the mechanics of materials at a microscopic level, it is necessary to view strain as a tensor field. In the present section, the kinematic approach to such a formulation of strain is reviewed. Fundamentally, kinematics is a branch of classical mechanics studying the motion of points, bodies, and systems of bodies under influence of external forces and stresses, in other words, it is a study of the geometry of motion. The kinematic study of continuum bodies focuses on quantifying strain and rate of strain in a body whose shape changes with time.

Of main concern are bodies composed of continuously distributed materials at the macroscopic level. Each of such bodies B is a smooth manifold of elements called particles and is assumed to occupy a connected open subset of a three-dimensional space that can be identified with the Euclidean point space $\mathbb{E}^3$. As the body deforms, the region occupied by the body will vary with time where the evolution of the body's behaviour is kept track. The identification of material particles with points $\boldsymbol{X} = (X_1, X_2, X_3)^T$ in the body B defines the configuration of the body at that instant. The configurations of the body B are elements of a set of one-to-one mappings of B into $\mathbb{E}^3$. The deformation of the body B is defined as a change of configuration between initial configuration B (reference configuration) and a subsequent configuration B' (deformed configuration). Such deformation is mathematically described by a function $\boldsymbol{\varphi} : B \to B'$, which maps each point $\boldsymbol{X} \in B$ to a point $\boldsymbol{x} \in B'$ (see Fig. 2.6) such that

$$\boldsymbol{x} = \boldsymbol{\varphi}(\boldsymbol{X}), \tag{2.1}$$

where $\boldsymbol{x} = (x_1, x_2, x_3)^T$ is called spatial coordinate for its location in B'. The mapping $\boldsymbol{\varphi}$ is called the deformation map relative to the reference configuration B. The distance of a material particle between its initial location $\boldsymbol{X}$ and its final location $\boldsymbol{x}$ is called displacement and is given as

$$\boldsymbol{u} = \boldsymbol{\varphi}(\boldsymbol{X}) - \boldsymbol{X} = \boldsymbol{x} - \boldsymbol{X}. \tag{2.2}$$

The mapping $\boldsymbol{u} : B \to \mathcal{V}$ is called displacement field associated with $\boldsymbol{\varphi}$. Here, $\mathcal{V}$ denotes a set of vectors associated to $\mathbb{E}^3$. The deformation of a material body is called admissible if for every point $\boldsymbol{X} \in B$, the following assumptions are met

i. The mapping $\boldsymbol{\varphi} : B \to B'$ is one-to-one, and

ii. $\det \boldsymbol{\nabla}\boldsymbol{\varphi}(\boldsymbol{X}) > 0$.

In particular, the first assumption implies that two or more distinct points in B cannot simultaneously occupy the same location in B'. The latter guarantees that the deformations preserves the orientation of a body in a sense that it cannot be continuously deformed onto its mirror image. (Gonzalez & Stuart, 2008)

By definition, any arbitrary small region Ω in B is mapped into a small region Ω' in B' by the definition map φ. The difference in shape between these two small

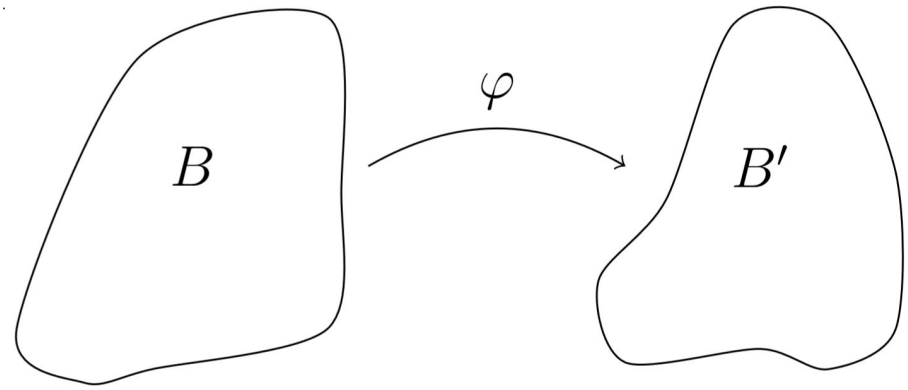

Figure 2.6: Reference and deformed configurations. The deformation map $\boldsymbol{\varphi}$ maps every point in reference configuration B to a point in deformed (current) configuration B'. The mapping $\boldsymbol{\varphi}$ is one-to-one.

regions Ω and Ω' leads to the concept of strain. The information on the local behaviour of a deformation $\boldsymbol{\varphi}$ is studied by its gradient

$$\boldsymbol{F}(\boldsymbol{X}) := \boldsymbol{\nabla}\boldsymbol{\varphi}(\boldsymbol{X}), \tag{2.3}$$

where $\boldsymbol{F}$ is called deformation gradient which provides a measure of strain. In fact, $\boldsymbol{F} : B \to \mathcal{V}^2$ is a second-order tensor field, where $\mathcal{V}^2$ denotes the set of second-order tensors. (Gonzalez & Stuart, 2008)

In the simplest case, the deformation map $\boldsymbol{\varphi}$ is assumed to be homogeneous meaning the corresponding deformation gradient field $\boldsymbol{F}$ is a constant. For such a case, $\boldsymbol{F}$ characters the amount of stretch and rotation that the body experiences when it is deformed from a configuration B onto configuration B'. For this reason, $\boldsymbol{F}$ can be decomposed into a stretch and a rotation operation about a same fixed point following the polar decomposition theorem

$$\boldsymbol{F} = \boldsymbol{R}\boldsymbol{U} = \boldsymbol{V}\boldsymbol{R}\,, \tag{2.4}$$

where $\boldsymbol{U} = \sqrt{\boldsymbol{F}^T\boldsymbol{F}}$ and $\boldsymbol{V} = \sqrt{\boldsymbol{F}\boldsymbol{F}^T}$ are symmetric, positive-definite tensors and $\boldsymbol{R}$ is a rotation tensor. Moreover, $\boldsymbol{U}$ and $\boldsymbol{V}$ are called the right and left stretch tensor, respectively. In general, $\boldsymbol{U}$ and $\boldsymbol{V}$ have same eigenvalues but different eigenvectors. (Gonzalez & Stuart, 2008)

In general, there is no assumption on the homogeneity of the deformation mapping $\boldsymbol{\varphi}$ associated with the deformation gradient $\boldsymbol{F}$. Accordingly, the measure of strain is defined as

$$\boldsymbol{C} = \boldsymbol{F}^T\boldsymbol{F} = \boldsymbol{U}^2, \tag{2.5}$$

and

$$\boldsymbol{B} = \boldsymbol{F}\boldsymbol{F}^T = \boldsymbol{V}^2, \tag{2.6}$$

where $\boldsymbol{C}, \boldsymbol{B} : B \to \mathcal{V}^2$ are respectively the right and left Cauchy-Green strain tensor fields associated with $\boldsymbol{\varphi}$. Furthermore, $\boldsymbol{C}$ and $\boldsymbol{B}$ are symmetric and possitive-definite

at every point $\boldsymbol{X} \in B$. Typically, $\boldsymbol{C}$ and $\boldsymbol{B}$ are more useful measures of strain than $\boldsymbol{F}$ since they contain information on stretch only instead of a mixture of information on both rigid body rotation and stretch contained in $\boldsymbol{F}$. (Gonzalez & Stuart, 2008)

The last quantity that is used to measure strain associated with the displacement gradient $\boldsymbol{\nabla u}$ is given

$$\boldsymbol{\epsilon}(\boldsymbol{u}) := sym(\nabla \boldsymbol{u}) = \frac{1}{2}\Big(\nabla \boldsymbol{u} + \nabla \boldsymbol{u}^T\Big), \tag{2.7}$$

where $\boldsymbol{\epsilon} : B \to \mathcal{V}^2$ is the infinitesimal strain tensor field associated with $\boldsymbol{\varphi}$ and is symmetric for every point in B. Here, the relation between $\boldsymbol{\epsilon}$ and the deformation gradient $\boldsymbol{F}$ and the Cauchy-Green tensor $\boldsymbol{C}$ is

$$\begin{aligned} \boldsymbol{\epsilon} &= sym(\boldsymbol{F} - \boldsymbol{I}) \\ &= \frac{1}{2}(\boldsymbol{C} - \boldsymbol{I}) - \frac{1}{2}\nabla \boldsymbol{u}^T \nabla \boldsymbol{u}. \end{aligned} \tag{2.8}$$

This particular strain tensor $\boldsymbol{\epsilon}$ provides a measure of strain for small deformation in the sense that for every point $\boldsymbol{x} \in B$ the rate of change of displacement in space $\frac{\partial u_i}{\partial X_j} = \mathcal{O}(\epsilon)$, where $0 \leq \epsilon \leq 1$. Essentially, for small deformation, $\boldsymbol{\epsilon}$ provides the same information as $\boldsymbol{C}$, however, $\boldsymbol{\epsilon}$ is crucially useful as it linearly depends on $\boldsymbol{u}$, whereas $\boldsymbol{C}$ is non-linear dependent on $\boldsymbol{u}$, hence $\boldsymbol{\varphi}$. (Gonzalez & Stuart, 2008)

2.3 Linear Viscoelasticity

In the late nineteenth century, the study of linear viscoelasticity in materials began several isolated contributors. The early stage of its development led to Boltzmann's first formulation of the three-dimensional theory for the isotropic viscoelasticity. Topics in linear viscoelasticity may roughly be divided into two principal categories: those concerned with the study of the intrinsic constitutive equations and those associated to the solution of boundary-value problems. The first category covers studies of alternative formulations of one-dimensional stress-strain relation and the connection between the corresponding alternative characteristics of material responses. The second category deals with integration methods associated with the fundamental boundary-value problems. (Gurtin & Sternberg, 1962)

Notwithstanding the triumphantly elegant mathematical structures of the classical theories of Linear Elasticity and Newtonian Fluid, they do not adequately describe the deformation of most real materials. Correspondingly, the theory of elasticity describes mechanical behaviour of materials that have the capacity to store mechanical energy without dissipation. In its counterpart, Newtonian viscous fluid accounts for materials which have the capacity for dissipating energy but not for storing it. Materials falling outside the scope of these two theories are those exhibit the mechanical behaviour, which combines properties both of a viscous liquid and an elastic solid, possesses a capacity to both store and dissipate mechanical energy. In particular, they store part of the deformational energy elastically as potential energy and dissipate the rest simultaneously through viscous forces. These materials are called viscoelastic materials.

The preceding classes of materials can be alternately characterized through the nature of their response to a suddenly applied loading state or stress state. To be more specific, a uniform distribution of surface tractions is suddenly applied on a specimen in such a way that the rates do not cause the excitation of a dynamic response in the specimen. Elastic material responses instantaneously when subjected to such a suddenly applied loading state and its state of deformation remains constant if the load is held constant thereafter. A Newtonian viscous fluid responds to such loading condition by a steady flow process. Nor is it surprising, viscoelastic deforms instantaneously to a suddenly applied loading followed by a steady flow process which may or may not be limited in magnitude as time advances. Such material is said to exhibit both an instantaneous elasticity effect and creep characteristics. (Christensen, 2012; Gurtin & Sternberg, 1962)

In a general setup of loading condition, the uniformly distributed tractions are applied on the specimen surface in such a way that there are two nonsimultaneously applied sudden changes superimposed upon each other. After the first application of stress, but before the second viscoelastic material response in some time-dependent manner which depends upon the magnitude of the first stress state. If there is an arbitrarily small interval of time after the sudden application of the second stress state, the material not only experiences the instantaneous response to the second change in surface tractions but also it experiences a continuing time-dependent

response due to the first applied level of stress. An elastic material, however, would respond only to the total stress level at every instant of time. Thus, viscoelastic materials belong to a more general class of materials who possesses a characteristic which can be descriptively referred to as a memory effect. The use of the term "memory" corresponds to materials whose response is determined not only by the current state of stress but also by the entire stress state history of the past. A similar situation exists in deformation of materials as the current stress state depends upon the entire prior history of deformation. This characteristic is completely different from the elastic materials, which would respond only to the total stress level at every instant in time. (Christensen, 2012)

Generally, all real materials can have a capacity for memory and can be mathematically characterised. The current section is devoted to study the formulation of the isothermal linear theory of homogeneous and isotropic viscoelastic mediums from a continuum mechanics point of view. In order to fully appreciate the many facets of this theory, a brief review of linear elasticity is presented in Fig. 2.3.1. The theory of linear viscoelasticity is studied in Fig. 2.3.2. Different representations are introduced including integral and differential representations.

2.3.1 Elastic Stress-Strain Constitutive Relations

The theory of linear elasticity is a simplification of the general nonlinear theory of elasticity that studies the deformation mechanisms of solid objects under different prescribed loading conditions. Linear elasticity is a branch of continuum mechanics where materials are modelled as continua. The theory is established under the fundamental assumptions of linear elasticity that strains are infinitesimal or deformations are "small" and the relationship of components of stress-strain is linear. A "small" or elastic deformation refers to a change of the shape of a solid object as a reaction to applied stress. This type of deformation is only temporary as the undeformed shape of the body is restored with the removal of stress. Depending on the loading mechanisms, there are corresponding measures to the inherent elastic properties of a material called elastic moduli such as Young's modulus, shear modulus, and bulk modulus.

The elastic relation between stress and strain (or the relative deformation) of materials is described by a stress-strain curve. Generally, the curve is nonlinear and is independent of time. Nevertheless, for sufficiently small deformation, the curve can be linearised by exploiting a Taylor series, wherein, higher-order terms are neglected. If the material is isotropic or exhibits a uniform behaviour in all orientations, its linear elastic stress-strain relation, thus, obeys the Hooke's law. Remaining in the elastic range, if materials undergo relatively large deformations, nonlinear elasticity is generally required to describe their constitutive relation. The theory of elasticity is no longer applied when materials deform irreversibly and do not recover to their original shape after stresses. (Gonzalez & Stuart, 2008)

Upon small strains or small deformations, the infinitesimal strain tensor described in Eq. (2.7) is utilised to measure strains while stresses are measured by the Cauchy

stress tensor. The corresponding (isotropic) material behaviour with respect to those measures is linear elasticity or generalised Hooke's law. If the stress at a point in an elastic solid depends only on a measure of present strain at that point. Particularly, it is independent of the past history and rate of strain

$$\boldsymbol{\sigma} = \boldsymbol{C}\boldsymbol{\epsilon} = 2\mu\boldsymbol{\epsilon} + \lambda \mathrm{tr}(\boldsymbol{\epsilon})\boldsymbol{I}, \tag{2.9}$$

where $\boldsymbol{C}$ is the forth-order elastic moduli tensor (note that this tensor differs than the right Cauchy-Green strain tensor form the previous section), μ and λ are Lamé constants, and $\boldsymbol{I}$ is second-order identity tensor. The trace of the infinitesimal strain tensor is defined as

$$tr(\boldsymbol{\epsilon}) = \sum_{i=1}^{3} \varepsilon_{ii}.$$

The relationship described in Eq. (2.9) for an elastic medium is an intrinsic property of the material. In particular, it depends only on material properties and the reference configuration.

2.3.2 Linear Viscoelastic Stress-Strain Constitutive Relations

The formulation of the isothermal viscoelastic stress-strain constitutive relations is discussed in the following section. The theory is developed based on assumptions that the materials are homogeneous and isotropic. Another important restriction is that the thermodynamic variables, temperature, and pressure are constant. The derivation of linear viscoelastic stress-strain relation is based upon the memory hypothesis and smoothness assumptions (Christensen, 2012). To be more specific, the memory effect is restricted to a particular type called fading memory, which was first discussed by Volterra, 2005. The linear viscoelastic hypothesis asserts that the current value of the stress tensor is assumed to depend linearly on the complete past history of the components of the strain tensor. In other words, the stress history at each material point of the body is completely determined by the strain history in the same location (Gurtin & Sternberg, 1962). Furthermore, the stress-strain constitutive equations are required to satisfy two fundamental hypotheses: (i.) Invariance for time translation, which means that "a time shift in the input results in an equal shift in the output"; (ii.) Causality, which means that " the output for any instant t_1 depends on the values of the input only for $t \leq t_1$" (Mainardi, 2010, p. 23). At sufficiently small strains, the behaviour of a viscoelastic body is well described by a linear constitutive relation between stress and strain of the classic form

$$\boldsymbol{\sigma} = \boldsymbol{\psi}\boldsymbol{\epsilon}, \tag{2.10}$$

where $\boldsymbol{\psi}$ is a linear tensor-valued functional which transforms each strain history $\boldsymbol{\epsilon}(t)$ into a corresponding stress history $\boldsymbol{\sigma}(t)$, $t \in \mathbb{R}$. In other words, $\boldsymbol{\psi}$ is a linear transformation on the space of symmetric tensors into itself. The functional $\boldsymbol{\psi}$ has a parametric dependence upon the current value of infinitesimal strain $\boldsymbol{\epsilon}$ at time t, corresponding to the instantaneous elasticity effect. Furthermore, linear viscoelasticity theory requires the strain history $\boldsymbol{\epsilon}$ to be continuous in its whole real

domain, and besides, the body is assumed to be in its undeformed state for all time t in $(-\infty, 0)$. The strain histories satisfying the aforementioned restrictions are called admissible strains. The analogous requirement applies to admissible stress histories. In addition, the transformation $\boldsymbol{\psi}$ is required to be linear. Thus, for arbitrary admissible strain histories $\boldsymbol{\epsilon}_1, \boldsymbol{\epsilon}_2$ satisfying $\boldsymbol{\sigma}_1 = \boldsymbol{\psi}\boldsymbol{\epsilon}_1$, $\boldsymbol{\sigma}_2 = \boldsymbol{\psi}\boldsymbol{\epsilon}_2$, the functional $\boldsymbol{\psi}$ must be (i) linear, (ii) translation invariance, (iii) nonretroactive, and (iv) continuous. Postulate (i) exhibits the principle of linear superposition, while (ii) guarantees the constitution of the materials is invariable with time. Nonretroactivity (iii) shows that the material is under stress-free state $\boldsymbol{\sigma}(t) = 0$ on $(-\infty, t]$ if it subjects to no strain histories before the time t of reference. This postulate is also referred to "principle of causality", if two strain histories coincide up to time t, so do the associated stress histories. Thus, the stresses $\boldsymbol{\sigma}(t)$ at each instant t depends only on the strains at time t and at all previous times. In other words, $\boldsymbol{\sigma}(t)$ is a functional of $\boldsymbol{\epsilon}(\tau)$, where $\tau \in (-\infty, t]$. The last postulate (iv.) demands that any two sufficiently close strain histories up to time t result in corresponding stress values at t which are arbitrarily close to each other. (Mainardi, 2010)

Generally, all field variables are not only functions of time but also are functions of position. However, based on the material homogeneity and isotropy assumptions, the spatial dependence of stress and strain can be suppressed. In other words, stress and strain are distributed uniformly across the body. Together with the above restrictions along with the Riesz's representation theorem (which lays out of the scope of this thesis), functional in Eq. (2.10) can be expressed by convolution integrals with difference kernels, linear differential equations with constant coefficients, frequency representation, and spectral representation.

2.3.3 Integral Representation

In this section, we are looking for an explicit linear functional which maps corresponding stress to strain at any time of interest. For a sake of simplicity, only local constitution equation,the stress at a certain position depends only on the strain at that position, is discussed. In particular, by the representation of linear hereditary laws theorem if the condition that the admissible strain history $\boldsymbol{\epsilon}$ is continuous on the time domain and the functional $\boldsymbol{\psi}$ is linear, there exists a real tensor valued function $\boldsymbol{G}$ such that

$$\boldsymbol{\sigma}(t) = \int_{-\infty}^{t} \boldsymbol{\epsilon}(t-s)\, \mathrm{d}\boldsymbol{G}(s), \qquad \text{for all } t \in \mathbb{R}, \tag{2.11}$$

where $\boldsymbol{G}$, a non-negative fourth-order tensor defined on a whole real domain, is termed relaxation function accounting for the mechanical property of the material. The above equation expresses that the value of stress at any time t of interest is determined by the corresponding strain value at t and all its past values. Here the time t is a fix point and s is integrating variable. This form of constitutive relation satisfies the time translation invariance as it is independent of any shifts in the time scales. The tensor valued function $\boldsymbol{G}$ has properties that $\boldsymbol{G}(t) = 0$ for all $t \in (-\infty, 0)$

and is integrable in the sense that

$$\int_{\mathbb{R}} \boldsymbol{G}(t)\,\mathrm{d}t < \infty. \tag{2.12}$$

In fact, Eq. (2.11) is a Riemann-Stieltjes integral, in other words, the stress $\boldsymbol{\sigma}$ defined on the whole real domain is the Stieltjes convolution of $\boldsymbol{\epsilon}$ and $\boldsymbol{G}$ over (∞, t). Thus, one can interpret the tensor functional $\boldsymbol{G}$ as a measure. The condition for which the integral in Eq. (2.11) exists is that each component of $\boldsymbol{G}$ is required to be of bounded variation in every closed subinterval of $\mathbb{R}$ (see Appendix A). In addition, $\boldsymbol{G}$ need to be continuous on the right in $\mathbb{R}$ which is to say $\boldsymbol{G}(t) = \boldsymbol{G}(t+)$. The symmetry of stress and strain tensors indicates that $\boldsymbol{G}$ is also symmetric in the sense that

$$G_{ijkl}(t) = G_{ijlk}(t) = G_{jikl}(t), \qquad \text{for all } t \in \mathbb{R}. \tag{2.13}$$

If the strain histories $\boldsymbol{\epsilon}(t) = 0$ for $t \in (-\infty, 0)$ and $\boldsymbol{G}$ is continuously differential over an interval $[0, \infty)$, then by the properties of the Stieltjes convolution the constitutive equation between stress and strain (2.11) can be written as a standard Riemann-Stieltjes integral form (Gurtin & Sternberg, 1962)

$$\boldsymbol{\sigma}(t) = \boldsymbol{G}(0)\,\boldsymbol{\epsilon}(t) + \int_0^t \boldsymbol{\epsilon}(t-s)\frac{\mathrm{d}\boldsymbol{G}(s)}{\mathrm{d}s}\,\mathrm{d}s, \qquad t \in [0, \infty), \tag{2.14}$$

in components,

$$\sigma_{ij}(t) = G_{ijkl}(0)\epsilon_{kl}(t) + \int_0^t \epsilon_{kl}(t-s)\frac{\mathrm{d}G_{ijkl}(s)}{\mathrm{d}s}\,\mathrm{d}s, \qquad t \in [0, \infty). \tag{2.15}$$

where $\boldsymbol{G}(0)$ is an instantaneous elastic modulus and takes account for the response to instantaneous changes in strain at time $t = 0$. Eq. (2.14) can be thought as being obtain from Eq. (2.11) through the integration of the Dirac delta function involved in the differential of the integrating functions $\boldsymbol{G}(t)$ at $t = 0$. The integral over the strain (or stress) history is referred to as hereditary integrals and materials whose constitutive relation contains such integrals are described as having memory. Another form of stress strain constitutive equation can be obtained from Eq. (2.14) by change of variable from s to $u = t - s$ and integration by parts

$$\boldsymbol{\sigma}(t) = \int_0^t \boldsymbol{G}(t-u)\frac{\mathrm{d}\boldsymbol{\epsilon}(u)}{\mathrm{d}u}\,\mathrm{d}u, \qquad t \in [0, \infty), \tag{2.16}$$

This form of constitutive equation has an advantage that when $\boldsymbol{\epsilon}$ is constant over certain time intervals, the hereditary integral vanishes in Eq. (2.16), then the constitutive relation reduces to Hook's law where the modulus is time dependent. Up to this point, the strain history has been required to be continuous with respect to time in order to satisfy the necessary condition stated in Riesz representation theorem. However, if the strain histories $\boldsymbol{\epsilon}$ experiences a discontinuity or a jump at the origin and differentiable over interval $[0, t)$, the hereditary integral form still holds true with the generalised form of Eq. (2.16)

$$\boldsymbol{\sigma}(t) = \boldsymbol{\epsilon}(0)\boldsymbol{G}(t) + \int_0^t \boldsymbol{G}(t-u)\frac{\mathrm{d}\boldsymbol{\epsilon}(u)}{\mathrm{d}u}\,\mathrm{d}u, \qquad t \in [0, \infty), \tag{2.17}$$

It is straightforward that Eq. (2.17) follows directly from Eq. (2.16) through the integration of the resulting delta function. However, one can avoid integrating over a delta function by approximating the discontinuous strain history by a sequence of continuous functions, thus the Riesz representation theorem holds. (Christensen, 2012; Gurtin & Sternberg, 1962; Mainardi, 2010)

An alternative form of the stress-strain relation is obtained by reversing the roles of stress and strain in the preceding derivation in such a way that the current strain is determined by the current value and past history of stress

$$\boldsymbol{\epsilon}(t) = \int_{-\infty}^{t} \boldsymbol{\sigma}(t-s)\,\mathrm{d}\boldsymbol{J}(s) \qquad t \in (-\infty, \infty). \tag{2.18}$$

in components

$$\epsilon_{ij}(t) = \int_{0}^{t} \sigma_{kl}(t-s)\mathrm{d}J_{ijkl}(s) \qquad \text{for all } t \in (-\infty, \infty). \tag{2.19}$$

The integrable function $\boldsymbol{J}$ is named retardation function or creep compliance function and is a fourth-order tensor defined on real domain. The tensor functional $\boldsymbol{J}$ is continuous on the right in $(-\infty, \infty)$ and vanishes for all $t \in (-\infty, 0)$. In addition, $\boldsymbol{J}$ is symmetric in the sense that

$$J_{ijkl}(t) = J_{ijlk}(t) = J_{jikl}(t), \qquad \text{for every } t \in (-\infty, \infty). \tag{2.20}$$

If stress and strain histories are admissible, Eq. (2.18) can be written as

$$\boldsymbol{\epsilon}(t) = \boldsymbol{J}(0^+)\boldsymbol{\sigma}(t) + \int_{0}^{t} \boldsymbol{\sigma}(t-s)\frac{\mathrm{d}\boldsymbol{J}(s)}{\mathrm{d}s}\,\mathrm{d}s, \qquad t \in [0, \infty). \tag{2.21}$$

A simple physical interpretation for the stress strain relation in Eq. (2.14) is that the current stress is determined by the superposition of the responses to the complete spectrum of increments of strain. This principle is called Boltzmann's superposition principle. Eq. (2.21) is interpreted similarly by interchanging the roles of stress and strain. The characteristic material functions $G(t)$ and $J(t)$ play as weighting functions. From experimental evidence, both material functions $\boldsymbol{G}$ and $\boldsymbol{J}$ are non-negative (Mainardi, 2010, p.25). Before further discussing the properties of the material functions, for a sake of simplicity and without loss of generality, we can restrict our attention to materials undergoing simple deformation in one direction, reducing Eq. (2.11) to a scalar equation. Under a restricted domain $[0, \infty)$, G behaves as a non-increasing function, while J is non-decreasing function. Assume G and J are differentiable monotonic functions of time, we get (Mainardi & Spada, 2011, 2012)

$$\begin{aligned} &\frac{\mathrm{d}G}{\mathrm{d}t} < 0 \implies +\infty \geq G(0^+) > G(t) > G(+\infty) \geq 0, \quad \text{for } t \in [0, \infty), \\ &\frac{\mathrm{d}J}{\mathrm{d}t} > 0 \implies +0 \leq J(0^+) < J(t) < J(+\infty) \leq +\infty, \quad \text{for } t \in [0, \infty), \end{aligned} \tag{2.22}$$

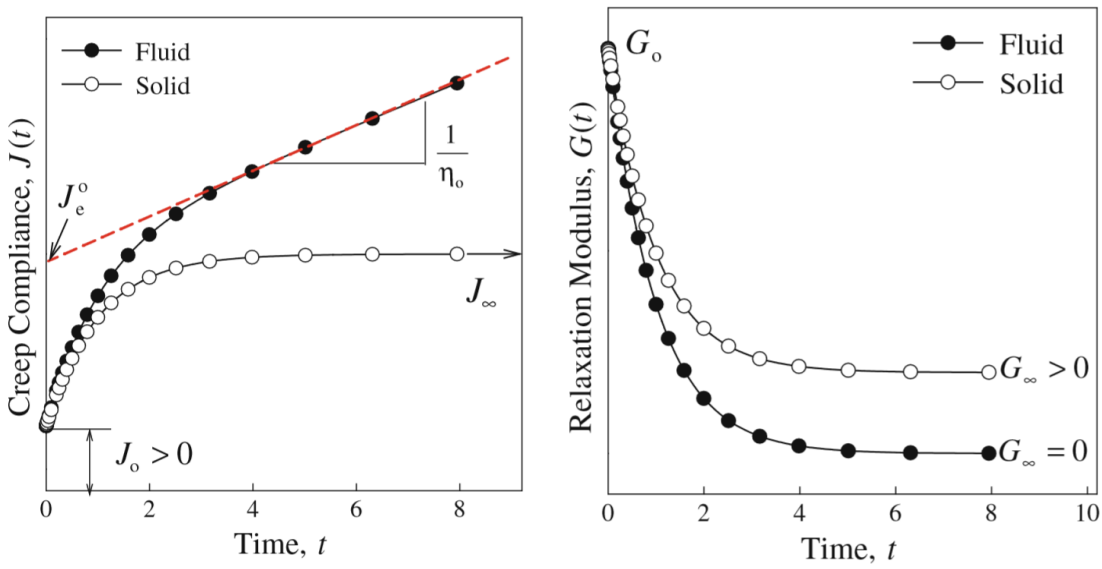

Figure 2.7: Schematic illustration of viscoelastic fluid and solid . (a) Compliance functions J of fluid-like viscoelastic materials diverges at large time t while compliance function of the solid-like viscoelastic material converges to a non-negative constant at the limit; (b) Relaxation Modulus G vanishes for viscolestic fluid and converges to a non-negative constant when time tends to infinity. (Cheneler, 2016)

where

$$\begin{cases} G(0^+) = \lim_{t\to 0^+} G(t) =: G_g & \text{elastic (glass) modulus,} \\ G(+\infty) = \lim_{t\to\infty} G(t) =: G_e & \text{equilibrium modulus,} \end{cases} \tag{2.23}$$

and

$$\begin{cases} J(0^+) = \lim_{t\to 0^+} J(t) =: J_g & \text{elastic (glass) compliance,} \\ J(+\infty) = \lim_{t\to\infty} J(t) =: J_e & \text{equilibrium compliance.} \end{cases} \tag{2.24}$$

Upon an observation of creep compliance, the equilibrium compliance $J(\infty)$ is often but not always finite. Intuitively, after the instantaneous finite jump at the time of a sudden stress, strain increases either to some final value or indefinitely. This suggests that the creep compliance may continue definitely for some certain materials. A rough quantitative pictures of the possible shapes of creep compliance and relaxation modulus are summarised in Fig. 2.7. Viscoelastic solid may exhibit relaxation function and compliance function that converge to non-negative constant while being observed in viscoelastic fluid, compliance function diverges and relaxation function vanishes in the limit when time tends to infinity. In general, it is not so easy to decide experimentally whether a viscoelastic material is a solid or fluid-like.

Physically, when compliance function converges to a non-negative constant suggestes that its time derivative tends to zero at large time t in viscoelastic solid causing strain in Eq. (2.11) to vanish. This justifies the behaviour that materials recover

completely from applied stress with time delays caused by internal friction losses. On the other hand, if the rate of change in compliance function is a finite number, then performance deformation is assumed to occur as a result of the application and removal of stress.

The simple approach to approximate the compliance function is with power law, which arisen as a application of the fractional calculus since 1920s. In particular, the relaxation function is said to obey the power law if it admits a form

$$G(t) = Ct^{-\alpha}, \tag{2.25}$$

where α is a non-negative real numbers at most 1, $0 < \alpha < 1$. This form of relaxation has an advantage of simplicity due to the numbers of unknown parameters. However, it is not efficient in describing the material response at short and long times as it give infinite at $t = 0$ and zero at $t = \infty$. Accordingly, the material shows zero instantaneous response to a suddenly applied stress and stress relaxes to zero at large time. (Hiel, Cardon, & Brinson, 1984)

Analogously, compliance function can be approximated by the power law form

$$J(t) = J_0 + Ct^{\alpha}, \quad C > 0, \quad \alpha \in (0, 1), \tag{2.26}$$

where J_0 is a non-negative constant accounting for an instantaneous elasticity of material under sudden stress at time $t = 0$, C is a non-negative constant, and α is the power law exponent. The parameter α is shown by Hiel et al., (1984) that it is most sensitive to experimental error. The value of the exponent α may vary with the length of the creep test used to collect data. However, it becomes stable after relatively large creep times.

2.3.4 Differential Representation

By no means that the integral form of the stress strain constitutive is the only possible form. In fact, another representation that satisfies the stress-strain constitutive relation (2.10) is a linear differential equation with constant coefficients. This representation is worth considering since it admits the familiar interpretation in terms of finite networks of springs and dash-pot models. Without loss in generality, one-dimensional stress-strain relation will be discussed in this section.

Assume that the pair of admissible stress-strain histories σ, ϵ is defined, continuous, and N times continuously differentiable on $[0, \infty)$, where N is an integer and at least 1. The functions σ, ϵ and their corresponding N continuously differentiable functions may have finite jump discontinuities at the origin. Then the aforementioned pair of stress and strain satisfies the following differential equation (Gurtin & Sternberg, 1962)

$$\sum_{n=0}^{N} p_n \frac{\mathrm{d}^n \sigma(t)}{\mathrm{d}t^n} = \sum_{n=0}^{N} q_n \frac{\mathrm{d}^n \epsilon(t)}{\mathrm{d}t^n}, \qquad \text{for all } t \in (0, \infty), \tag{2.27}$$

where p_n, q_n are constant coefficients and either $p_N \neq 0$ or $q_N \neq 0$. This is a linear differential equation with constant coeffients contain derivatives up to order N.

Together with the appropriate initial conditions Eq. (2.27) adequately describes the time dependent viscoelastic behavior of an isotropic material subjected to an infinitesimally small deformation. Compactly, the differential equation (2.27) can be written as

$$P(D)\sigma(t) = Q(D)\epsilon(t), \qquad \text{for all } t \in (0,\infty), \tag{2.28}$$

where

$$P(D)\Big\{.\Big\} = \sum_{n=0}^{N} p_n \frac{\mathrm{d}^n}{\mathrm{d}t^n}\Big\{.\Big\} \qquad \text{and} \qquad Q(D)\Big\{.\Big\} = \sum_{n=0}^{N} q_n \frac{\mathrm{d}^n}{\mathrm{d}t^n}\Big\{.\Big\}$$

are linear differential operators. Furthermore, σ and ϵ also meet the initial condition (Gurtin & Sternberg, 1962)

$$\sum_{n=k}^{N} p_n \frac{\mathrm{d}^{n-k}}{\mathrm{d}t^{n-k}}\sigma(t)\Big|_{t=0} = \sum_{n=k}^{N} q_n \frac{\mathrm{d}^{n-k}}{\mathrm{d}t^{n-k}}\epsilon(t)\Big|_{t=0}, \qquad k = 1,2,\ldots,N. \tag{2.29}$$

The relationship between differential form and integral form of stress strain constitutive relation (2.10) is that if the relaxation function G associated with aforementioned σ, ϵ is defined, continuous, and N times continuously differentiable on $[0,\infty)$, then

$$P(D)G(t) = q_0, \qquad t \in (0,\infty) \tag{2.30}$$

and

$$q_r = \sum_{n=r}^{N} p_n \frac{\mathrm{d}^{n-r}}{\mathrm{d}t^{n-r}}G(t)\Big|_{t=0}, \qquad r = 1,2,\ldots,N. \tag{2.31}$$

In order words, G is the solution of the initial-value problem governed by Eq. (2.14) subjected to the following initial conditions

$$\begin{aligned}
&\text{if } N = 1, \qquad G_0 = \frac{q_1}{p_1}.\\
&\text{if } N > 1, \qquad G_0 = \frac{q_N}{p_N}, \text{ and}\\
&\qquad \frac{\mathrm{d}^r}{\mathrm{d}t^r}G\Big|_{t=0} = \frac{1}{p_N}\Big[q_{N-r} - \sum_{k=0}^{r-1} p_{N-r+k}\frac{\mathrm{d}^k}{\mathrm{d}t^k}G\Big|_{t=0}\Big], \qquad (r = 1,2,\ldots,N-1),
\end{aligned} \tag{2.32}$$

which imply

$$\frac{\mathrm{d}^k}{\mathrm{d}t^k}\sigma(t)\Big|_{t=0} = \sum_{r=0}^{k} \frac{\mathrm{d}^{k-r}}{\mathrm{d}t^{k-r}}G(t)\Big|_{t=0}\frac{\mathrm{d}^r}{\mathrm{d}t^r}\epsilon\Big|_{t=0}, \qquad (k = 0,1,2,\ldots,N-1). \tag{2.33}$$

The pair of linear differential operators $[P(D), Q(D)]$ is said to be of order N if either $p_N \neq 0$ or $q_N \neq 0$ or equivalently, at least one of the two polynomials P and Q is of degree N. (Gurtin & Sternberg, 1962)

Laplace transformation can be applied to the Eq. (2.27) to get

$$P(\xi)\bar{\sigma}(\xi) - \frac{1}{\xi}\sum_{k=1}^{N} p_k \sum_{r=1}^{k} \xi^r \frac{\mathrm{d}^{k-r}}{\mathrm{d}t^{k-r}}\sigma(t)\Big|_{t=0} = Q(\xi)\bar{\epsilon}(\xi) - \frac{1}{\xi}\sum_{k=1}^{N} q_k \sum_{r=1}^{k} \xi^r \frac{\mathrm{d}^{k-r}}{\mathrm{d}t^{k-r}}\epsilon(t)\Big|_{t=0} \tag{2.34}$$

where $P(\xi)$ and $Q(\xi)$ are polynomials in the complex number ξ. By the property described in Eq. (2.29), we obtain a stress strain relationship in the complex plane

$$P(\xi)\bar{\sigma}(\xi) = Q(\xi)\bar{\epsilon}(\xi). \tag{2.35}$$

Comparing this with the Laplace transform of one-dimensional integral form in (2.11), $\bar{\sigma}(\xi) = \xi\bar{G}(\xi)\bar{\epsilon}(\xi)$, we archive

$$\xi P(\xi)\bar{G}(\xi) = Q(\xi) \qquad \text{or} \qquad \bar{G}(\xi) = \frac{Q(\xi)}{\xi P(\xi)}\ . \tag{2.36}$$

Analogously, we get

$$\bar{J}(\xi) = \frac{P(\xi)}{\xi Q(\xi)}, \tag{2.37}$$

where $\bar{G}$ and $\bar{J}$ are Laplace transform of relaxation and retardation (creep compliance) functions.

To illustrate, we consider the case when $N = 1$ and the strain is given by a form

$$\epsilon(t) = \epsilon_0\, h(t), \tag{2.38}$$

where ϵ_0 is a given amplitude and $h(t)$ is unit step function or Heavyside function defined as

$$h(t) = \begin{cases} 1, & t > 0 \\ 0, & t \leq 0 \end{cases}$$

The relation (2.11) immediately gives

$$\sigma(t) = G(t)\epsilon_0, \tag{2.39}$$

which indicates that the resulting stress relates directly to the relaxation function. The relaxation function is strictly non-increasing, moreover, it typically adopts a form of decaying function with respect to time. In order to be consistent with the fading hypothesis, the slope of $\mathrm{d}G(t)/\mathrm{d}(t)$ is expected to decay with time. A candidate of such a function is single decaying exponential:

$$G(t) = G(0)e^{-t/\lambda}h(t), \tag{2.40}$$

where G_0 is the relaxation amplitude and λ is a positive time constant that determines the rate of decay and typically called retardation time. By applying Laplace transformation to Eq. (2.40), we get

$$\frac{G_0}{s + (1/\lambda)} = \frac{\sum_{k=0}^{N} q_k(s)^k}{\sum_{k=0}^{N} p_k(s)^{k+1}}. \tag{2.41}$$

As $N = 1$, we find

$$p_0 = \frac{1}{\lambda}, \quad p_1 = 1, \quad q_0 = 0, \quad \text{and } q_1 = G_0.$$

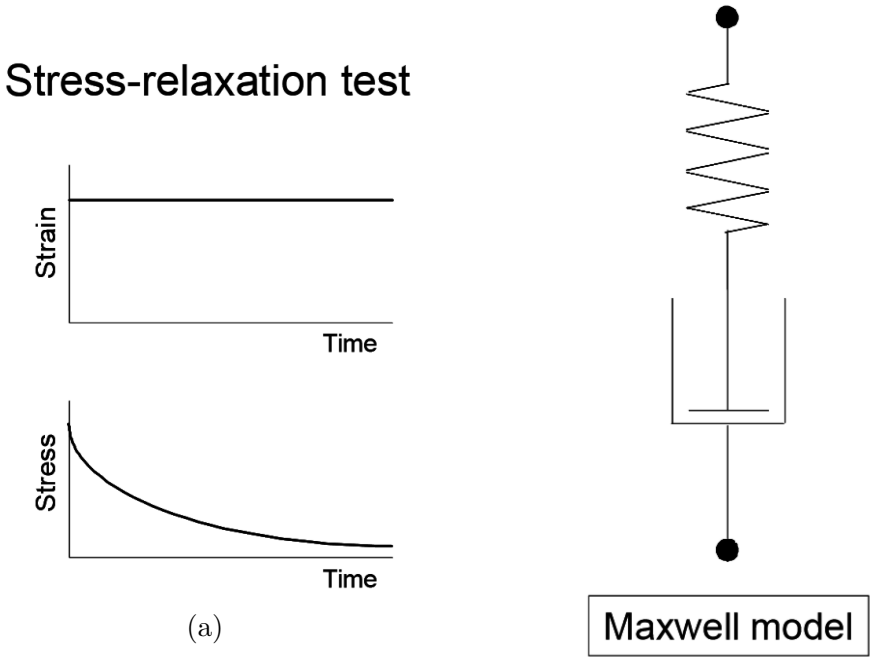

(a) (b)

Figure 2.8: Maxwell single element model.(a) Strain input as a constant function, strain rate $\dot{\epsilon} = 0$ and material stress response. (b) Single Maxwell spring-dashpot element model. (Murata, 2012)

Consequently, the corresponding differential operator stress strain relation is

$$\frac{1}{\lambda}\sigma(t) + \frac{\mathrm{d}\sigma(t)}{\mathrm{d}t} = G_0 \frac{\mathrm{d}\epsilon(t)}{\mathrm{d}t} \tag{2.42}$$

Let us define $\eta := G_0\,\lambda$ and $G_0 := E$. Physically, η is the material coefficient of viscosity and E is the elastic Young modulus. Eq. (2.42) ends up to be the Maxwell model involving a spring and a dashpot (see Fig. 2.8)

$$\frac{\sigma(t)}{\eta} + \frac{1}{E}\frac{\mathrm{d}\sigma(t)}{\mathrm{d}t} = \frac{\mathrm{d}\epsilon(t)}{\mathrm{d}t} \qquad \text{or} \qquad \frac{1}{\eta}\sigma + \frac{1}{E}\dot{\sigma} = \dot{\epsilon}. \tag{2.43}$$

Analogously, if the stress is given as a state of a simple shear which can be specified in terms of a unit step function:

$$\sigma(t) = \sigma_0 h(t), \tag{2.44}$$

where σ_0 is the amplitude. The creep compliance integral (2.18) gives

$$\epsilon(t) = J(t)\sigma_0. \tag{2.45}$$

Thus, by a single creep test the creep function is given directly by the strain response. By definition, creep compliance function is non-decreasing function but with a

decreasing slope. One of a simplest creep function is

$$J(t) = J_0(1 - e^{-t/\tau})h(t), \tag{2.46}$$

where J_0 is the retardation amplitude and τ is relaxation time a positive time constant which determines the rate of decay of the first derivative of $J(t)$. By Laplace transformation of Eq. (2.46), we get

$$\frac{1 + \tau s}{J_0} = \frac{\sum_{k=0}^{N} q_k(s)^k}{\sum_{k=0}^{N} p_k(s)^k}, \tag{2.47}$$

and with $N = 1$, the coefficients are

$$p_0 = J_0, \quad p_1 = 0, \quad q_0 = 1, \quad \text{and } q_1 = \tau.$$

Hence, the differential operator stress strain relation which corresponds to simple stress state (2.44) is

$$J_0\sigma(t) = \epsilon(t) + \tau\frac{\mathrm{d}\epsilon(t)}{\mathrm{d}t}. \tag{2.48}$$

In particular, the equation (2.48) is the well-known Kelvin–Voigt model, where the spring and dashpot are connected in parallel as shown in Fig. 2.9. The Kelvin–Voigt model has a connection to that of Maxwell seen from

$$J_0 = \frac{1}{G_0}, \quad \lambda = \frac{E}{\eta} \quad \text{and} \quad \tau = \frac{\eta}{E} \tag{2.49}$$

Thus, the Eq. (2.44) can be written as

$$E\epsilon(t) + \eta\frac{\mathrm{d}\epsilon}{\mathrm{d}t} = \sigma(t) \qquad \text{or} \qquad E\epsilon + \eta\dot{\epsilon} = \sigma. \tag{2.50}$$

2.3.5 Frequency Representation

When viscoelastic bodies are subjected to steady-state oscillatory conditions or harmonic excitations, the viscoelastic representation is expected to be formulated in term of frequency, instead of time. The concept of harmonic excitation in viscoelasticity arises due to simplicity and accuracy in experiment performance. The corresponding responses are preferred as the dynamic functions.

Under a harmonic strain excitation, the strain histories are exerted a harmonic function of time of either of the two equivalent forms

$$\epsilon(t) = \epsilon_0 \sin\omega t \qquad \text{or} \qquad \epsilon(t) = \epsilon_0 \cos\omega t\ , \tag{2.51}$$

where ϵ_0 is the strain amplitude and ω is the angular frequency of oscillation. The two forms in Eq. (2.51) are shifted $\pi/2$ radians with respect to each other. Since the choice of the harmonic representation is arbitrary, it is also an option to utilise both forms of the excitation simultaneously by means of the complex form

$$\epsilon(t) = \epsilon_0(\cos\omega t + i\sin\omega t) = \epsilon_0\, e^{i\omega t}\ , \tag{2.52}$$

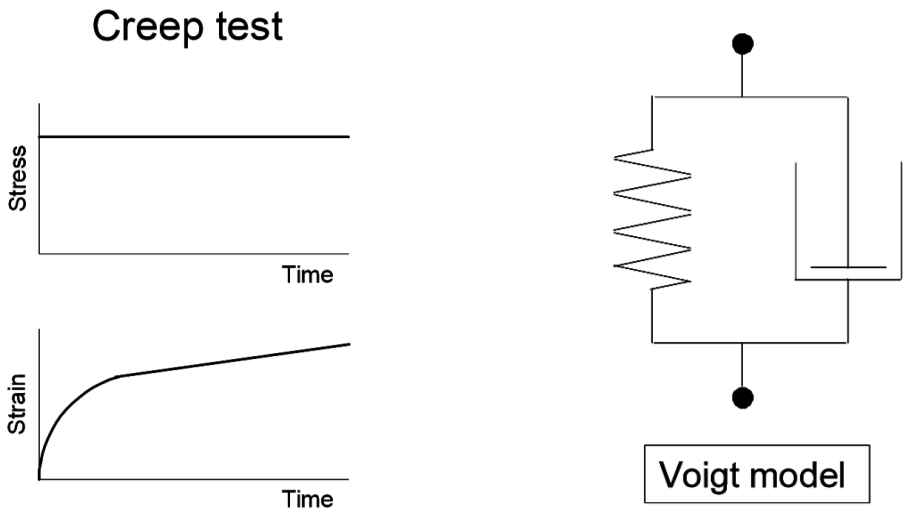

(a) (b)

Figure 2.9: Voigt single element model.(a) Stress input as a constant function, stress rate $\dot{\sigma} = 0$ and strain response. (b) Single Voigt spring-dashpot element model. (Murata, 2012)

where now ϵ is called the generalised harmonic strain and $i = \sqrt{-1}$, imaginary axis of the complex variable. An analogous technique is employed to define a generalised harmonic stress excitation with the stress amplitude σ_0. The Laplace transformation of Eq. (2.52) is

$$\mathcal{L}(\epsilon) := \bar{\epsilon}(\xi) = \frac{\epsilon_0}{\xi - i\omega} \,. \tag{2.53}$$

Consequently, the constitutive equation in the complex time axis is

$$\bar{\sigma}(\xi) = \frac{\epsilon_0 \xi \bar{G}(\xi)}{\xi - i\omega} \,. \tag{2.54}$$

Retransforming the above equation into the real time axis yields the total stress response

$$\sigma(t) = \epsilon_0 \, \mathcal{L}^{-1}\left(\frac{\xi \bar{G}(\xi)}{\xi - i\omega}\right) . \tag{2.55}$$

However, this expression of stress response does not immediately elicit a steady-state response from the harmonic steady-state excitation. To see that, the response is decomposed into two distinct parts: steady-state response and transient response. By rewriting Eq. (2.54) using the definition of $\bar{G}(\xi)$ in Eq. (2.36) and decomposing into partial fractions, we obtain (Tschoegl, 2012)

$$\frac{\bar{\sigma}(\xi)}{\epsilon_0} = \frac{Q(\xi)}{(\xi - i\omega)P(\xi)} = \frac{A}{\xi - i\omega} + \frac{B(\xi)}{P(\xi)} \,, \tag{2.56}$$

where

$$A\,P(\xi) + (\xi - i\omega)B(\xi) = Q(\xi) \,, \tag{2.57}$$

where $B(\xi)$ is a function of ξ but A is not since $(\xi - i\omega)$ is linear in ξ. In general, $B(\xi)$ is a polynomial in ξ and of degree one less than that of $P(\xi)$. The first partial fraction $A/(\xi - i\omega)$ represents the steady-state response corresponding to the driving transform pole. The second partial fraction $B(\xi)/P(\xi)$ accounts for the transient response corresponding to the rise of the poles of the relaxance $\bar{G}(\xi)$, that is, the zeros of the denominator $P(\xi)$. Rearranging Eq. (2.57) gives (Tschoegl, 2012)

$$A = \xi \bar{G}(\xi) - \frac{(\xi - i\omega)B(\xi)}{P(\xi)} \ . \tag{2.58}$$

In the steady-state response, the transform variable ξ is set to be equal to $i\omega$, in which the transient term vanishes, giving

$$A = \left[\xi \bar{G}(\xi)\right]_{\xi = i\omega} = i\omega \bar{G}(i\omega) \ . \tag{2.59}$$

Therefore, for the steady-state of (2.56) we find

$$\frac{\bar{\sigma}_{ss}(\xi)}{\epsilon_0} = \frac{i\omega \bar{G}(i\omega)}{\xi - i\omega} \ . \tag{2.60}$$

After a transformation to the real time axis, the generalised harmonic stress response reads

$$\sigma_{ss}(t) = i\omega \bar{G}(i\omega)\epsilon_0 e^{i\omega t} \ . \tag{2.61}$$

The steady stress response is no longer of the time t but the angular frequency ω for which the response varies with t in a periodic manner. More precisely, it varies with the frequency of the excitation. Consequently, it allows us to write $\epsilon(\omega)$ instead of $\epsilon_0 e^{i\omega t}$ and $\sigma(\omega)$ instead of $\sigma_{ss}(t)$,

$$\sigma(\omega) = G^*(\omega)\epsilon(\omega) \ , \tag{2.62}$$

where $G^*(\omega) := i\omega \bar{G}(i\omega)$ is called complex modulus and has the dimensions of a modulus. $G^*(\omega)$ dictates the relationship of the sinusoidal steady-state stress and strain.

An analogous analysis is applied for a harmonic stress excitation of amplitude σ_0, $\sigma(t) = \sigma_0 e^{i\omega t}$, for which the response of a sinusoidal steady-state strain takes the form

$$\epsilon(\omega) = i\omega \bar{J}(i\omega)\sigma(\omega) = J^*(\omega)\sigma(\omega) \ , \tag{2.63}$$

where $J^*(\omega) = \xi \bar{J}(\xi)|_{\xi = i\omega}$ is the complex shear compliance or harmonic retardance. The complex quantities $G^*(\omega)$ and $J^*(\omega)$ can be decomposed into real and imaginary parts as

$$G^*(\omega) = G_1(\omega) + iG_2(\omega) = |G^*(\omega)|\, e^{i\delta(\omega)} \tag{2.64}$$

and

$$J^*(\omega) = J_1(\omega) - iJ_2(\omega) = |J^*(\omega)|\, e^{-i\delta(\omega)} \ . \tag{2.65}$$

Here, $G_1(\omega)$ and $J_1(\omega)$ are called storage modulus and storage compliance, respectively, due to the fact that they are proportional to the average energy stored during

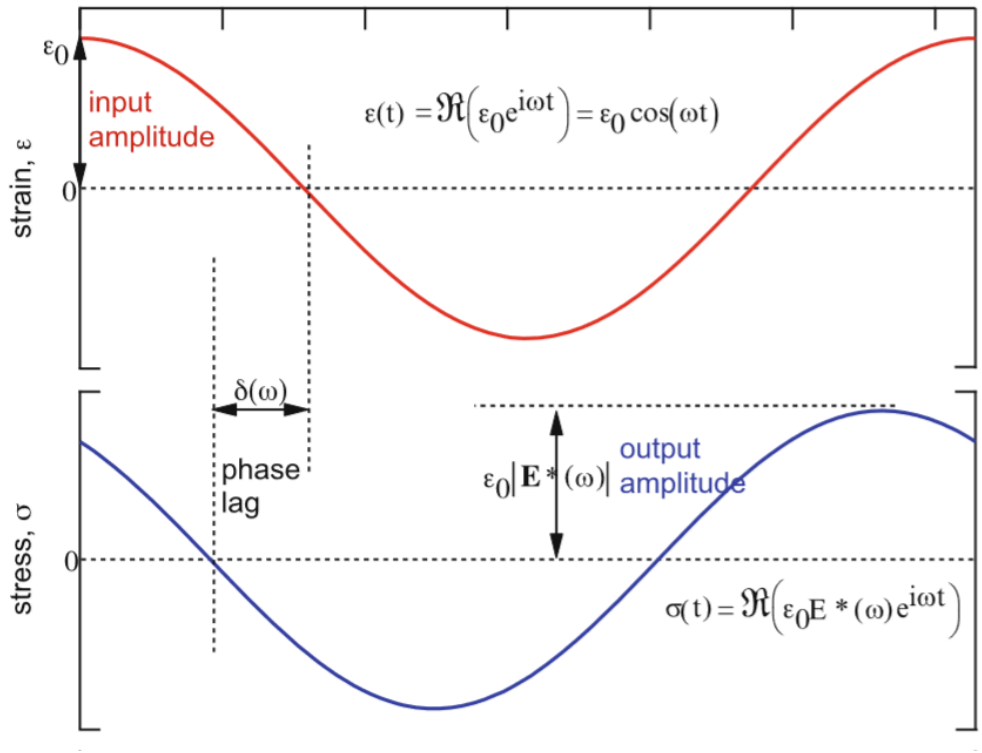

Figure 2.10: Input and output for a steady state vibration test at a single frequency. The stress output is oscillatory, but is out of phase with the strain input. (Brinson & Brinson, 2015)

a cycle of deformation per unit volume of the material. $|G^*|$ and $|J^*|$ are defined as the absolute modulus and absolute compliance, respectively

$$|G^*(\omega)| = \sqrt{G_1(\omega)^2 + G_2(\omega)^2} \quad \text{and} \, |J^*(\omega)| = \sqrt{J_1(\omega)^2 + J_2(\omega)^2} \tag{2.66}$$

The term $\delta(\omega)$ is refered to as the loss angle, whereas the loss tangent is defined as (Tschoegl, 2012)

$$\tan \delta(\omega) = \frac{G_2(\omega)}{G_1(\omega)} = \frac{J_2(\omega)}{J_1(\omega)} \, . \tag{2.67}$$

The loss angle $\delta(\omega)$ is a function of ω containing the information of the phase angle between the steady-state stress and strain. As $\tan \delta(\omega)$ is the ratio of the two moduli, the phase angle is always positive. Conversely, the storage and loss moduli and compliance can be written as

$$G_1(\omega) = |G| \cos \delta(\omega) \quad \text{and} \quad G_2(\omega) = |G| \sin \delta(\omega), \tag{2.68}$$

and

$$J_1(\omega) = |J| \cos \delta(\omega) \quad \text{and} \quad J_2(\omega) = |J| \sin \delta(\omega). \tag{2.69}$$

2.3.6 Spectral Representation

Viscoelastic mechanical properties of materials are primarily determined by experimental means under an applied excitation and observed response. In a natural manner, the applied excitation is necessarily a function of time such as a step function, sinusoidal steady-state function, or any other functions of time (Tschoegl, 2012, p.157). Spontaneously, the observed response always inherits the signature of the time regime in the sense the material functions derived from it contain the same information but with different weights in different regions of the time (or frequency) scale. However, the material functions can be presented in such a way that is independent of the time regime of the driving functions. Those functions are called spectral distribution functions or spectra. Obviously, these functions cannot be accessible directly from experiments but approximated through the application of mathematical techniques. The viscoelastic spectra can be distinguished as relaxation and retardation spectra in relation that they are obtained from the response to a stress or strain excitation respectively. The concept of spectral distribution function turns out to be extremely useful in the theory of linear viscoelasticity due to their independence of any time regime (Tschoegl, 2012, p.57). Once the spectrum is known along with viscoelastic constants, they can be used to generate the response to any desired type of excitation and all other linear viscoelastic properties.

Viscoelastic spectra can be either continuous or discrete and are required to contain complete information on the time-dependent part of the response. Accordingly, they must consist of the appropriate viscoelastic constants extracted from the integral over the spectrum multiplied by a kernel function characterised by the chosen type of the excitation. In the case of continuity, the relaxation time spectra are derived from an assumption that the relaxation times become closely spaced such that the sum of the discrete contribution of the relaxation G_n can be replaced by the integral with respect to time τ over appropriate continuous function (Tschoegl, 2012)

$$G(t) = G(+\infty) + \int_0^\infty H(\tau) e^{-t/\tau} \frac{d\tau}{\tau}, \tag{2.70}$$

where, $G(+\infty) = \lim_{t\to\infty} G(t)$ is the long-time asymptote or equilibrium modulus as defined in Sec. 2.3.4, $H(\tau)$ is un-normalised nonnegative density function associated with a continuous range of relaxation times τ, thus is a function of τ, is called continuous relaxation spectrum. The continuous spectrum form of $H(\tau)$ in Eq. (2.70) directly gives the relative weighting of the different time ranges involved in the relaxation process. The corresponding complex moduli related to the relaxation spectrum are

$$G^*(\omega) = G(+\infty) + \int_0^\infty H(\tau) \frac{i\omega\tau}{1+i\omega\tau} \frac{d\tau}{\tau}, \tag{2.71}$$

$$G_1(\omega) = G(+\infty) + \int_0^\infty H(\tau) \frac{\omega^2\tau^2}{1+\omega^2\tau^2} \frac{d\tau}{\tau}, \tag{2.72}$$

$$G_2(\omega) = \int_0^\infty H(\tau) \frac{\omega\tau}{1+\omega^2\tau^2} \frac{d\tau}{\tau}. \tag{2.73}$$

Since the kernel in Eq. (2.71) has a real part as

$$\frac{\omega^2\tau^2}{1+\omega^2\tau^2} = \frac{1}{2}\Big(1+\tanh(\ln(\omega\tau))\Big), \tag{2.74}$$

while the imaginary part of the kernel in Eq. (2.71) is

$$\frac{\omega\tau}{1+\omega^2\tau^2} = \frac{1}{2}\mathrm{sech}(\ln(\omega\tau)). \tag{2.75}$$

Thus, as a consequence, the storage and loss moduli can be expressed real and imaginary parts of the complex modulus

$$G_1(\omega) = G(+\infty) + \frac{1}{2}\int_0^\infty \Big(1+\tanh(\ln(\omega\tau))\Big)\frac{H(\tau)}{\tau}\mathrm{d}\tau, \tag{2.76}$$

$$G_2(\omega) = \frac{1}{2}\int_0^\infty \mathrm{sech}(\ln(\omega\tau))\frac{H(\tau)}{\tau}\mathrm{d}\tau. \tag{2.77}$$

The determination of $H(\tau)$ from $G(t)$ or from complex moduli is ill-posed inverse in the sense of Hadamard. In particular, small perturbations in the measurement of $G(t)$, or $G_i(\omega), i = 1, 2$ leads to arbitrary large perturbation in $H(\tau)$ since the inverse of the integral operator is not continuous. The ill-posedness of the inversion of Laplace transformation associated with Eq. (2.71) is known as exponentially ill-posed. In term of ill-posedness for identification problems in the sense of Hadamard, the inverse problem does not necessarily have a solution. Even if the solution exists, it can be neither unique nor stable, that is it does not continuously depend on the data.

In an attempt to stabilise the ill-posedness, the discrete spectral representation of viscoelastic material function is considered. In particular, a continuous relaxation modulus G can be approximated arbitrarily closely by a general Dirichlet or Prony series of form

$$G(t) = G_0 + \sum_{k=1}^{N} G_k e^{-t/\tau_k}, \tag{2.78}$$

where $G_1, G_2, \ldots, G_N$ are nonnegative constants and $\tau_1, \tau_2, \ldots, \tau_N$ are distinct positive constants. This equivalent discrete dual presentation of relaxation function corresponds to a generalised Maxwell model. To see the connection, we consider a N-mode Maxwell model with a discrete relaxation spectrum given by (Davies & Goulding, 2012)

$$H(\tau) = \sum_{k=1}^{N} \eta_k\, \delta(t-\tau_k), \tag{2.79}$$

where δ is a Dirac measure. The corresponding storage and loss moduli are given by

$$G_1(\omega) = G(+\infty) + \sum_{k=1}\frac{\eta_k}{\tau_k}\frac{\omega^2\tau_k^2}{1+\omega^2\tau_k^2}, \quad \text{and} \quad G_2(\omega) = \sum_{k=1}\frac{\eta_k}{\tau_k}\frac{\omega\tau_k}{1+\omega^2\tau_k^2}. \tag{2.80}$$

The ill-posedness can be kept under control by various different techniques. One possible method is to keep N sufficiently small. The restriction of numbers of terms in

the sums also prevents fitting the noise inherited from measurement process. Methods for determining discrete spectra include the use of nonlinear regression (Baumgaertel & Winter, 1989), Prony series (Carrot & Verney, 1996), maximum entropy regularisation (Elster & Honerkamp, 1991), Tikhonov regularisation (Honerkamp & Weese, 1989), and sampling localisation (Anderssen & Davies, 2001). In this thesis work, we attempt to fit experimental data based on constrained nonnegative least square introduced by Liu, (1999).

In corresponding of creep behaviour representation, the creep compliance can be expressed in its continuous spectrum as

$$J(t) = J_0 + \int_0^\infty L(\tau)(1 - e^{-t/\tau})\frac{d\tau}{\tau}, \tag{2.81}$$

where $L(\tau)$ is retardation spectrum, $J_0 = J(0)$ the instantaneous creep compliance. Similar to the case of the relaxation modulus G, the retardation modulus or creep compliance function is arbitrarily approximated by a Dirichlet or Prony series of form

$$J(t) = j_0 - \sum_{k=1}^{N} j_k e^{-t/\tau_k}, \qquad N \in \mathbb{N} = \{1, 2, \dots\}, \tag{2.82}$$

where $\tau_1, \tau_2, \dots, \tau_N$ are discrete non-negative retardation times and $j_0, j_1, \dots, j_N$ are non-negative constant parameters called retardation strength. This particular form of creep compliance function corresponds to a generalised Kelvin (Voigt) model. Observe that the instantaneous elastic compliance is evaluated at $t = 0$, that is

$$J_0 = J(0) = j_0 + \sum_{k=1}^{N} j_k. \tag{2.83}$$

In comparison, the Power Law form of creep compliance function in Eq. (2.26) is relatively simple as opposed to the generalised Kelvin model. Indeed, the formulation of Power Law consists of only two terms. Thus there are only two unknown parameters, while the Kelvin model requires $2N + 1$ parameters to be determined. However, the Power Law model generates a compliance function which is unbounded in $\mathbb{R}$, that is, it does not capture the asymptotic behaviour of compliance in the longtime limit. On the contrary, the linear combination of exponential terms in the Kelvin model accounts for such behaviour.

3 Estimates on Compliance Function

The properties of the compliance function of the lab-grown S2 ice under uniaxial compression stress, as described in Sec. 2.3.3, are now discussed in great detail. Compliance data of viscoelastic materials can be obtained from a creep test wherein the suddenly applied stress is kept constant for a finite period of time (see Fig. 3.1). This discrete sampled data from experiments may be used to reconstruct the continuous compliance function up to some degree of accuracy. In this section, we attempt to approximate the compliance function with simple Power Law and to reconstruct the discrete compliance spectrum by the non-negative least squares method described by Liu, (1999).

Consider the one-dimensional form of the linear viscoelastic stress-strain relation given in the Eq. (2.21)

$$\epsilon(t) = J_0\sigma(t) + \int_0^t \sigma(t-s)\frac{\mathrm{d}J(s)}{\mathrm{d}s}\,\mathrm{d}s, \qquad t \in [0,\infty), \tag{3.1}$$

where ϵ is a measured strain response of the specimen subjected to an input stress σ (measured in Pascals), t is time measured in seconds, and J is compliance measured in Pa^{-1}. Eq. (3.1) above implies that if the creep compliance function J is known then the strain ϵ can be determined from any given stress state at any time $t \in [0,\infty)$. To obtain compliance data, a creep test is performed wherein the input stress is a constant function of the form $\sigma(t) = \sigma_0 > 0$ for all time $t \in [0,\infty)$, and σ_0 is sufficiently small to guarantee linearity in the sense of viscoelastic theory. Accordingly, Eq. (3.1) yields

$$\epsilon(t) = J_0\sigma_0 + \int_0^t \sigma_0\frac{\mathrm{d}J(\tau)}{\mathrm{d}\tau}\,\mathrm{d}\tau = J_0\sigma_0 + \sigma_0\int_0^t \frac{\mathrm{d}J(\tau)}{\mathrm{d}\tau}\,\mathrm{d}\tau = J(t)\sigma_0, \quad t \in [0,\infty). \tag{3.2}$$

The last equality follows directly from the fundamental theorem of calculus. Therefore, the compliance function is given simply by

$$J(t) = \frac{\epsilon(t)}{\sigma_0}, \qquad t \in [0,\infty). \tag{3.3}$$

As was discussed in the Sec. 2.3.3, we impose the requirements for the creep compliance J to be a non-negative monotonically increasing function of time:

$$J(t) = \begin{cases} J(t) \geq 0, & t \geq 0 \\ 0, & t < 0, \end{cases}$$

and

$$\frac{\mathrm{d}J(t)}{\mathrm{d}t} \geq 0 \qquad \text{and} \qquad \frac{\mathrm{d}^2J(t)}{\mathrm{d}t^2} \leq 0 \qquad \text{for } t \geq 0.$$

We will study two different approximations for compliance function J. The first approximation is given by a simple Power Law model described by Eq. (2.26) and

the second approximation is given by a Dirichlet series of form or generalised Kelvin model in Eq. (2.82).

Theoretically, the compliance function is evaluated from a creep test in which a constant load is applied infinitely fast. However, such a test is impossible to perform without invoking shockwaves propagating in the material. In practice, an ideal creep test is realised by increasing the load linearly to a predetermined value or a ramp test. The ramp-up phase is required to be short, typically in the order of a second. Obviously, it is not a correct creep test and thus an error must be involved. This error, yet, may be negligible if the ramp time t_1 is small compared to the retardation time of the material. However, due to the fading memory property, the material soon "forget" the precise history to which the load has been applied, thus the viscoelastic response during the initial or transient portion of the ramp-strain history cannot be captured. In order to compensate for this loss of information, a certain analysis method is devised and described by Sorvari and Malinen, (2006).

Let the stress state be given by

$$\sigma(t) = \begin{cases} \frac{\sigma_0}{t_1}\, t, & t < t_1, \\ \sigma_0, & t_1 \leq t, \end{cases} \tag{3.4}$$

where σ_0 is the constant stress input, t_1 denotes time when the maximum stress is achieved. The strain output can be split into two integrals

$$\begin{aligned} \epsilon(t) &= \int_{-\infty}^{t_1} J(t-s)\frac{\mathrm{d}\sigma(s)}{\mathrm{d}s}\mathrm{d}s + \int_{t_1}^{t} J(t-s)\frac{\mathrm{d}\sigma(s)}{\mathrm{d}s}\mathrm{d}s \\ &= \frac{\sigma_0}{t_1}\int_{-\infty}^{t_1} J(t-s)\mathrm{d}s + \int_{t_1}^{t} J(t-s)\frac{\mathrm{d}\sigma(s)}{\mathrm{d}s}\mathrm{d}s \end{aligned} \tag{3.5}$$

Integration by parts the second term on the right hand side, we obtain

$$\begin{aligned} \int_{t_1}^{t} J(t-s)\frac{\mathrm{d}\sigma(s)}{\mathrm{d}s}\mathrm{d}s &= \int_{0}^{t-t_1} J(u)\frac{\mathrm{d}\sigma(t-u)}{\mathrm{d}u}\mathrm{d}u \\ &= J(u)\sigma(t-u)\Big|_0^{t-t_1} - \int_0^{t-t_1}\sigma(t-s)\frac{\mathrm{d}J(s)}{\mathrm{d}s}\mathrm{d}s \\ &= J(t)\sigma_0 - \int_0^{t-t_1}\sigma(t-s)\frac{\mathrm{d}J(s)}{\mathrm{d}s}\mathrm{d}s. \end{aligned} \tag{3.6}$$

Change of variable from s to $u = t - s$, $du = -ds$ and change of integral limits when $s = 0, u = t$, and $s = t_1, u = t - t_1$ yield

$$\epsilon(t) = \frac{\sigma_0}{t_1}\int_{t-t_1}^{t} J(u)\mathrm{d}u. \tag{3.7}$$

Differentiating Eq. (3.7) with respect to time yields

$$\dot{\epsilon}(t) = \frac{\sigma_0}{t_1}\Big(J(t) - J(t-t_1)\Big) \implies J(t) = \frac{t_1\dot{\epsilon}(t)}{\sigma_0} + J(t-t_1) \tag{3.8}$$

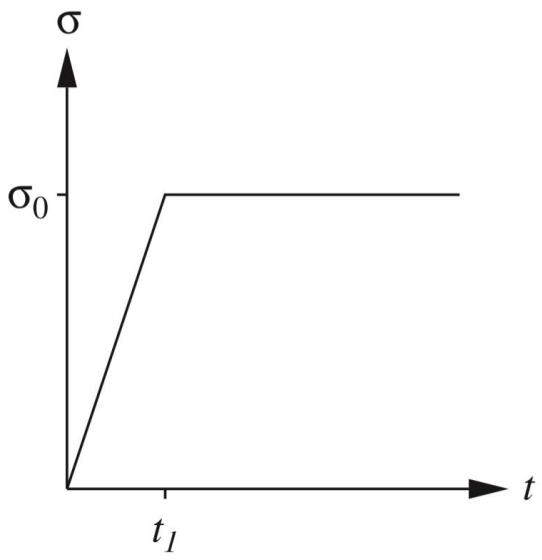

Figure 3.1: Stress input in a creep test.

On the other hand, we apply the two point trapezoidal rule to integrate Eq. (3.7) numerically to achieve

$$\epsilon(t) = \frac{t_1}{2}\frac{\sigma_0}{t_1}\Big(J(t) + J(t-t_1)\Big) = \frac{\sigma_0}{2}\Big(J(t) + J(t-t_1)\Big). \tag{3.9}$$

To this end, substituting Eq. (3.8) to Eq. (3.9) gives

$$J(t-t_1) = \frac{\epsilon(t)}{\sigma_0} - \frac{t_1\dot{\epsilon}(t)}{2\sigma_0}, \quad t \geq t_1. \tag{3.10}$$

Equivalently, the compliance data can be obtained by

$$J(t) = \frac{\epsilon(t+t_1)}{\sigma_0} - \frac{t_1\dot{\epsilon}(t+t_1)}{2\sigma_0}, \quad t \geq 0. \tag{3.11}$$

3.1 Power Law Creep Compliance

The fundamental idea behind the Power Law is to have a simple model with few parameters that describes the material functions efficiently. In this work, the instantaneous creep value $J_0 = J(0)$ is assumed to be known and is taken to be the reciprocal value of the material elastic modulus or Young modulus. As a consequence, there are only two parameters C and α needed to be determined. In principle, there are two methods for determination of parameter values. The choice between them depends on availability of the data. The first method allows us to work with measured strain response data while the second one suggests employing the corresponding measured creep compliance data. The two methods and their pros and cons are discussing in the following section.

If the stress history is assumed to have the form (see Fig. 3.2)

$$\sigma(t) = \begin{cases} \sigma_0\,, & \text{if} \quad 0 \le t < t_1, \\ 0\,, & \text{if} \quad t < 0 \ \text{ and } t \ge t_1, \end{cases} \tag{3.12}$$

where t_1 is the time when the load is removed, then the strain response takes the form

$$\epsilon(t) = \left(J_0 + Ct^{\alpha}\right)\sigma_0 = J_0\sigma_0 + C\sigma_0 t^{\alpha}, \quad 0 < \alpha < 1, \quad t \in [0, t_1). \tag{3.13}$$

In the first approach, choosing two different values of the transient strain at two different points in time, say $\epsilon_{t_a} = \epsilon(t = t_a)$ and $\epsilon_{t_b} = \epsilon_t(t = t_b)$, yields a system of two equations

$$\begin{cases} \epsilon_{t_a} - J_0\sigma_0 = C\sigma_0 t_a^n, \\ \epsilon_{t_b} - J_0\sigma_0 = C\sigma_0 t_b^n, \end{cases} \qquad t_a < t_b < t_1, \tag{3.14}$$

from which it follows that

$$\frac{\epsilon_{t_a} - J_0\sigma_0}{\epsilon_{t_b} - J_0\sigma_0} = \frac{C\sigma_0 t_a^{\alpha}}{C\sigma_0 t_b^n} = \left(\frac{t_a}{t_b}\right)^{\alpha}. \tag{3.15}$$

In consequence, the Power Law exponent is obtained by taking a logarithm of both sides of Eq. (3.15),

$$\alpha = \log\left(\frac{\epsilon_{t_a}}{\epsilon_{t_b}}\right) \log^{-1}\left(\frac{t_a}{t_b}\right), \tag{3.16}$$

and the constant parameter C is determined by

$$C = \frac{\epsilon_{t_a} - J_0\sigma_0}{\sigma_0 t_a^{\alpha}} = \frac{\epsilon_{t_b} - J_0\sigma_0}{\sigma_0 t_b^{\alpha}}. \tag{3.17}$$

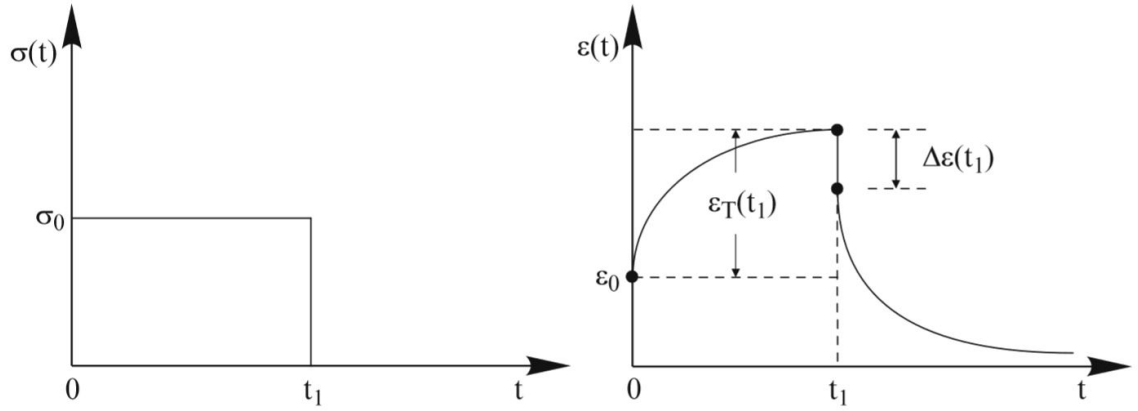

Figure 3.2: Single step creep load and material response. (Brinson & Brinson, 2015) (a) Applied stress. (b) Creep and creep recovery: Instantaneous strains at $t = t_1$ and $t = t_1$ denoted as ϵ_0 and $\Delta\epsilon(t_1)$. The time dependent strain or transient strain has a magnitude depicted at $t = t_1$.

Graphically, under linear viscoelastic response, the plot of the strain versus time on a log-log scale is a straight line for a long time interval. The slope of the line, hence, is the power law exponent, α.

In the second approach, the parameters can be solved straightforwardly from a given creep compliance data by taking logarithm both sides of Eq. (2.26)

$$\log\Big(J(t) - J_0\Big) = \log C + \alpha \log(t). \tag{3.18}$$

In this case, the parameter C can be solved by choosing $t = 1$ and thus, the above equation obtains solutions

$$\begin{cases} C = J(t=1) - J_0, \\ \alpha = \frac{\log\Big(J(t) - J_0\Big) - \log C}{\log(t)}, \quad t \geq 1. \end{cases} . \tag{3.19}$$

In consideration of noisy measured data, the aforementioned methods show the downside in the accuracy of the determined values C and α as they depends strongly on the choice of the point in time at which they are evaluated. To overcome this obstacle, the data obtained by measurement over the whole time domain is suggested to be taken into consideration. As a consequence, the problem of determining parameter values are necessarily formulated as an inverse problem. In addition, as measurement data are often contaminated by errors, some numerical regularisation techniques when working with compliance data will be studied; in particular, the regularisation by singular value truncation and the Tikhonov regularisation.

For the sake of ease in computation, the nonlinear Power Law is reformulated as a linear system. Let $\tilde{\boldsymbol{J}} \in \mathbb{R}^M$ denote the vector of measured value of creep compliance with the corresponding vector of measured time $\boldsymbol{t}$. Denote

$$y_k = \log(\tilde{J}_k - J_0) \quad \text{and} \quad \hat{t}_k = \log(t_k), \quad k = 2, 3, \ldots, M. \tag{3.20}$$

Note that the set of indices k starts from 2, as the logarithm is not defined at $t_1 = 0$. Now the problem reduces to finding the line $\hat{\boldsymbol{J}} = c + \alpha\,\hat{\boldsymbol{t}}$ that best fits the $M - 1$ ordered pairs $(\hat{J}_k, \hat{t}_k)$. As a result, we obtain the following overdetermined system of linear equations

$$\hat{\boldsymbol{J}} = \boldsymbol{A}\boldsymbol{x} = \begin{bmatrix} 1 & \hat{t}_2 \\ 1 & \hat{t}_3 \\ \vdots & \vdots \\ 1 & \hat{t}_M \end{bmatrix} \begin{bmatrix} c \\ \alpha \end{bmatrix}. \tag{3.21}$$

3.1.1 Regularisation by Singular Value Truncation

The matrix $\boldsymbol{A} \in \mathbb{R}^{(M-1)\times 2}$ can be represented in terms of its singular system called singular value decomposition of $\boldsymbol{A}$, abbreviated as SVD of $\boldsymbol{A}$. In particular, $\boldsymbol{A}$ can be decomposed as $\boldsymbol{A} = \boldsymbol{U}\boldsymbol{\Lambda}\boldsymbol{V}^T$ where $\boldsymbol{U} \in \mathbb{R}^{(M-1)\times(M-1)}$ and $\boldsymbol{V} \in \mathbb{R}^{2\times 2}$ are orthogonal matrices, and $\boldsymbol{\Lambda} \in \mathbb{R}^{(M-1)\times 2}$ is a diagonal matrix with diagonal elements:

$\lambda_1 \geq \lambda_2 \geq ... \geq \lambda_{min(M-1,2)} \geq 0$. Therefore, the minimum norm solution of the problem $\hat{\boldsymbol{J}} = \boldsymbol{A}\boldsymbol{x}$ is of form

$$\boldsymbol{x} = \boldsymbol{A}^{\dagger}\hat{\boldsymbol{J}}, \tag{3.22}$$

where $\boldsymbol{A}^{\dagger}$ is called pseudoinverse or Moore–Penrose inverse of A and is defined as

$$\boldsymbol{A}^{\dagger} = \boldsymbol{V}\boldsymbol{\Lambda}^{\dagger}\boldsymbol{U}^{T}, \tag{3.23}$$

where

$$\boldsymbol{\Lambda}^{\dagger} = \begin{bmatrix} 1/\lambda_1 & 0 \\ 0 & 1/\lambda_2 \\ 0 & 0 \\ \vdots & \vdots \\ 0 & 0 \end{bmatrix} \in \mathbb{R}^{(M-1)\times 2}. \tag{3.24}$$

More details on the Moore-Penrose inverse and on the corresponding SVD techniques can be found in (Kaipio & Somersalo, 2006).

3.1.2 Tikhonov regularisation

The idea of the Tikhonov regularisation is that instead of minimising the norm of the residual, it proposes to minimise the so-called Tikhonov functional

$$F_{\delta}(x) := \left\| \boldsymbol{A}\boldsymbol{x} - \hat{\boldsymbol{J}} \right\|^2 + \delta \left\| \boldsymbol{x} \right\|^2, \tag{3.25}$$

where $\delta > 0$ is the regularisation parameter. A Tikhonov regularised solution exists, is unique, and is given by

$$\boldsymbol{x}_{\delta} = (\boldsymbol{A}^{T}\boldsymbol{A} + \delta \boldsymbol{I})^{-1}\boldsymbol{A}^{T}\hat{\boldsymbol{J}}. \tag{3.26}$$

For matrices, the Tikhonov regularised functional is written as

$$F_{\delta}(x) = \left\| \begin{bmatrix} \boldsymbol{A} \\ \sqrt{\delta}\boldsymbol{I} \end{bmatrix} \boldsymbol{x} - \begin{bmatrix} \hat{\boldsymbol{J}} \\ \boldsymbol{0} \end{bmatrix} \right\|^2, \quad \boldsymbol{I} \in \mathbb{R}^{(M-1)\times 2}, \quad \boldsymbol{0} \in \mathbb{R}^2. \tag{3.27}$$

The normal equation corresponding to this least squares problem is

$$\begin{bmatrix} \boldsymbol{A} \\ \sqrt{\delta}\boldsymbol{I} \end{bmatrix}^{T} \begin{bmatrix} \boldsymbol{A} \\ \sqrt{\delta}\boldsymbol{I} \end{bmatrix} \boldsymbol{x} = \begin{bmatrix} \boldsymbol{A} \\ \sqrt{\delta}\boldsymbol{I} \end{bmatrix}^{T} \begin{bmatrix} \hat{\boldsymbol{J}} \\ \boldsymbol{0} \end{bmatrix} \tag{3.28}$$

or equivalently,

$$(\boldsymbol{A}^{T}\boldsymbol{A} + \delta \boldsymbol{I})\boldsymbol{x} = \boldsymbol{A}^{T}\hat{\boldsymbol{J}}. \tag{3.29}$$

The regularisation parameter δ can be chosen by different methods such as discrepancy principle, quasi optimality criterion, and L-curve method. In this work, we consider the Morozov principle advises to choose the regularisation parameter δ. The main idea of the Morozov principle in the framework of the Tikhonov regularisation is to choose δ so that the residual satisfies

$$\left\| \boldsymbol{A}\boldsymbol{x}_{\delta} - \hat{\boldsymbol{J}} \right\|^2 = e > 0, \tag{3.30}$$

where e is defined as a norm difference between noisy measurement $\hat{\boldsymbol{J}}$ and the 'exact' data $\boldsymbol{J}$

$$\left\|\hat{\boldsymbol{J}} - \boldsymbol{J}\right\| \approx e. \tag{3.31}$$

The discrepancy between the measured data and the underlying 'exact' data may be assumed to equal the square root of the expectation value of the squared norm of the noise vector

$$e = \sqrt{2 \cdot 0.001^2}. \tag{3.32}$$

The detailed analysis of Tikhonov regularisation is referred in the work of Kaipio and Somersalo, (2006).

Solving this minimisation problem in MATLAB is rather simple as we can employ the `backlash` or `mldivide` command of MATLAB. The reason is that for non-square matrices these commands try to solve the corresponding least squares problem.

Once parameters C and α are known, substituting Eq. (2.26) into Eq. (3.1) yields

$$\epsilon(t) = J_0\sigma(t) + C\int_0^t \sigma(t-s)\frac{\mathrm{d}s^\alpha}{\mathrm{d}s}\mathrm{d}s = J_0\sigma(t) + \alpha C\int_0^t \sigma(t-s)\, s^{\alpha-1}\,\mathrm{d}s. \tag{3.33}$$

3.1.3 Power Law Complex Compliance

Depending on the form of the approximation, a corresponding complex compliance is derived. Assume that the oscillatory stress has been imposed for a long time so that transient vibrations have disappeared:

$$\sigma(t) = \sigma_0 \sin^2(\frac{\omega t}{2}), \tag{3.34}$$

where σ_0 is the amplitude or the maximum value of the oscillating stress, ω is the angular velocity, and t is time measured in second. The input stress function in Eq. (3.34) follows Haversine formula. The time derivative of σ

$$\frac{\mathrm{d}\sigma(t)}{\mathrm{d}t} = \sigma_0\omega \sin(\frac{\omega t}{2})\cos(\frac{\omega t}{2}) = \frac{\sigma_0\omega}{2}\sin(\omega t). \tag{3.35}$$

Inserting Eq. (3.35) into Eq. (3.1) yields

$$\epsilon(t) = \frac{i\omega\sigma_0 e^{i\omega t}}{2}\int_0^\infty J(u)e^{i\omega(-u)}\mathrm{d}u, \tag{3.36}$$

which implies

$$J(\omega) = i\omega\int_0^\infty J(u)e^{-i\omega u}\mathrm{d}u = \mathcal{L}(J(u))|_{s=i\omega}. \tag{3.37}$$

Eq. (3.37) shows the relationship between the complex compliance J^* and the static creep compliance J. The right-hand side in Eq. (3.37) involves the Laplace transform of J at point u evaluated at point $s = i\omega$.

If the creep compliance $J(t)$ obeys the Power Law, it can be expressed as a power function of time $J(t) = J_0 + Ct^\alpha, \alpha \in (0,1)$, then the corresponding complex compliance can be obtained by inserting the Laplace transform as follows

$$J^*(\omega) = i\omega \int_0^\infty J(u)e^{-i\omega u}\,\mathrm{d}u = i\omega\mathcal{L}[J(u)]_{s=i\omega} = i\omega\Big[\frac{J_0}{i\omega} + \frac{C\,\Gamma(\alpha+1)}{(i\omega)^{\alpha+1}}\Big], \tag{3.38}$$

or

$$J^*(\omega) = J_1(\omega) + iJ_2(\omega) = J_0 + C\,\Gamma(\alpha+1)(i\omega)^{-\alpha}, \tag{3.39}$$

where Γ is the Gamma-function. Applying the relation

$$\begin{aligned} i^{-p} &= (-1)^{-k/2} = e^{\frac{-p\log(-1)}{2}} = e^{\frac{-ip\pi}{2}} \\ &= \cos(-\frac{p\pi}{2}) + i\sin(-\frac{p\pi}{2}) = \cos(\frac{p\pi}{2}) - i\sin(\frac{p\pi}{2}) \quad \text{for } 0 < p < 1, \end{aligned} \tag{3.40}$$

Eq. (3.39) yields

$$J_1(\omega) + iJ_2(\omega) = J_0 + C\omega^{-\alpha}\Gamma(\alpha+1)\Big[\cos(\frac{\alpha\pi}{2}) - i\sin(\frac{\alpha\pi}{2})\Big]. \tag{3.41}$$

Explicitly, the real and imaginary parts of the complex compliance are described by

$$\begin{aligned} J_1(\omega) &= J_0 + C\omega^{-\alpha}\Gamma(\alpha+1)\cos(\alpha\pi(2k+\frac{1}{2})), \\ J_2(\omega) &= C\omega^{-\alpha}\Gamma(\alpha+1)\sin(\alpha\pi(2k+\frac{1}{2})), \\ &\text{where } k = 0,1,2. \end{aligned} \tag{3.42}$$

3.2 Discrete Creep Spectrum - Generalised Kelvin Compliance Model

3.2.1 Estimating Unknown Parameters by Nonnegative Least Squares Method

Recall that the Kelvin compliance model is given by Eq. (2.82)

$$J(t) = j_0 - \sum_{k=1}^{N} j_k e^{-t/\tau_k}, \qquad N \in \mathbb{N} = \{1,2,\dots\}.$$

The model contains $2N+1$ parameters, $j_0, j_1, \dots, j_N$ and $\tau_1, \tau_2, \dots, \tau_N$. We observe that the model is highly nonlinear with respect to parameters τ_k, while being linear in j_k. In practice, the step-stress experiment only gives discrete sampled values of creep compliance function $J(t)$ and this experimental data is always contaminated by noise. Let us denote a set of experimental discrete creep compliance $\{\tilde{J}_i\}_{i=1}^M$, which is measured at the set of time points $\{t_i\}_{i=1}^M$ in the interval $[0,\infty)$, where M is

the number of measurements. Thus the values of the compliance function at times $t_i, i = 1, 2, \ldots, M$, are given by

$$\boldsymbol{J} = \begin{bmatrix} J_1 \\ J_2 \\ \vdots \\ J_M \end{bmatrix} = \begin{bmatrix} j_0 - \sum_{k=1}^{N} j_k e^{-t_1/\tau_k} \\ j_0 - \sum_{k=1}^{N} j_k e^{-t_2/\tau_k} \\ \vdots \\ j_0 - \sum_{k=1}^{N} j_k e^{-t_M/\tau_k} \end{bmatrix} = \begin{bmatrix} 1 & -e^{-t_1/\tau_1} & \ldots & -e^{-t_1/\tau_M} \\ 1 & -e^{-t_2/\tau_1} & \ldots & -e^{-t_2/\tau_M} \\ \vdots & \vdots & \ddots & \vdots \\ 1 & -e^{-t_N/\tau_1} & \ldots & -e^{-t_N/\tau_M} \end{bmatrix} \begin{bmatrix} j_0 \\ j_1 \\ \vdots \\ j_N. \end{bmatrix}$$

Denote

$$\boldsymbol{A} = \begin{bmatrix} 1 & -e^{-t_1/\tau_1} & \ldots & -e^{-t_1/\tau_M} \\ 1 & -e^{-t_2/\tau_1} & \ldots & -e^{-t_2/\tau_M} \\ \vdots & \vdots & \ddots & \vdots \\ 1 & -e^{-t_N/\tau_1} & \ldots & -e^{-t_N/\tau_M} \end{bmatrix} \quad \text{and} \quad \boldsymbol{j} = \begin{bmatrix} j_0 \\ j_1 \\ \vdots \\ j_N. \end{bmatrix} \tag{3.43}$$

Given M experimentally measured values of the compliance $\tilde{\boldsymbol{J}}$, the problem of finding the $2N + 1$ unknown parameters τ_k and j_k, corresponds to an optimisation problem. However, due to the appearance of the parameters τ_k in the exponent, only nonlinear optimisation regimes can be utilised. However, we can make use of linear optimisation if values of τ_k are provided a priori. In particular, then Eq. (**??**) becomes a system of M equations in $N + 1$ unknowns. A brief account of dealing with such optimisation problems is presented in the Appendix X.

The set of $\{j_k\}, k = 1, 2, \ldots$ are estimated in such a way that a cost function or residual term is minimised:

$$\text{minimise } \left\| \boldsymbol{A}\boldsymbol{j} - \tilde{\boldsymbol{J}} \right\|_2^2 \tag{3.44}$$

subject to an inequality constrain

$$j_k \geq 0, \qquad k = 0, 1, 2, \ldots, N$$

where $\boldsymbol{A} = (a)_{ij}$ is an $M \times (N+1)$ matrix with $M > N+1$, $\tilde{\boldsymbol{J}}$ is an $M-$dimensional vector, $\tilde{\boldsymbol{J}} = (\tilde{J}_1, \tilde{J}_2, \ldots, \tilde{J}_M)^T$ is an M-dimensional vector, $\boldsymbol{j} = (j_0, j_1, \ldots, j_N)^T$ is an $(N + 1)$-dimensional vector, and $\|.\|_2$ is Euclidean norm or norm 2. In fact, Eq. (3.44) is a constrain quadratic optimisation problem involving minimising the convex quadratic function

$$\left\| \boldsymbol{A}\boldsymbol{j} - \tilde{\boldsymbol{J}} \right\|_2^2 = \boldsymbol{j}^T \boldsymbol{A}^T \boldsymbol{A}\boldsymbol{j} - 2\boldsymbol{j}\boldsymbol{A}\boldsymbol{j} + \tilde{\boldsymbol{J}}\boldsymbol{j}, \tag{3.45}$$

where $\boldsymbol{j}^T$ is transpose of $\boldsymbol{j}$. This problem is simple enough to have the well known analytical solution $\boldsymbol{j} = \boldsymbol{A}^\dagger \tilde{\boldsymbol{J}}$, where $\boldsymbol{A}^\dagger$ is the pseudo-inverse of $\boldsymbol{A}$.

The software package MATLAB is used to conduct the numerical experiments in this subsection. The MATLAB 'lsqnonneg' function is utilised to implement the nonnegative least square method.

Differentiating the compliance function in Eq. (2.82) with respect to time gives

$$\frac{\mathrm{d}J(t)}{\mathrm{d}t} = \sum_{k=1}^{N} \frac{j_k}{\tau_k} e^{-t/\tau_k}. \tag{3.46}$$

Substituting the above result into Eq. (3.1) yields

$$\epsilon(t) = J_0\sigma(t) + \int_0^t \sigma(t-s)\Big(\sum_{k=1}^{N} \frac{j_k}{\tau_k} e^{-s/\tau_k}\Big)\mathrm{d}s. \tag{3.47}$$

The sequence of discrete retardation time $\{\tau_k\}_{k=1}^N$ can be openly chosen in such a way that they satisfy the following condition

$$\sum_{k=1}^{\infty} \frac{\tau_k}{1+\tau_k^2} = \infty. \tag{3.48}$$

3.2.2 Generalised Kelvin Dynamic Compliance

Give a creep compliance or retardation function J of form described by Eq. (2.82), applying the Laplace transformation, we get

$$J^*(\omega) = i\omega\mathcal{L}(J(t)) = i\omega\Big[\frac{j_0}{i\omega} - \sum_{k=1}^{N} \frac{j_k}{i\omega + \frac{1}{\tau_k}}\Big] = j_0 - \sum_{k=1}^{N} \frac{j_k i\omega\tau_k}{1+i\omega\tau_k}. \tag{3.49}$$

or

$$\begin{aligned} J^*(\omega) = J_1(\omega) + iJ_2 &= j_0 - \sum_{k=1}^{N} \frac{j_k i\omega\tau_k}{1+i\omega\tau_k}\Big(\frac{1-i\omega\tau_k}{1-i\omega\tau_k}\Big) \\ &= j_0 - \sum_{k=1}^{N} \frac{j_k(i\omega\tau_k + \omega^2\tau_k^2)}{1+\omega^2\tau_k^2} = j_0 - \sum_{k=1}^{N} \frac{j_k\omega^2\tau_k^2}{1+\omega^2\tau_k^2} - i\sum_{k=1}^{N} \frac{j_k\omega\tau_k}{1+\omega^2\tau_k^2}. \end{aligned} \tag{3.50}$$

Explicitly,

$$\begin{aligned} J_1(\omega) &= j_0 - \sum_{k=1}^{N} \frac{j_k\omega^2\tau_k^2}{1+\omega^2\tau_k^2}, \\ J_2(\omega) &= \sum_{k=1}^{N} \frac{j_k\omega\tau_k}{1+\omega^2\tau_k^2}, \end{aligned} \tag{3.51}$$

$$J(\omega) = \sqrt{J_1(\omega)^2 + J_2(\omega)^2} = \sqrt{\Big(j_0 - \sum_{k=1}^{m} \frac{j_k\omega^2\tau_k^2}{1+\omega^2\tau_k^2}\Big)^2 + \Big(\sum_{k=1}^{N} \frac{j_k\tau_k\omega}{1+\omega^2\tau_k^2}\Big)^2}, \tag{3.52}$$

and

$$\tan\delta = \frac{J_2(\omega)}{J_1(\omega)} = \Big(\sum_{k=1}^{N} \frac{j_k\tau_k\omega}{1+\omega^2\tau_k^2}\Big)\Big(j_0 - \sum_{k=1}^{N} \frac{j_k\omega^2\tau_k^2}{1+\omega^2\tau_k^2}\Big)^{-1}. \tag{3.53}$$

4 Results and Discussion

In the following section, we investigate the accuracy of the schemes described in the preceding section in determining parameters of the Power Law and Kelvin models for creep compliance. The compliance data obtained from these models is compared with the compliance computed from numerically generated stress and strain data (as described in Sec. 4.1). In studying the robustness of the schemes, Gaussian noise is added to the compliance data.

Later in this project, these schemes are used to estimate creep compliance of sea ice from strain response obtained experimentally via a creep test. Once the parameters of the Power Law and Kelvin models are known, they are used to predict strain response from different loading scenarios, namely, from static and cyclic loading.

4.1 Numerical Results

The performance of the approximation schemes is tested on a set of numerically generated creep compliance data over the time range of $[0, 120]s$. In order to simulate creep compliance data, we employ the nonlinear viscoelastic model for strain response introduced by LeClair, Schapery, and Dempsey, (1999). The nonlinear viscoelastic model is a generalization of a linear model. Thus, by inputting low enough values for stress, the linear viscoelastic strain response is produced. Specifically, LeClair et al. suggested that the strain response can be modelled as a function of time and stress by

$$\epsilon(t) = J_0\sigma(t) + S_1 \int_{-\infty}^{t} \sigma^3(s)\mathrm{d}s + S_2 \int_{-\infty}^{t} (t-s)^{1/3} \frac{\mathrm{d}\sigma^{3/2}(s)}{\mathrm{d}s}\mathrm{d}s, \tag{4.1}$$

where σ is stress in units of MPa. We choose to model stress as a constant function, given by

$$\sigma(t) = \begin{cases} 0.5 \text{ MPa}, & \text{if} \quad 0 \leq t \leq 120, \\ 0, & \text{otherwise} . \end{cases} \tag{4.2}$$

Time t is measured in seconds and the model parameters are

$$\begin{aligned} J_0 &= 13.5 \times 10^{-11} \frac{\mathrm{m}^2}{\mathrm{N}}, \\ S_1 &= 8.0 \times 10^{-25} \frac{\mathrm{m}^6}{\mathrm{N}^3 \cdot \mathrm{s}}, \\ S_2 &= 8.25 \times 10^{-14} \frac{\mathrm{m}^3}{\mathrm{N}^{3/2} \cdot \mathrm{s}^{4/3}}. \end{aligned} \tag{4.3}$$

Thus the theoretical compliance data is obtained by

$$J(t) = \frac{\epsilon(t)}{\sigma_0}. \tag{4.4}$$

We can now study how accurate the schemes are in terms of estimating the compliance function as compared to the compliance obtained from Eq. (4.4). Furthermore, we

investigate how sensitive to noise the schemes are by adding Gaussian noise to the compliance. Variance of the noise is taken to be $1\%, 2\%, 5\%$, and 10% of the maximal compliance value. In what follows, all integrals are evaluated by the trapezoidal integration rule. The error is measured by the root mean square (RMS) scheme given by

$$error = \sqrt{\frac{\sum_{k=1}^{N}(\hat{J}_k - J_k)^2}{N}}, \tag{4.5}$$

where $\hat{J}_k$ are predicted values and J_k are exact values. Results for each model are summarized and discussed in the following subsections.

4.1.1 Power Law

The numerical results of fitting noiseless compliance data to the Power Law form are shown in Fig. 4.2a, in which the theoretical compliance function is plotted against the optimized result in Pa^{-1} while time is measured in seconds. The Fig. 4.1 presents the results from a simple '`fit`' command from MATLAB. These results are employed to compare with results obtained from the singular value truncation and Tikhonov regularization techniques.

In general, the three methods produce remarkable outcomes in approximating noiseless measurement data. The MATLAB '`fit`' command produces exceptional results, as the obtained curve has pointwise differences from the 'exact' solution of magnitude 10^{-25}. The relative error, of order of magnitude is 10^{-13}, is observed to be the largest in case of Tikhonov regularization. Even though the creep compliance curve nearly coincides with the test data, as shown in Fig. 4.3a, the plot of pointwise differences between the two compliance functions in Fig. 4.3b reveals that this method overestimates the data in the first rapid growth of creep compliance curve. In

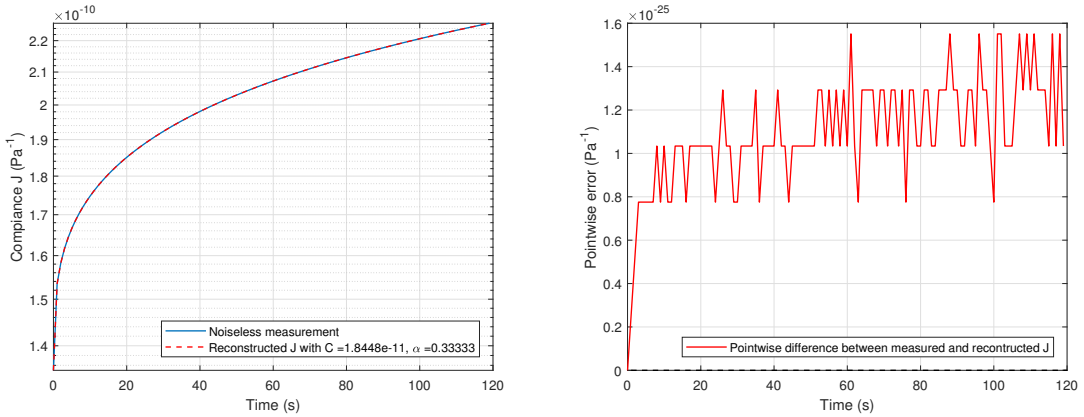

(a) (b)

Figure 4.1: (a) Plot of 'exact' and reconstructed compliance function obtained by 'fit' command. Parameters are reported to be $C = 1.8448 \times 10^{-11}$ and $\alpha = 0.33333$ (b) Pointwise error.

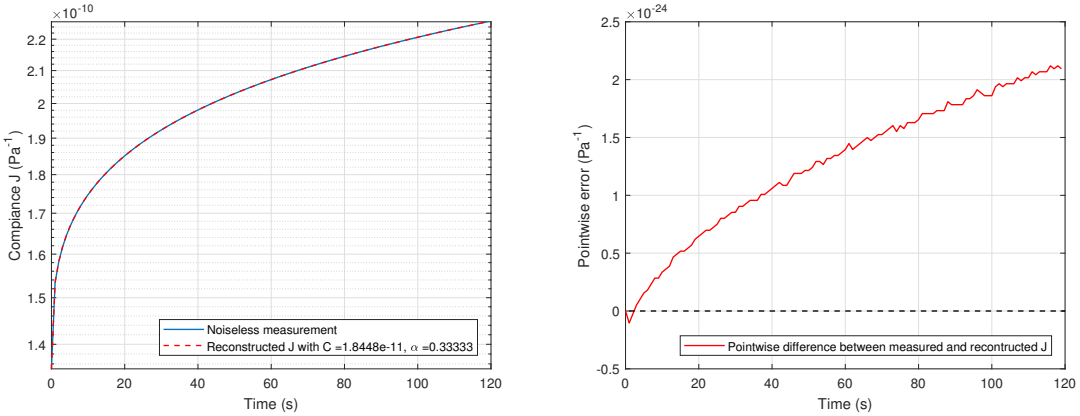

(a) (b)

Figure 4.2: (a) Plot of 'exact' and reconstructed compliance function obtained by SVD method. Parameters are reported to be $C = 1.8448 \times 10^{-11}$ and $\alpha = 0.33333$ (b) Pointwise error.

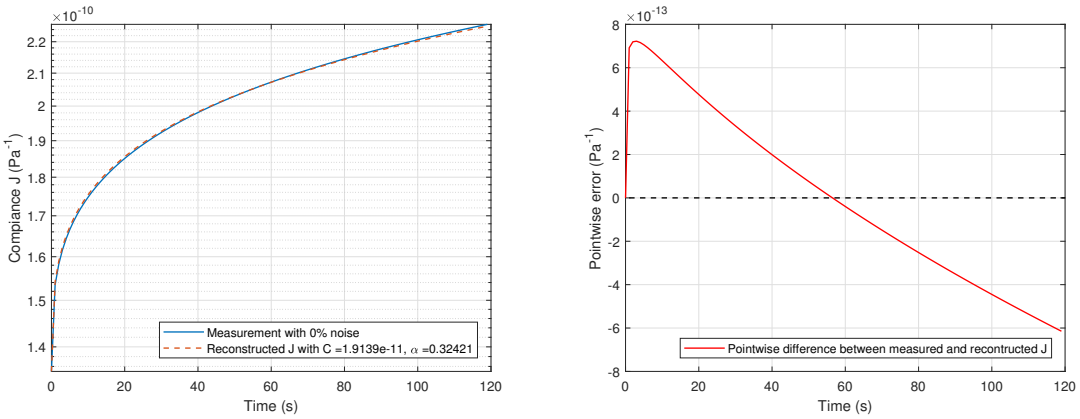

(a) (b)

Figure 4.3: (a) Plot of 'exact' and reconstructed compliance function obtained by Tikhonov regularization method. Parameters are reported to be $C = 1.9139 \times 10^{-11}$ and $\alpha = 0.32421$ (b) Pointwise error.

addition, the compliance curve generated by this method tends to be more concave compared to the test compliance data. Obviously, the steep gradient of the compliance near the origin has a strong impact on the accuracy of the approximation. In other words, a small deviation in compliance data in the first few seconds would give a large error in the approximation. As for Tikhonov regularization, the solutions tend to underestimate the test data as observed in Fig. 4.3a when time passes 70s, while the curve obtained by truncated SVD tends to overestimate when time passes 2s. This shows a disagreement between the numerical solutions and the test data in a long time limit. However, the magnitude of errors is less than 0.1% indicating that the models are still good in a short time regime.

Table 2: Constant C and the exponent α obtain by scheme of SVD truncation and Tikhonov regularization for estimating the compliance data of different Gaussian noise variance levels.

Method	Noise %	Constant C	Exponent α	Error %
'fit' command	0	$1.8448 \cdot 10^{-11}$	0.33	5.32×10^{-14}
	1	$1.8314 \cdot 10^{-11}$	0.34	0.11
	2	$1.7121 \cdot 10^{-11}$	0.35	0.38
	5	$1.3478 \cdot 10^{-11}$	0.41	1.49
	10	$3.3212 \cdot 10^{-11}$	0.18	3.95
Truncated SVD	0	$1.9139 \cdot 10^{-11}$	0.32	6.11×10^{-13}
	1	$1.8478 \cdot 10^{-11}$	0.33	0.09
	2	$1.7983 \cdot 10^{-11}$	0.34	0.01
	5	$1.8787 \cdot 10^{-11}$	0.33	0.81
	10	$2.0448 \cdot 10^{-11}$	0.30	4.05
Tikhonov regularization	0	$1.9139 \cdot 10^{-11}$	0.32	0.17
	1	$1.9374 \cdot 10^{-11}$	0.32	0.14
	2	$1.9263 \cdot 10^{-11}$	0.32	0.05
	5	$1.819 \cdot 10^{-11}$	0.34	1.04
	10	$1.9198 \cdot 10^{-11}$	0.31	3.75

When noise is added to the test compliance, the study shows that the '`fit`' command and Tikhonov regularization are sensitive to noisy data compared to singular value truncation method. The dependence of noise levels on the degree of accuracy of these models is summarised in table 2. In general, these techniques appear to be conceivably applicable to approximate the test data contaminated with the level of noise less than 5%. As noise level increases, these models tend to underestimate the data. In fact, the mean absolute percentage error is increasing almost linearly with the noise levels as observed in the last column of table 2. Among the three methods, the MATLAB '`fit`' command shows its limitation in estimating noisy data (see Fig. 4.4). In particular, when the noise level is over 5%, solutions obtained from this method do not show a tendency of converging to the 'exact' solution. On the contrary, singular value truncation and Tikhonov regularization methods are relatively stable when the test data oscillates with different variances as demontrated in Fig. 4.5 and 4.6.

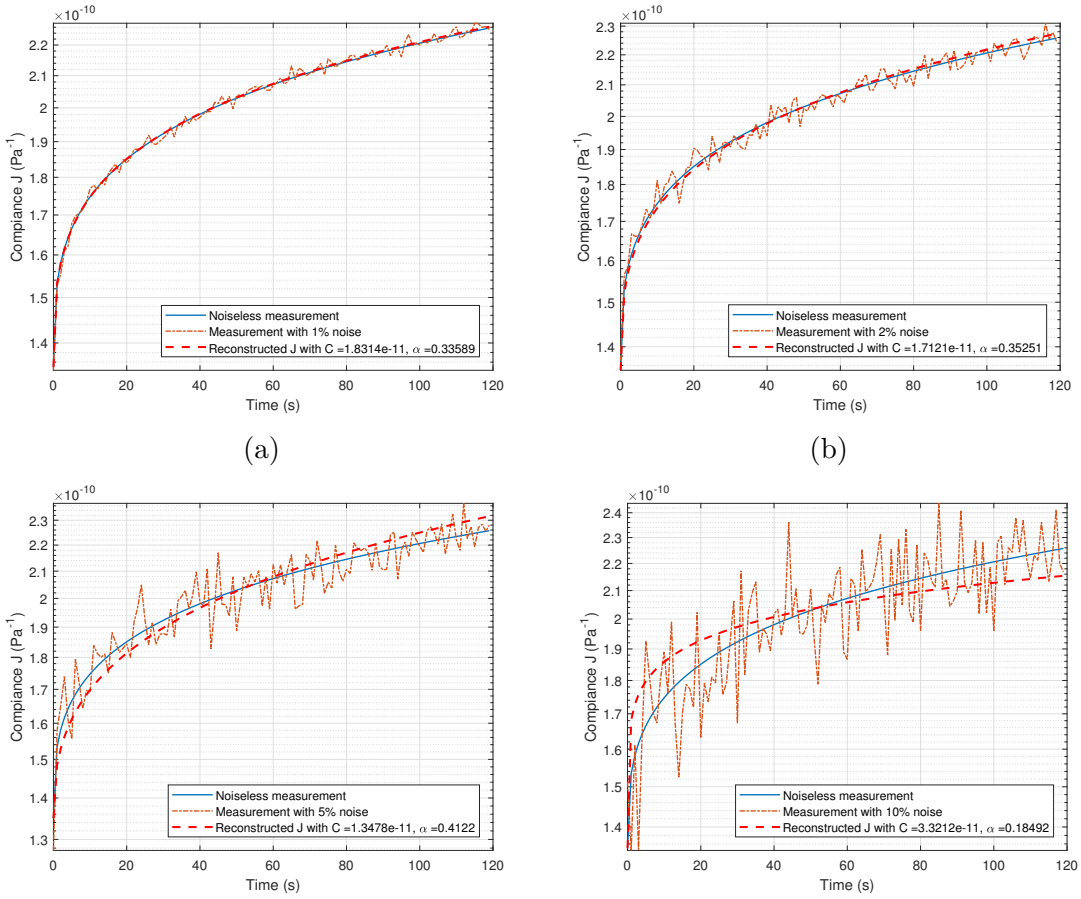

Figure 4.4: Estimated compliance functions obtained via the Power Law with 'fit' command. Gaussian noise of different variance was added to the simulated strain response data.

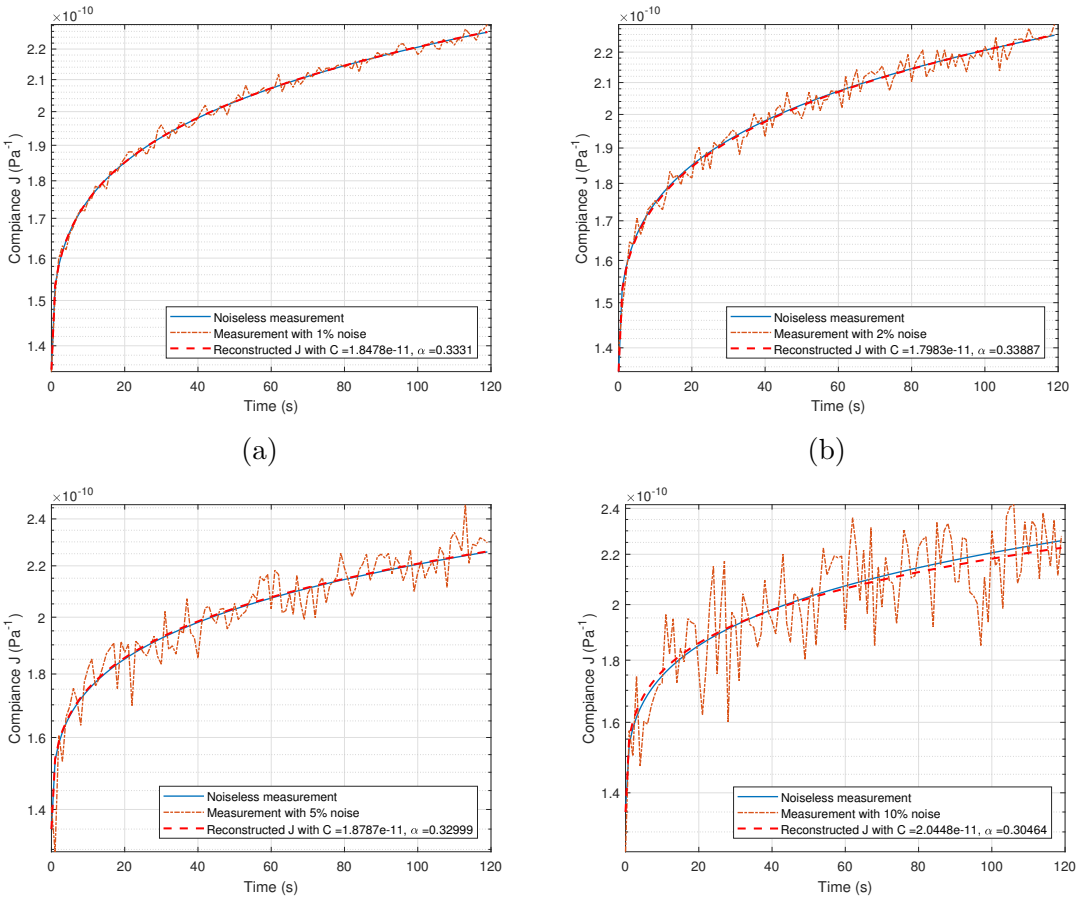

Figure 4.5: Estimated compliance functions obtained via the Power Law with SVD truncated model. Gaussian noise of different variance was added to the simulated strain response data.

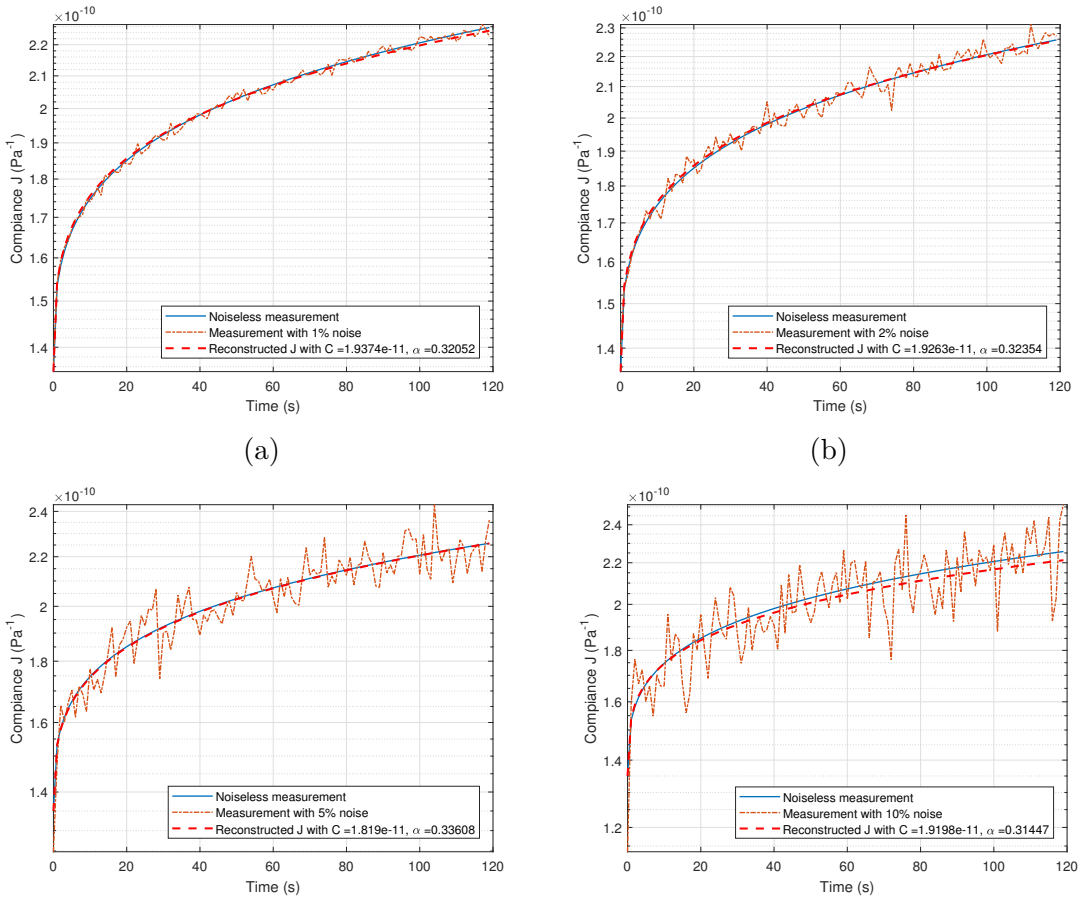

Figure 4.6: Estimated compliance functions obtained via the Power Law with Tikhonov regularization. Gaussian noise of different variance was added to the simulated strain response data.

4.1.2 Kelvin (Voigt) Model

The identification results of optimization algorithm for Kelvin (Voigt) model is reported in Fig. 4.7a, 4.7b. The dash blue curve represents the final outcome of the standard procedure wherein a total $N = 40$ retardation times were employed. The procedure produces 3 significant retardation strength values and the other strength values turn out to be zero. The set of chosen retardation times forms the basis for the identification of the unknown parameters. It is evident that the number of non-zero retardation strength values is strongly affected by the values of preselected retardation time τ. The creep curve, corresponding to the retardation strength, generally agrees well with the exact compliance data in Fig. 4.7a. Upon observation, the shape of the estimated compliance is of greater curvature and the curve shows a tendency to stabilize or to converge after $t = 100s$. The pointwise value differences between the exact and estimated data plotted in Fig. 4.7b shows that the Kelvin model underestimates the values of compliance in the first 40s and the last 20s. The largest error recorded in the first few seconds suggests poor accuracy when the compliance experiences a steep gradient at the origin.

Upon examination, Fig. 4.8 shows that the approximate creep curves are very similar to each other for different perturbation levels. It demonstrates stability of the method with respect to perturbations of the data. Observe that at all noise levels, the largest difference appears during the initial rapid growth period of the compliance function. In contrast to the Power Law model, the mean absolute percentage error observed in this model does not grow proportionally to the increase of noise.

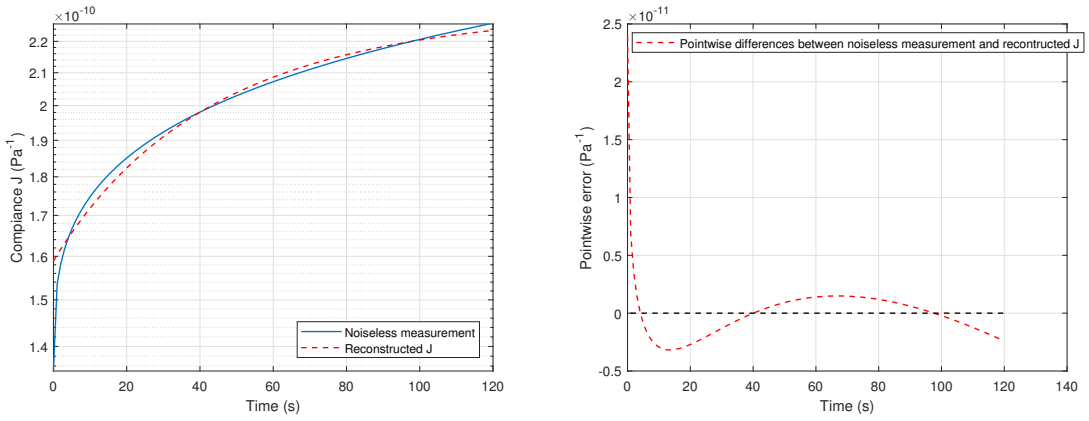

(a) (b)

Figure 4.7: (a) Plot of the 'exact' and the reconstructed compliance functions obtained by Kelvin (Voigt) model. (b) Pointwise error. The visualised times are limited to 120s.

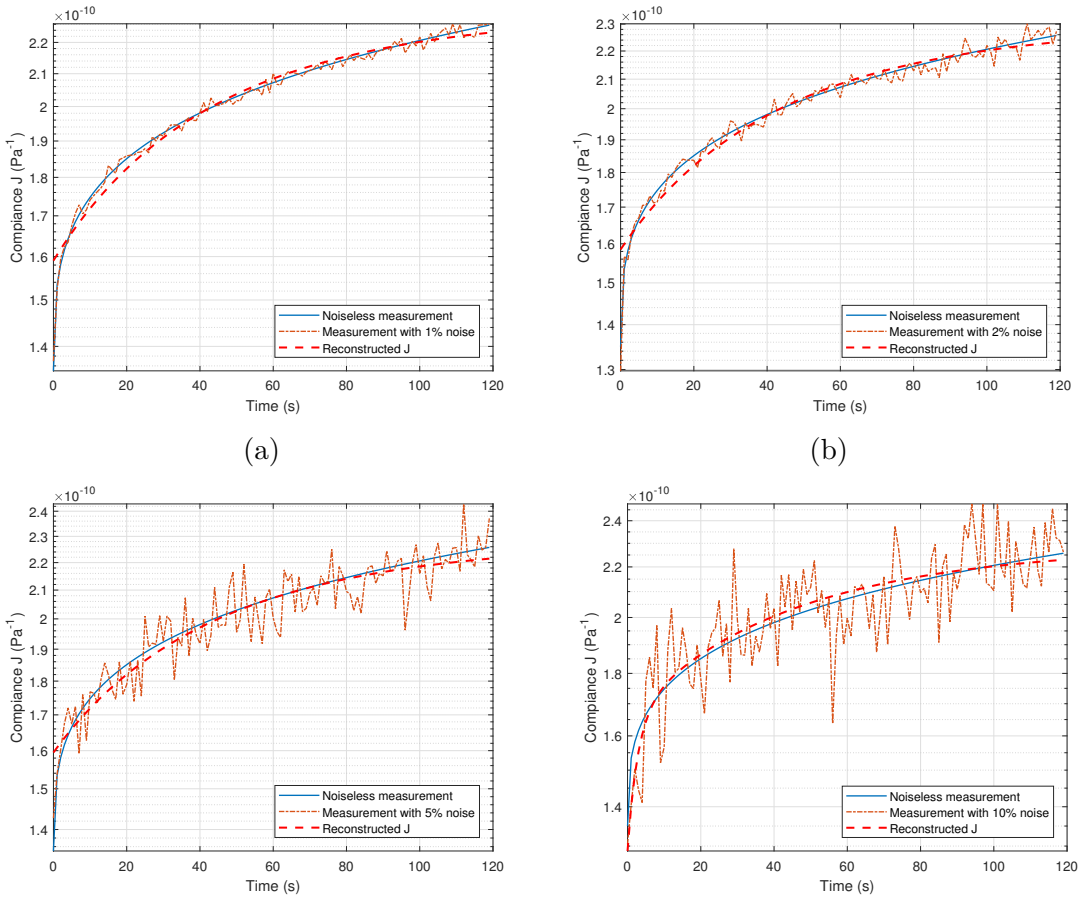

Figure 4.8: Estimated compliance functions obtained via the Kelvin model with nonnegative least squares method. Gaussian noise of different variance was added to the simulated strain response data.

4.2 Predicting experimental compliance and strain responses

4.2.1 Compliance functions

In this section, we present the results of applying the schemes to determine parameters of the compliance function from experimentally obtained data for loading and strain responses. The ice specimen with volume of $60 \times 30 \times 10$ cm^3 was cut from at sheet of lab-grown S2 saline ice at the Ice Tank located at Aalto University. The creep test was performed for a period of 100s with the magnitude of the applied stress was 0.3MPa. The loading and unloading stress rate was 0.3MPa/s. The instantaneous creep compliance value was measured to be 27.027×10^{-9} Pa^{-1} which is the reciprocal of the Young's modulus of 3.7GPa. This value of the instantaneous creep compliance is used for all of the tests in this project. The procedure of estimating the compliance function is as described in the preceding sections, where the schemes were tested on numerically generated data. As before, the Power Law model is considered first, and then the Kelvin model.

Fig. 4.9 presents plots of creep compliance as function of time. The plots indicate that, when it comes to the Power Law model, the truncated singular value decomposition scheme and the Tikhonov regularization technique give the most reliable compliance function values, compared to the other two schemes. This fact corresponds well with the observations made in Sec. 4.1 where the schemes were compared when applied to computer simulated data. While the truncated SVD and Tikhonov regularization appear to be indistinguishable in terms of accuracy of prediction, the former scheme is more practical. The reason being, that with SVD we can utilize the Matlab built-in backslash routine, which is optimized in a number of parameters, whereas Tikhonov regularization is sensitive to the choice of a regularization parameter. Kelvin model, as seen in Fig. 4.9d, also produces relatively good reconstruction, only underestimating values of the compliance at the start of measurement, as expected (see Sec. 4.1.2).

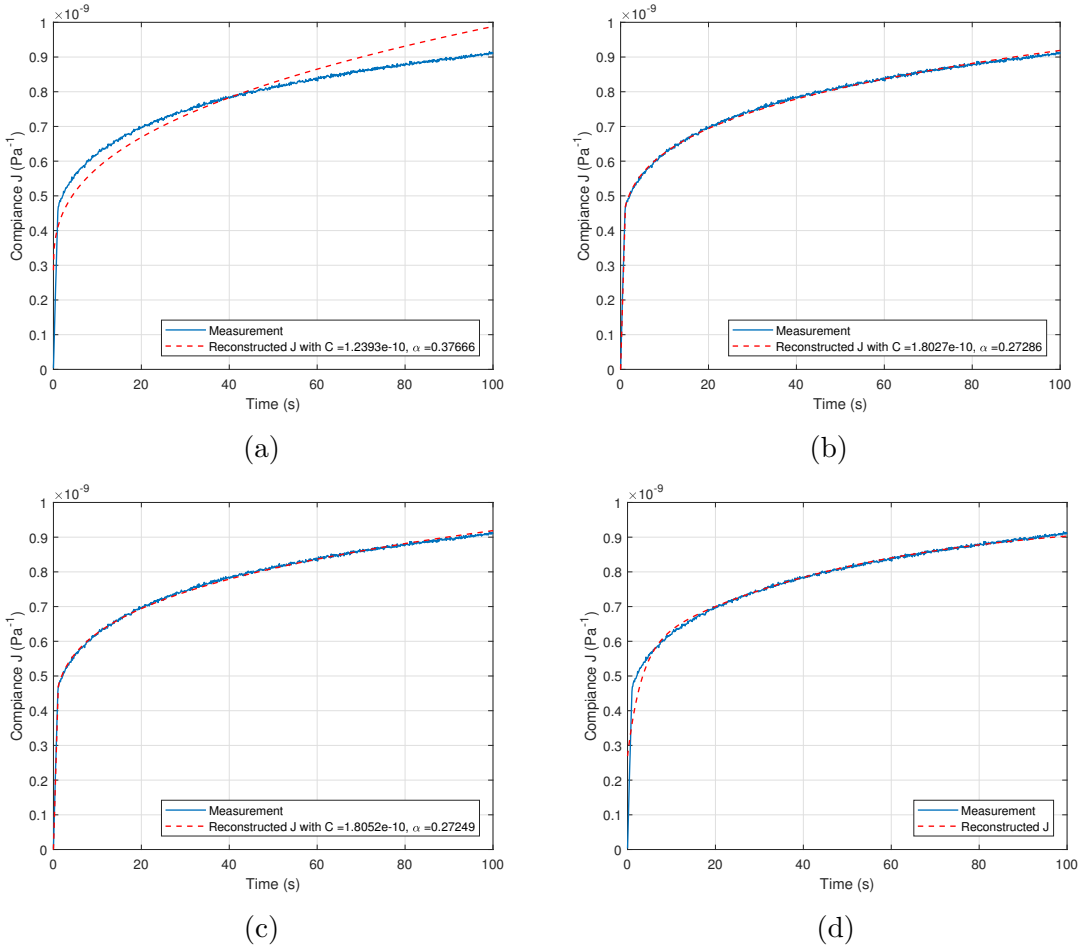

Figure 4.9: Estimated compliance curves obtained by Power Law model (through (a) by 'fit' command, (b) by SVD truncated method, (c) Tikhonov regularization method) and by generalized Kelvin model (through (d) nonnegative least squares method).

4.2.2 Predicting experimental strain responses

The compliance function parameters obtained from the SVD for the Power Law model, as well as the values obtained from the Kelvin model, were then utilized in order to predict the strain response to a given stress loading. Predicted values of strain response are also to be compared with the measured response.

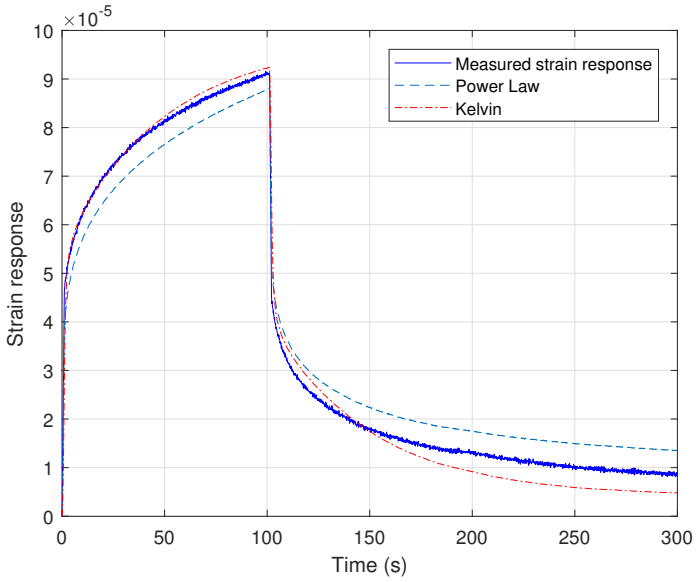

(a)

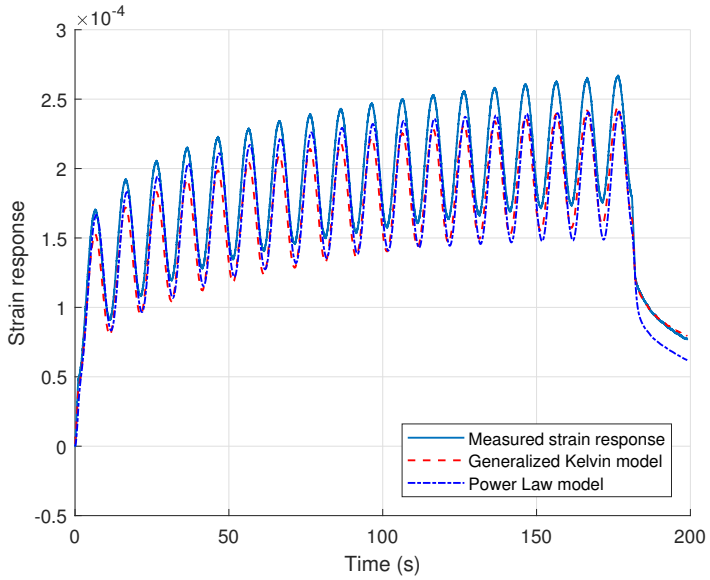

(b)

Figure 4.10: Experimental strain response versus the predicted strain response according to the Power Law and the Kelvin model, in case of (a) static and (b) cyclic loading cases.

In order to apply the above techniques in practice, we used a creep-recovery test wherein a stress is applied to a specimen with the loading speed of 0.1MPa/s until the stress reaches a level of 0.1MPa at which it is held for 100s; then the specimen is unloaded with the same velocity. The measured strain response together with the approximation from Power Law and Kelvin model are plotted in Fig. 4.10a. In general, the Kelvin model shows better agreement with the material response than the Power Law. The Power law tends to underestimate the strain response during the creep period but overestimates it during the recovery period. In contrast, the Kelvin model performs well in predicting the strain response during the creep phase even though it underestimates the strain response during the recovery time.

Furthermore, the same models were used to predict the strain response in case of a cyclic loading. The load was applied with a magnitude of 0.2MPa and angular frequency of $0.1s^{-1}$. Fig. 4.10b presents the results obtained from the two methods together with the strain response. Both models appear to underestimate the strain

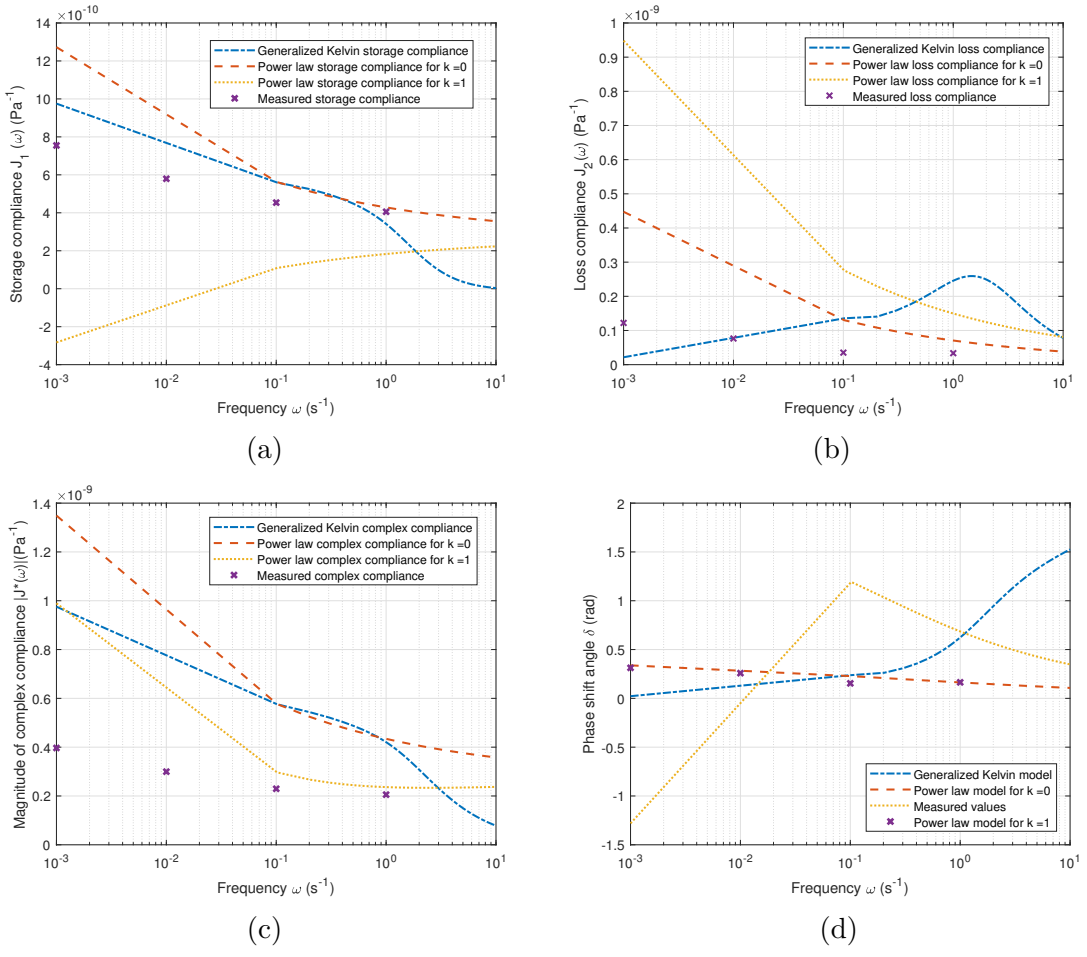

Figure 4.11: Experimental complex compliance data and estimated complex compliances by Power Law and Kelvin model. (a) Storage compliance, (b) loss compliance, (c) magnitude of complex compliance, and (d) phrase shift angle.

response. In general, the Power Law model shows better agreement with the material response than the Kelvin model does. The Power Law appears to be exceptionally accurate during the first loading cycle; however, after that the accuracy deteriorates toward the end of the experiment. Overall, both models capture the cyclic nature of strain response, its approximate values and shape of its graph. The mismatch between the prediction and the measurement can be explained by linear nature of the models, whereas the observed phenomena are highly nonlinear. Other factors contributing to errors are random noise in measurements as well as inaccuracies in algorithms used to treat and analyze data.

In case of both creep-recovery and cyclic loading, the reason behind the mismatch between predicted values of strain response and measured ones is that creep test was run for relatively short times. Normally, creep tests are to be executed over the span of hours, if not longer. This is dictated by the viscoelastic nature of ice.

Harmonic retardation or complex compliance derived from the Power Law and Kelvin models are illustrated by Fig. 4.11 displays . The figures present complex compliance at four different frequencies, ranging from $0.001s^{-1}$ to $1s^{-1}$. The storage J_1 and loss compliance J_2 are plotted as functions of frequency as demonstrated in Fig. 4.11a and Fig. 4.11b respectively. The associated complex compliance $|J^*|$ as a function of frequency is depicted in Fig.4.11c and phrase shift angle δ in Fig. 4.11d. As seen from the Fig. 4.11a and 4.11b, the Power Law with $k = 0$ returns negative values for the storage compliance, which is not physically possible, therefore we disregard this solution. In general, results shown in Fig. 4.11 indicate that the complex compliance predicted by the Kelvin model is closer in magnitude to the measured values, however, interestingly, the Power Law appears to much better capture the overall trend of compliances as function of frequency, as well as its monotonicity and convexity. In discussion of the harmonic retardation or complex compliances derived from the two models Power Law and Kelvin, from the preceding result, the two identification methods provide excellent approximations of the compliance data in the time range of experiment.

5 Conclusions

With the purpose of studying the nature of sea ice, we performed a literature survey on the topic of polycrystalline sea ice; for this project, the S2 ice was of particular interest. A review of relevant literature and work done in the field was presented. Linear viscoelastic behavior of ice was described from the continuum-mechanical point of view and four equivalent representations of the constitutive relation were examined. As the major objective was to develop and research on ways of predicting strain response from a given loading of ice, material functions in the constitutive relations play the key role.

The focus was set on the examination of the creep compliance function, which is one possible link between stress and strain. Specifically, two analytical models for the compliance function were discussed: the Power Law model and the Generalized Kelvin model. In order to meet the main goal of current work, we applied various numerical techniques to approximate the analytical forms of the compliance function. These numerical schemes allowed us to formulate and to solve the problem of determining the ice compliance function based on measured stress and strain response. Once the parameters that constitute approximate forms of the compliance function were established, the numerical schemes were compared on the basis of how well the compliance function that they produce predicts the strain response of ice.

In order to test the accuracy of these numerical schemes, both computer-simulated measurement data and experimentally recorded data were used. Experimental part of this project consisted of creep tests and loading/unloading creep cycles at various stress rates and frequencies; experiments were performed on lab-grown S2 sea ice. Overall, the numerical methods were shown to determine the parameters of the approximate forms of compliance function rather well. Both in case of computer-simulated measurements and in case of experiments, the truncated Singular Value Decomposition technique demonstrated optimal results with highest accuracy in predicting the strain response.

The continuation of current work may lie in conducting more experiments, and over longer stretches of time, in order to ensure better accuracy of measurements. In addition, it would be important to devise a technique for determining optimal values of retardation times τ_k of the Power Law model to be used with the non-negative least squares method. Unless it is done, this method is not reliable in computing parameters of the compliance models.

References

Anderson, D. L., & Weeks, W. F. (1958). A theoretical analysis of sea-ice strength. *Eos, Transactions American Geophysical Union*, *39*(4), 632–640.

Anderssen, R. S., & Davies, A. (2001). Simple moving-average formulae for the direct recovery of the relaxation spectrum. *Journal of Rheology*, *45*(1), 1–27.

Baumgaertel, M., & Winter, H. (1989). Determination of discrete relaxation and retardation time spectra from dynamic mechanical data. *Rheologica Acta*, *28*(6), 511–519.

Brinson, H. F., & Brinson, L. C. (2015). *Polymer engineering science and viscoelasticity: An introduction*. Springer.

Carrot, C., & Verney, V. (1996). Determination of a discrete relaxation spectrum from dynamic experimental data using the pade-laplace method. *European polymer journal*, *32*(1), 69–77.

Cheneler, D. (2016). Viscoelasticity of polymers: Theory and numerical algorithms. *APPLIED RHEOLOGY*, *26*(4), 10–52.

Christensen, R. (2012). *Theory of viscoelasticity: an introduction*. Elsevier.

Davies, A., & Goulding, N. (2012). Wavelet regularization and the continuous relaxation spectrum. *Journal of Non-Newtonian Fluid Mechanics*, *189*, 19–30.

Elster, C., & Honerkamp, J. (1991). Modified maximum entropy method and its application to creep data. *Macromolecules*, *24*(1), 310–314.

Gonzalez, O., & Stuart, A. M. (2008). *A first course in continuum mechanics*. Cambridge University Press.

Gurtin, M. E., & Sternberg, E. (1962). On the linear theory of viscoelasticity. *Archive for Rational Mechanics and Analysis*, *11*(1), 291–356.

Hiel, C., Cardon, A., & Brinson, H. (1984). Viscoelastic modelling of epoxy-resins for adhesive and composite applications.

Honerkamp, J., & Weese, J. (1989). Determination of the relaxation spectrum by a regularization method. *Macromolecules*, *22*(11), 4372–4377.

Kaipio, J., & Somersalo, E. (2006). *Statistical and computational inverse problems* (Vol. 160). Springer Science & Business Media.

LeClair, E., Schapery, R., & Dempsey, J. (1999). A broad-spectrum constitutive modeling technique applied to saline ice. *International journal of fracture*, *97*(1-4), 209.

Liu, Y. (1999). Calculation of discrete relaxation modulus and creep compliance. *Rheologica acta*, *38*(4), 357–364.

Luo, R., Liu, H., & Zhang, Y. (2016). Characterization of linear viscoelastic, nonlinear viscoelastic and damage stages of asphalt mixtures. *Construction and Building Materials*, *125*, 72–80.

Mainardi, F. (2010). *Fractional calculus and waves in linear viscoelasticity: an introduction to mathematical models*. World Scientific.

Mainardi, F., & Spada, G. (2011). Creep, relaxation and viscosity properties for basic fractional models in rheology. *The European Physical Journal Special Topics*, *193*(1), 133–160.

Mainardi, F., & Spada, G. (2012). On the viscoelastic characterization of the jeffreys–lomnitz law of creep. *Rheologica acta*, *51*(9), 783–791.

Murata, H. (2012). Rheology-theory and application to biomaterials. In *Polymerization*. InTech.

Riska, K. (2011). Ship-ice interaction in ship design: theory and practice. *Course Material NTNU*.

Shokr, M., & Sinha, N. (2015). *Sea ice: physics and remote sensing*. John Wiley & Sons.

Sinha, N. K. (1977). Technique for studying structure of sea ice. *Journal of Glaciology*, *18*(79), 315–324.

Sorvari, J., & Malinen, M. (2006). Determination of the relaxation modulus of a linearly viscoelastic material. *Mechanics of Time-Dependent Materials*, *10*(2), 125–133.

Staroszczyk, R. (2018). *Ice mechanics for geophysical and civil engineering applications*. Springer.

Thomas, D. N. (2017). *Sea ice*. John Wiley & Sons.

Tschoegl, N. W. (2012). *The phenomenological theory of linear viscoelastic behavior: an introduction*. Springer Science & Business Media.

Weeks, W., et al. (1998). Growth conditions and the structure and properties of sea ice. *Physics of ice-covered seas*, *1*, 25–104.

Weeks, W. F., & Ackley, S. F. (1986). The growth, structure, and properties of sea ice. In *The geophysics of sea ice* (pp. 9–164). Springer.

Weeks, W. F., & Gow, A. J. (1978). Preferred crystal orientations in the fast ice along the margins of the arctic ocean. *Journal of Geophysical Research: Oceans*, *83*(C10), 5105–5121.

A Function of Bounded Variation

A function $f : [a, b] \to \mathbb{R}$ is said to be of *bounded variation* if

$$\sup \sum_{i=1}^{n} |f(a_i) - f(a_{i+1})| < \infty \tag{A1}$$

where the supremum is taken over all nonoverlapping subintervals $[a_1, b_2], \cdots [a_n, b_n]$ of $[a, b]$. If a function is of bounded variation, it can be written as a difference of two increasing functions. Functions of bounded variation are almost everywhere differentiable but the fundamental theorem of calculus may fail for them.

B Laplace Transform

Laplace transform is a classical tool to study problems that are set in the half-line of positive real numbers with prescribed initial data. The most important property of the Laplace transformation is the fact that it works on functions with exponential growth, that is objects that cannot undergo the Fourier transform, neither in functional nor in the distributional setting. Definition Let $f : \mathbb{R} \to \mathbb{C}$ be a $\mathcal{L}$ transformable function, the the Laplace transform of f is the function F defined by

$$F(s) = \int_0^\infty e^{-zt} f(t)\, dt = \int_{\mathbb{R}} e^{-zt} f(t)\, dt \quad \text{for all } z \in \mathbb{C}. \tag{B1}$$

C The Dirac Delta Function

The Dirac delta function $\delta(t)$ can be obtained by scaling an integrable function g which satisfies

$$\int_{-\infty}^{\infty} g(t)\mathrm{d}t = 1. \tag{C1}$$

Let

$$g_\epsilon(t) = \frac{1}{\epsilon} g(\frac{1}{\epsilon}) \tag{C2}$$

A Dirac delta function can then be defined as the limit

$$\delta(t) = \lim_{\epsilon \to 0} g_\epsilon(t), \tag{C3}$$

with the property that for any continuous function f at the origin

$$\int_{-\infty}^{\infty} \delta(t) f(t) = f(0). \tag{C4}$$

The symbolic integral over a Dirac is useful notation because it has the same properties as a usual integral, including change of variables and integration by parts. A translated Dirac $\delta_t = \delta(t - u)$ has a mass centered at u and

$$\int_{-\infty}^{\infty} f(t)\delta(u - t)dt = f(u). \tag{C5}$$

D Matlab code

D.1 Preliminary functions

D.1.1 Simulated stress for a creep test

```
function [sigma, t] = teststress(value_at_t0, constant_value)
% Returning the simulated stress array for 120s
% In put
% value_at_t0: is value at t=0,
% constant_value: value of the constant stress
minute = 60;
t = linspace(0, 2*minute, 2*minute+1)';
sigma = zeros(length(t), 1);
sigma(t <= 2*minute) = constant_value;
sigma(t <= 0*minute) = value_at_t0;
end
```

D.1.2 Numerical generated creep compliance

```
function [J,time, res] = Num_Gen_Comp(J0 ,sigma, t)
% Return numerical generate compliance data.
% Input
% J0 : instantaneous creep compliance value
% sigma : M-by-1 array of stress value
% t  : M-by-1 array of time value
% Output
% J : N-by-1 array of ceep compliance value, N is the number of
% nozero term in stress vector.
% time : N-by-1 array of corresponding time value
S1 = 8e-25;
S2 = 8.25e-14;
sigma = sigma*1e6 ;% MPa to Pa
m = length(t);
e1 = J0*sigma;
e2 = zeros(m, 1);
e3 = zeros(m, 1);
dt = diff(t);
ds = diff(sigma.^(3/2))./dt;
for i = 1:m-1
e2(i+1) = e2(i) + sigma(i)^3*dt(i);
temp = 0;
for j = 1 : i
temp = temp + (t(i) - t(j))^(1/3)*ds(j)*dt(j);
end
e3(i+1) = temp;
```

```
end
res = e1 + S2*e3;
idx = find(sigma > 0);
J =  res(idx)./sigma(idx);
time =  t(1:length(J));
end
```

D.1.3 Kelvin compliance by nonnegative least squares method

```
function [Jk, J_const, J0, tau] = Kelvin_compliance(time,J_meas,N)

% Assembles the matrix for forward problem.
% Input:
% N          = degree of accuracy
% time       = M-by-1 vector of discrete measurement times
%starting from point t.
% J_meas     = M-by-1 vector of measured compliance data.
%  tau       = N-by-1 vector of retardation times.
% Output
% Jk         = (N+1)-by-1 vector of retardation strength
% J_const    = N-by-1 vector of constructed compliance data
% J0         = (scalar) Instantaneous compliance at t=0.
% tau

%%%%% CHOOSE A SUITABLE TAU VECTOR
lambda  = pi;
%tau_inv    = lambda * [1:N]'.^(-1) ;
%tau_inv = lambda * [1:N]'.^(-2) ;
%tau = 2.8*10.^([-4 : (N-5)])';
%tau_inv = lambda * rho.^[1:N]' ;
%tau = [ 1/(.2*pi); [1:N-2]' ;1/pi ];
%tau =  1./tau_inv;
%tau = 250*[1:N]'.^(-2);
%tau = (250 ./(2.^[1:N]))';
% tau = 50*[1:N]'.^(-2);
% tau = [50 6.25 3.12 0.7 0.617 0.1*ones(1,N-5)]';
tau = 50*[1:N]'.^(-4)
%tau = (50 ./(2.^[0:(N-1)]))';
%tau   = exp([-1.5 -1 0.5 0 0.5 1 1.5 2 3 20*ones(1,N-9)]')
%tau = [ 1/(.2*pi), 1./[1:1000], 1/(400*pi) ]';
Jmat    = time * (1./tau'); %create M x N - matrix of time/tau
Jmat    = -exp( -Jmat );    % matrix of- e^(-time/tau)
Jmat    = [ones(size(time)), Jmat]; % create (M+1) x N - matrix
Jk      = lsqnonneg(Jmat, J_meas) ; % nonnegative least square returns
% (N+1)- vector
```

```
J_const = Jmat*Jk;      % estimated/constructed compliance funtion
J0      = Jk(1) - sum(Jk(2:end)) ; % instantaneous compliance
% or compliance value at t=0.
end
```

D.1.4 Kelvin compliance by weighted nonnegative least squares method

```
function  [Jk, J_const, J0, tau] = ...
   Weighted_Kelvin_compliance(time, J_meas, N )
% Weighted Kelvin compliance
% Input
% N          = degree of accuracy
% time       = M-by-1 vector of discrete measurement times starting from
% point t.
% J_meas     = M-by-1 vector of measured compliance data.
%  tau       = N-by-1 vector of retardation times.
% Output
%%%%% CHOOSE A SUITABLE TAU VECTOR
lambda  = pi;
%tau_inv    = lambda * [1:N]'.^(-1) ;
%tau_inv = lambda * [1:N]'.^(-2) ;
%tau = 0.358*10.^([-4 : (N-5)])';
%tau_inv = lambda * rho.^[1:N]' ;
%tau = [ 1/(.2*pi); [1:N-2]' ;1/pi ];
%tau =  1./tau_inv;
%tau       = 250*[1:N]'.^(-2);
%tau = (250 ./(2.^[1:N]))';
%tau = (250 ./(2.^[0:(N-1)]))';
%tau = 10*[1:N]'.^(-2);
%tau = 50*[1:N]'.^(-2);
tau = (50 ./(2.^[0:(N-1)]))';
%tau = 250*[1:N]'.^(-2);
weight    = [time(2) - time(1); (time(3:end) - time(1:end-2));...
time(end) - time(end-1)]./(2); % weight vector
sqw       = sqrt(weight);              % square root of weight
b         = sqw.*J_meas;
expt      =  time * (1./tau');  %create M x N - matrix of time/tau
expt      = -exp( -expt);              % matrix of- e^(-time/tau)
Jmat      = [ ones(size(time)) expt ]; % create (M+1) x N - matrix
WJmat     = bsxfun(@times, sqw, Jmat); % elementwise multiplication
   % of column vectors of matrix
Jk        = lsqnonneg(WJmat, b); % nonnegative least squares...
% return (N+1)- vector
J_const   = Jmat*Jk;  % estimated/constructed compliance funtion
J0        = Jk(1)-sum(Jk(2:end)); % instantaneous compliance...
```

```
% or compliance value at t=0.
end
```

D.1.5 Power Law compliance by Matlab 'fit' command

```
function [C, n, J_const] = PL_fit(J0, J_meas, time)
% Returning the creep compliance estimate by Matlab fit command
% Input
% time       = M-by-1 vector of discrete measurement time.
% J_meas     = M-by-1 vector of measured compliance data.
% J0         = (scalar) Instantaneous compliance at t=0.
% Output
% C          = scalar
% n          = power law exponent
% J_const    = M-by-1 vector of constructed compliance data

J        = J_meas - J0;
fo = fitoptions('Method','NonlinearLeastSquares',...
'Lower',[0,0])

curvefit = fit(time(10:end),J(10:end),'power1',fo);
C        = curvefit.a;

n        = curvefit.b;
J_const  = J0 + C*time.^n; % reconstructing compliance function
end
```

D.1.6 Power Law compliance by truncated SVD method

```
function [C, alpha, J_const] = PL_SVD(J0,J_meas, time, idx)
% Returning the creep compliance estimate by truncated SVD method
% Input
%J0  = the instantaneous creep value at t = 0,
%J_meas = N-by-1 array of measured creep data
%time  = N-by-1 array of measured time data
% idx  = the index where the stress obtains the constant value
%Output
% C   = the constant value
% alpha = the power law exponent
% J_const= N-by-1 array of creep compliance data
% Take logarithms
J_meas  = J_meas - J0;
x_log   = log(time(idx+10: end)); % Ignore the linear region
y_log   = log(J_meas(idx+10:end));
% Build matrix A
A       = [ ones(size(y_log)), x_log ];
```

```
[U S V] = svd(A);
d       = diag(S);
Sp      = zeros(size(S))'; % Relocate the pseuoinverse of S
dp      = 1./d;
Sp(1:length(d),1:length(d)) = diag(dp);
% Place the inversed singular values
% on the diagonal
Ap      = V*Sp*U';
x       = Ap*y_log;
alpha   = x(2) ;
C       = exp(x(1))  ;
if idx <=1
J_const = J0+ C*time.^alpha;
else
speed   = (J0+ C*time(idx).^alpha)/(time(idx));
J_const =[time(1:idx)*speed  ; J0+ C*time(idx+1:end).^alpha];
end
end
```

D.1.7 Power Law compliance by Tikhonov regularisation method

```
function [C, alpha, J_const] = PL_Tik_reg(J0,J_meas, time, idx)
% Returning the creep compliance estimate
%   by Tikhonov regularisation method
% Input
%J0  = the instantaneous creep value at t = 0,
%J_meas = N-by-1 array of measured creep data
%time  = N-by-1 array of measured time data
% idx  = the index where the stress obtains the constant value
%Output
% C   = the constant value
% alpha = the power law exponent
% J_const= N-by-1 array of creep compliance data
% Take logarithms
J_meas  = J_meas - J0;
x_log   = log(time(idx+1: end)); % Ignore the linear region
y_log   = log(J_meas(idx+1:end));
% Build matrix A
A       = [ ones(size(y_log)), x_log ];
moro2 =0.1^2;           % Mozorov discrepancy principle parameter
y_aug = [ y_log ; zeros(2,1)]; % Stacked form of the emasurement date
delta = moro2 ; % Initial guess for the regularisation parameter
K = [A; sqrt(delta)*eye(2)] ; % Stacked form of the Tikhonov operator
x = K\y_aug; %backflash Tikhonov regularised solution
alpha   = x(2) ;
```

```
C       = exp(x(1))  ;
if idx <=1
J_const = J0+ C*time.^alpha;
else
speed   = (J0+ C*time(idx).^alpha)/(time(idx));
J_const =[time(1:idx)*speed  ;
J0+ C*time(idx+1:end).^alpha];
end
end
```

D.1.8 Strain response by Power Law model

```
function  strain = PL_Strain_response(stress,time,J0,C,n)
%Return strain response from an input stress by Power Law model
%Input
%stress= N-by-1 array of stress value
%t     = N-by-1 array of time value
%J0    =instantaneous creep compliance value
%C     = Power Law constant value
%alpha = Power Law exponent
%Output
% strain = N-by-1 array of strain value

M = length(t);
stress = stress*1e6;
strain = J0*stress;
delt = t(2) - t(1);
dj   = diff(J0 + t.^alpha);
dt   = diff(t);
for i = 1:M
temp = stress(i:-1:1);
for s_idx = 1:i-1
temp(s_idx) = temp(s_idx) * dj(s_idx)/dt(s_idx);
end
strain(i) = strain(i) + C*trapezoidal(temp, delt);
end
end
```

D.1.9 Strain response by generalised Kelvin model

```
function strain = Kelvin_Strain_response(stress,time,tau,Jk, J0)
%Input
% stress      = M-by-1 vector of stress in Pa
% tau         = N-by-1 vector of retardation times.
% Jk          = (N+1)-by-1 vector of creep compliance strength data.
% Output
```

```
M           = length(time) ;% Number of integration points.
delt        = time(end)/(M-1); % Delta t.
%strain      = (Jk(1)- sum(Jk(2:end)))*stress;
stress = stress*1e6;
strain      = J0*stress;
for i       = 1:M
temp    = stress(i:-1:1);
for s_idx = 1:i
s     = (s_idx-1)*delt;
temp(s_idx)  = temp(s_idx) * (sum(Jk(2:end).*exp(-s./tau)./tau));
end
strain(i) = strain(i) + trapezoidal(temp, delt);
end
end
```

D.1.10 Complex/Dynamic compliance by generalised Kelvin model

```
function [J1, J2, J_omega, delta] = Dynamic_K_compliance(Jk,tau,omega)
% Input
% Jk    = (N+1)-by-1-vector discrete compliance strength
% tau   =  N-by-1-vector retardation time
% omega =  M-by-1 -vector frequence
% Output
% J1    = M-by-N vetor of storage compliance
% J2    = M-by-N vetor of loss compliance
% J_omega = M-by-N vetor of magnitude of complex compliance
% delta = M-by-N vetor of phase shift angle in rad.

if(length(omega) <= 1) % If omega is a scalar then do
S1      = 0;
S2      = 0;
for i   = 1: length(tau)
S1      = S1 + (Jk(i+1)*tau(i)^2*omega^2/(1+omega^2*tau(i)^2));
S2      = S2 + (Jk(i+1)*tau(i)*omega/(1+omega^2*tau(i)^2));
end
J1       = Jk(1)- S1 ; % Storage compliance
J2       = S2 ;               % Loss compliance
J_omega  = sqrt(J2^2 + J1^2); % Magnitude of the complex compliance
delta    = atan(J2/J1) ;      % Phase shift angle in rad

else            % If omega is a vector, do

J1       = zeros(size(omega));
J2       = zeros(size(omega));
for j   = 1: length(omega)
```

```
S1       = 0;
S2       = 0;
for n = 1: length(tau)
S1       = S1 + (Jk(n+1)*tau(n)^2*omega(j)^2/(1+omega(j)^2*tau(n)^2));
S2       = S2 + (Jk(n+1)*tau(n)*omega(j)/(1+omega(j)^2*tau(n)^2));
end
J1(j)    = Jk(1)- S1;  % Storage compliance vector of length N-by-1
J2(j)    = S2;         % Loss compliance vector of length N-by-1
end
J_omega  = sqrt(J1.^2+ J2.^2);   % Magnitude of the complex compliance
% vector of length N-by-1
delta    = atan(J2./J1) ;        % Phase shift angle in rad
% vector of length N-by-1
end
end
```

D.1.11 Complex/Dynamic compliance by Power Law model

```
function [J1, J2, J_omega, delta]  = Dynamic_PL_compliance(C,n,J0,k,omega)
% Input
% C     = constant
% n     = power law exponental constant number
% J0    = instantaneous creep compliance
% omega = N-by-1 -vector frequence
% k     = M-by-1 vector of cycle
% Output
% J1    = N-by-M vetor of storage compliance
% J2    = N-by-M vetor of loss compliance
% J_omega = N-by-M vetor of magnitude of complex compliance
% delta = N-by-M vetor of phase shift angle in rad.


J1         = zeros(length(omega), length(k));
J2         = zeros(length(omega), length(k));
J_omega    = zeros(length(omega), length(k));
delta      = zeros(length(omega), length(k));
for      i =1 : length(omega)
for  j = 1:length(k)
J1(i,j)    = J0 + C * omega(i)^(-n) * gamma(n+1)...
*cos(n*pi*(2*k(j) +0.5));% Storage compliance vector of length N-by-M
J2(i,j)    = C * omega(i)^(-n) * gamma(n+1) * sin(n*pi*(2*k(j) +0.5));
% Loss compliance vector of length N-by-M
J_omega(i,j)= sqrt(J1(i,j).^2+ J2(i,j).^2);
% Magnitude of Complex compliance vector of length N-by-M
delta(i,j) = atan(J2(i,j)./J1(i,j));
```

```
% Phase shift angle in rad vector of length N-by-M
end
end
end
```

D.1.12 Error estimate

```
function [ error] = Error_estimate(True, Estimate)
% Input
% True      = N-by-1-vector of true data
% Estimate  = N-by-1-vector of estimated data
% Output
% error      = 1-by-1 scalar of percentage root mean square error
N    = length(True) ;
error = 100* sqrt( (sum(True - Estimate))^2 /N) ;
% Root mean square deviation
end
```

D.1.13 Numeriacal Trapezoidal integration

```
function res = trapezoidal(y, dx)
%%% This function assumes that the values of function have been evaluated
%%% using constant time step.
%%%     y  = function values
%%%     dx = step size
if(length(y) <= 1) % If only one sample, integral is zero
res = 0;
% Else apply the trapezoidal rule
else
y(2:end-1) = 2*y(2:end-1); % Double each element except for
% the first and the last sample
res        = dx*sum(y)*.5; % Compute the integral
end
end
```

D.2 Compliance studies

```
%% Kelvin compliance studies
close all; clear all;
%Generating compliance data
J0          = 13.5e-11; % Instantaneous compliance,
% where E is Young Modulus
[sigma, t]  = teststress(0,.05) ; % Numerically generate stress
[J_noiseless,time, noiseless_strain] = Num_Gen_Comp(J0 ,sigma, t) ;

N           = 40;                     % Degree of accuracy
```

```
noise       = [0 0.01 0.02 0.05 0.1]; % Noise array
Err         = zeros(size(noise));     % Error array
for k = noise     % let k run through component of noise vector
if k ==0      % if k = 0, return noise less compliance data
[K_jk, J_K, K_J0, tau] = Kelvin_compliance(time,J_noiseless,N) ;
Diff        = J_K - J_noiseless ; % pointwise difference between
% true J and constructed J
MAPE        = Error_estimate(J_noiseless,J_K); % Mean absolute
Err(find(noise == k))  = Error_estimate(J_noiseless, J_K);
% Plot results
figure()
semilogy(time,J_noiseless,'-', 'LineWidth',1),hold on, grid on
semilogx(time,J_K, 'r--','LineWidth',1);hold off
xlabel('Time (s)')
ylabel('Compiance J (Pa^{-1})')
legend('Noiseless measurement','Reconstructed J',...
'Location', 'SouthEast')
% Plot pointwise difference
figure ()
plot(time,Diff,'r--','LineWidth',1); hold on;
plot(zeros(size(t)),'--k','LineWidth',1);grid on;hold off
xlabel('Time (s)');ylabel('Pointwise error (Pa^{-1})')
legend('Pointwise differences between noiseless measurement...
 and recontructed J','Location', 'SouthEast')

else   % if k differs than 0, return noisy compliance data
J_noisy = J_noiseless + k*min(J_noiseless)*randn(size(J_noiseless));
% Add noise
[Jk, J_K, J0, tau] = Kelvin_compliance(time,J_noisy,N);
Err(find(noise == k))  = Error_estimate(J_noiseless, J_K);
% Plot results
figure()
semilogy(time,J_noiseless,'-', 'LineWidth',1), hold on, grid on
semilogy(time,J_noisy,'-.', 'LineWidth',1)
semilogx(time,J_K, 'r--','LineWidth',1.5)
xlabel('Time (s)')
ylabel('Compiance J (Pa^{-1})')
legend('Noiseless measurement',...
['Measurement with ',num2str(k*100),'% noise' ],...
'Reconstructed J ',...
'Location', 'SouthEast')
end
end
% Plot RMSD
figure ()
```

```
plot(noise*100,Err,'r--<','LineWidth',1);
strValues = strtrim(cellstr(num2str(Err(:))));
text(noise*100,Err,strValues,'VerticalAlignment','top');
grid on
xlabel('Noise level (%)') ; ylabel('Error (%)')
legend('Mean absolute percentage error',...
'Location', 'SouthEast')

%% Power Law compliance study - 'Fit' command
close all; clear all;
%Generating compliance data
J0          = 13.5e-11; % Instantaneous compliance,
% where E is Young Modulus
[sigma, t]  = teststress(0,.05) ; % Numerically generate stress
[J_noiseless,time, noiseless_strain] = Num_Gen_Comp(J0 ,sigma, t) ;
noise = [0 0.01 0.02 0.05 0.1];
Err   = zeros(size(noise));
for k = noise % let k run through component of noise vector
idx = 1;
if k == 0
[C, alpha, PL_J] = PL_Tik_reg( J0,J_noiseless, time, idx);
Diff             = PL_J - J_noiseless; % Pointwise differences
Err(noise == k)  = Error_estimate(J_noiseless, PL_J);

figure()
semilogy(time,J_noiseless,'-', 'LineWidth',1), hold on, grid on
semilogx(time,PL_J, 'r--','LineWidth',1);hold off
xlabel('Time (s)')
ylabel('Compiance J (Pa^{-1})')
legend('Noiseless measurement',...
['Reconstructed J with C =',num2str(C), ', \alpha =', num2str(alpha)],...
'Location', 'SouthEast')
% Plot pointwise difference
figure ()
plot(time,Diff,'r--','LineWidth',1); hold on;
plot(zeros(size(t)),'--k','LineWidth',1);grid on;hold off
xlabel('Time (s)');ylabel('Pointwise error (Pa^{-1})')
legend('Pointwise differences between noiseless measurement...
 and recontructed J', 'Location', 'SouthEast')

else
J_noisy = J_noiseless + k*mean(J_noiseless)*randn(size(J_noiseless));
% Add noise
[C, alpha, PL_J] = PL_Tik_reg( J0,J_noisy, time, idx);
Err(noise == k)  = Error_estimate(J_noiseless, PL_J);
```

```
% Plot results
figure()
semilogy(time,J_noiseless,'-', 'LineWidth',1), hold on, grid on
semilogy(time,J_noisy,'-.', 'LineWidth',1)
semilogx(time,PL_J, 'r--','LineWidth',1.5)
xlabel('Time (s)')
ylabel('Compiance J (Pa^{-1})')
legend('Noiseless measurement ',...
['Measurement with ', num2str(k*100),'% noise'],  ...
['Reconstructed J with C =',num2str(C), ', \alpha =', num2str(alpha)],...
'Location', 'SouthEast')
end
end
% Plot RMSD
figure ()
plot(noise*100,Err,'r--<','LineWidth',1);
strValues = strtrim(cellstr(num2str(Err(:))));
text( noise*100,Err,strValues,'VerticalAlignment','top');
grid on
xlabel('Noise level (%)') ; ylabel('Error (%)')
legend('Mean absolute percentage error',...
'Location', 'SouthEast')

%% Power Law compliance study - SVD method
close all; clear all;
%Generating compliance data
J0          = 13.5e-11; % Instantaneous compliance,
% where E is Young Modulus
[sigma, t]  = teststress(0,.05) ; % Numerically generate stress
[J_noiseless,time, noiseless_strain] = Num_Gen_Comp(J0 ,sigma, t) ;
noise = [0 0.01 0.02 0.05 0.1];
Err   = zeros(size(noise));
for k = noise % let k run through component of noise vector
idx = 1;
if k == 0
[C, alpha, PL_J] = PL_SVD( J0,J_noiseless, time, idx);
Diff             = PL_J - J_noiseless; % Pointwise differences
Err(noise == k)  = Error_estimate(J_noiseless, PL_J);

figure()
semilogy(time,J_noiseless,'-', 'LineWidth',1), hold on, grid on
semilogx(time,PL_J, 'r--','LineWidth',1);hold off
xlabel('Time (s)')
ylabel('Compiance J (Pa^{-1})')
```

```
legend('Noiseless measurement',...
['Reconstructed J with C =',num2str(C), ', \alpha =', num2str(alpha)],...
'Location', 'SouthEast')
% Plot pointwise difference
figure ()
plot(time,Diff,'r--','LineWidth',1); hold on;
plot(zeros(size(t)),'--k','LineWidth',1);grid on;hold off
xlabel('Time (s)');ylabel('Pointwise error (Pa^{-1})')
legend('Pointwise differences between noiseless measurement...
 and recontructed J','Location', 'SouthEast')

else
J_noisy = J_noiseless + k*mean(J_noiseless)*randn(size(J_noiseless));
% Add noise
[C, alpha, PL_J] = PL_SVD( J0,J_noisy, time, idx);
Err(noise == k)  = Error_estimate(J_noiseless, PL_J);

% Plot results
figure()
semilogy(time,J_noiseless,'-', 'LineWidth',1), hold on, grid on
semilogy(time,J_noisy,'-.', 'LineWidth',1)
semilogx(time,PL_J, 'r--','LineWidth',1.5)
xlabel('Time (s)')
ylabel('Compiance J (Pa^{-1})')
legend('Noiseless measurement ',...
['Measurement with ', num2str(k*100),'% noise'],  ...
['Reconstructed J with C =',num2str(C), ', \alpha =', num2str(alpha)],...
'Location', 'SouthEast')
end
end
% Plot RMSD
figure ()
plot(noise*100,Err,'r--<','LineWidth',1);
strValues = strtrim(cellstr(num2str(Err(:))));
text( noise*100,Err,strValues,'VerticalAlignment','top');
grid on
xlabel('Noise level (%)') ; ylabel('Error (%)')
legend('Mean absolute percentage error',...
'Location', 'SouthEast')

%% Power Law compliance study - Tikhonov regularisation method
close all; clear all;
%Generating compliance data
J0          = 13.5e-11; % Instantaneous compliance,
% where E is Young Modulus
```

```
[sigma, t]  = teststress(0,.05) ; % Numerically generate stress
[J_noiseless,time, noiseless_strain] = Num_Gen_Comp(J0 ,sigma, t) ;
noise = [0 0.01 0.02 0.05 0.1];
Err   = zeros(size(noise));
for k = noise % let k run through component of noise vector
idx = 1;
if k == 0
[C, alpha, PL_J] = PL_Tik_reg( J0,J_noiseless, time, idx);
Diff             = PL_J - J_noiseless; % Pointwise differences
Err(noise == k)  = Error_estimate(J_noiseless, PL_J);

figure()
semilogy(time,J_noiseless,'-', 'LineWidth',1), hold on, grid on
semilogx(time,PL_J, 'r--','LineWidth',1);hold off
xlabel('Time (s)')
ylabel('Compiance J (Pa^{-1})')
legend('Noiseless measurement',...
['Reconstructed J with C =',num2str(C), ', \alpha =', num2str(alpha)],...
'Location', 'SouthEast')
% Plot pointwise difference
figure ()
plot(time,Diff,'r--','LineWidth',1); hold on;
plot(zeros(size(t)),'--k','LineWidth',1);grid on;hold off
xlabel('Time (s)');ylabel('Pointwise error (Pa^{-1})')
legend('Pointwise differences between noiseless measurement...
 and recontructed J','Location', 'SouthEast')

else
J_noisy = J_noiseless + k*mean(J_noiseless)*randn(size(J_noiseless));
% Add noise
[C, alpha, PL_J] = PL_Tik_reg( J0,J_noisy, time, idx);
Err(noise == k)  = Error_estimate(J_noiseless, PL_J);

% Plot results
figure()
semilogy(time,J_noiseless,'-', 'LineWidth',1), hold on, grid on
semilogy(time,J_noisy,'-.', 'LineWidth',1)
semilogx(time,PL_J, 'r--','LineWidth',1.5)
xlabel('Time (s)')
ylabel('Compiance J (Pa^{-1})')
legend('Noiseless measurement ',...
['Measurement with ', num2str(k*100),'% noise'],  ...
['Reconstructed J with C =',num2str(C), ', \alpha =', num2str(alpha)],...
'Location', 'SouthEast')
end
```

```
end
% Plot RMSD
figure ()
plot(noise*100,Err,'r--<','LineWidth',1);
strValues = strtrim(cellstr(num2str(Err(:))));
text( noise*100,Err,strValues,'VerticalAlignment','top');
grid on
xlabel('Noise level (%)') ; ylabel('Error (%)')
legend('Mean absolute percentage error',...
'Location', 'SouthEast')


%% Experiemental studies
close all; clear all;
measured_data    = csvread('creeptest.csv');
time    = measured_data(1:500,1);
measured_stress = measured_data(1:500,2)*1e6;
measured_strain = measured_data(1:500,3);
idx        = find(measured_stress == max(measured_stress));
dt         = time(2)-time(1);
measured_J     = zeros(length(time)-(idx+1),1);
for i = 1:length(time)-(idx+1)
measured_J (i)  = measured_strain(i+1)./(0.1*1e6) -...
 time(idx)*((measured_strain(i+idx)- ...
 measured_strain(idx+i+1) ) /(4*0.1*dt*1e6)) ;
end

time(length(measured_J):end-1) = [];

J0         =  1/(3.7e9) ;
[C, alpha, J_PL] = PL_SVD( J0,measured_J, time,idx); %Power Law
N = 40;
[Jk, J_K, JK0, tau] = Kelvin_compliance(time,measured_J,N); %Kelvin
figure()
plot(time,measured_J,'-', 'LineWidth',1), hold on, grid on
plot(time,J_PL, 'r--','LineWidth',1);hold off
xlabel('Time (s)')
ylabel('Compiance J (Pa^{-1})')
legend('Measurement',...
['Reconstructed J with C =',num2str(C), ', \alpha =', num2str(alpha)],...
'Location', 'SouthEast')
title('Power law model')
figure()
plot(time,measured_J,'-', 'LineWidth',1), hold on, grid on
plot(time,J_K, 'r--','LineWidth',1);hold off
```

```
xlabel('Time (s)')
ylabel('Compiance J (Pa^{-1})')
legend('Measurement','Reconstructed J',...
'Location', 'SouthEast')
title('Generalised Kelvin model')

% Strain response
mdata    = csvread('creeptest.csv');
t    = mdata(1:3000,1);
mstress = mdata(1: 3000,2); %figure; plot(time, tstress)
mstrain = mdata(1:3000,3);
PLs    = PL_strain_response(mstress,t,J0,C,alpha);
Ks =  Kelvin_Strain_response(mstress,t,tau,Jk, JK0);
figure;plot(t,mstrain, 'b-'), hold on; plot(t,PLs, '--');
hold on, plot(t,Ks,'r-.'); grid on
xlabel('Time (s)')
ylabel('Strain response')
legend('Measured strain response',...
'Power Law','Kelvin',   'Location', 'NorthEast')
% Cyclic
data    = csvread('harmonic.csv');
t    = data(1:end,1);
stress = data(1:end,2); %figure; plot(t, stress)
strain_response = data(1:end,3); %figure; plot(time, strain_response)
strain = PL_Strain_response(stress,t,J0,C,alpha);
str     = PL(stress,t,J0,C,alpha);
strainK =  Kelvin_Strain_response(stress,t,tau,Jk, JK0);
figure;  hold on ; plot(t,strain_response, '-', 'LineWidth',1); grid on
plot(t,str, 'r--','LineWidth',1)
plot(t,strainK, 'b-.','LineWidth',1)
xlabel('Time (s)')
ylabel('Strain response')
legend('Measured strain response','Generalised Kelvin model',...
'Power Law model', 'Location', 'SouthEast')



% Dynamic Compliance
Frequency       = linspace(1e-3, 10, 100)';
[K_J1, K_J2, K_J_omega, K_delta]        = ...
Dynamic_K_compliance(Jk,tau,Frequency);
k               = [0,1,2]';
[PL_J1, PL_J2, PL_J_omega, PL_delta]    = ...
Dynamic_PL_compliance(C,alpha,J0,k,Frequency);
%plotting loss compliance
```

```
Data = csvread('storage and loss.csv');
omega = Data(:,1);
omega = 1./omega;
measured_storage_compliance = Data(:,2);
measured_loss_compliance = Data(:,3);
measured_complex_compliance = (measured_storage_compliance.^2 +...
measured_loss_compliance.^2).^(0.5);
measured_delta    = ...
atan(measured_loss_compliance./measured_storage_compliance);
figure()
semilogx(Frequency, K_J1, '-.', 'LineWidth',1.5); hold on; grid on
semilogx(Frequency, PL_J1(:,1), '--', 'LineWidth',1.5);
semilogx(Frequency, PL_J1(:,2), ':', 'LineWidth',1.5);
semilogx(omega,measured_storage_compliance, 'x', 'LineWidth',2);
hold off
xlabel('Frequency \omega (s^{-1})');
ylabel('Storage compliance J_1 (\omega) (Pa^{-1})')
legend('Generalised Kelvin storage compliance', ...
'Power law storage compliance for k =0',...
'Power law storage compliance for k =1',...
'Measured storage compliance',...
'Location', 'SouthEast')

figure ()
semilogx(Frequency, K_J2, '-.', 'LineWidth',1.5);hold on;grid on
semilogx(Frequency, PL_J2(:,1), '--', 'LineWidth',1.5);
semilogx(Frequency, PL_J2(:,2), ':', 'LineWidth',1.5);
semilogx(omega,measured_loss_compliance, 'x','LineWidth',1.5); hold off
%ylim([-1.5e-9  3e-9])
xlabel('Frequency \omega (s^{-1})');
ylabel('Loss compliance J_2(\omega) (Pa^{-1})')
legend('Generalised Kelvin loss compliance',...
'Power law loss compliance for k =0',...
'Power law loss compliance for k =1',...
'Measured loss compliance',...
'Location', 'SouthEast')

figure ()
semilogx(Frequency, K_J_omega, '-.', 'LineWidth',1.5); hold on;grid on
semilogx(Frequency, PL_J_omega(:,1), '--', 'LineWidth',1.5);
semilogx(Frequency, PL_J_omega(:,2), ':', 'LineWidth',1.5);
semilogx(omega,measured_complex_compliance, 'x', 'LineWidth',2); hold off
xlabel('Frequency \omega (s^{-1})');
ylabel('Magnitude of complex compliance |J*(\omega)|(Pa^{-1})');
legend('Generalised Kelvin complex compliance',...
```

```
'Power law complex compliance for k =0',...
'Power law complex compliance for k =1',...
'Measured complex compliance',...
'Location', 'SouthEast')

figure ()
semilogx(Frequency, K_delta, '-.', 'LineWidth',1.5); hold on; grid on
semilogx(Frequency, PL_delta(:,1), '--', 'LineWidth',1.5);
semilogx(Frequency, PL_delta(:,2), ':', 'LineWidth',1.5);
semilogx(omega,measured_delta, 'x', 'LineWidth',2)
xlabel('Frequency \omega (s^{-1})');
ylabel('Phase shift angle \delta (rad)'); grid on
legend('Generalised Kelvin model', 'Power law model for k =0',...
'Measured values',...
'Power law model for k =1','Location', 'SouthEast')
%% Ramp test studies
clear all; close all;
J0   = 1/(9e9) ;
C = 1e-11;
alpha=1/3;
time      = linspace(0, 60*20,2*421)';
stress_level = 1;
noiseless_s = stress_level*ones(size(time));
noiseless_strain = PL(noiseless_s,time,J0,C,alpha);
noiseless_J = noiseless_strain./(noiseless_s*1e6);
noise       = [0 0.01 0.02 0.05 0.1];
ramp_time   = [.5 1 2 10];
m = 2;
for i = noise
for j = ramp_time
stress    = stress_level*[(1/(m*j))*linspace(0,(m*j),(m*j+1))';...
ones(length(time)- (m*j+1),1)] ;
stress      = stress + 1e6*i*stress_level*randn(size(stress));
measured_strain = PL(stress,time,J0,C,alpha);
J  = measured_strain/(stress_level*1e6);
idx        = m*j+20;
t1      = time(idx);
dt         = time(2)-time(1);
measured_J     = zeros(length(time)-(idx+1),1);
for k = 1:length(time)-(idx+1)
measured_J (k)  = measured_strain(k+1)./(stress_level*1e6) ...
- time(idx)*((measured_strain(k+idx)- measured_strain(idx+k+1) )...
/(4*stress_level*dt*1e6)) ;
end
figure();  plot(measured_J), hold on, plot(noiseless_J) , plot(J)
```

```
xlabel('time (sec)'); ylabel('Strain');
legend(['Complian with ramp time = ',num2str(j), 's and noise = ',...
num2str(i), '%'],'Noiseless Compliance','J_divided',...
'Location', 'SouthEast')
end
end
```